UNIVERSIDADE FEDERAL DE MINAS GERAIS
Escola de Engenharia
Programa de Pós-Graduação em Saneamento, Meio Ambiente e Recursos Hídricos

Isabel Pereira da Silva

EVALUATION OF COMPOSITE FROM DISPOSED ULTRAFILTRATION MEMBRANES AS ADSORBENT FOR THE REMOVAL OF ANTIBIOTICS FROM WATER

Belo Horizonte
2024

Isabel Pereira da Silva

EVALUATION OF COMPOSITE FROM DISPOSED ULTRAFILTRATION MEMBRANES AS ADSORBENT FOR THE REMOVAL OF ANTIBIOTICS FROM WATER

Tese apresentada ao Programa de Pós-graduação em Saneamento, Meio Ambiente e Recursos Hídricos da Universidade Federal de Minas Gerais, como requisito parcial à obtenção do título de Doutora em Saneamento, Meio Ambiente e Recursos Hídricos.

Área de concentração: Meio Ambiente

Linha de pesquisa: Caracterização, prevenção e controle da poluição

Orientador: Prof. Dr. Eduardo Coutinho de Paula

Coorientadora: Prof.ª Dr.ª Sônia Denise Ferreira Rocha

Belo Horizonte
2024

Silva, Isabel Pereira da.
S586e Evaluation of composite from disposed ultrafiltration membranes as adsorbent for the removal of antibiotics from water [recurso eletrônico] / Isabel Pereira da Silva. - 2024.
1 recurso online (169 f. : il., color.) : pdf.

Orientador: Eduardo Coutinho de Paula.
Coorientadora: Sônia Denise Ferreira Rocha.

Tese (doutorado) - Universidade Federal de Minas Gerais, Escola de Engenharia.

Anexos: f. 163-169.

Inclui bibliografia.
Exigências do sistema: Adobe Acrobat Reader.

1. Engenharia sanitária - Teses. 2. Meio ambiente - Teses. 3. Bentonita - Teses. 4. Adsorventes - Teses. 5. Pirólise - Teses. 6. Resíduos sólidos - Administração Teses. I. Paula, Eduardo Coutinho de. II. Rocha, Sônia Denise Ferreira. III. Universidade Federal de Minas Gerais. Escola de Engenharia. IV. Título.

CDU: 628(043)

Ficha catalográfica elaborada pelo bibliotecário Reginaldo César Vital dos Santos CRB/6 2165
Biblioteca Prof. Mário Werneck, Escola de Engenharia da UFMG

UNIVERSIDADE FEDERAL DE MINAS GERAIS
ESCOLA DE ENGENHARIA
PROGRAMA DE PÓS-GRADUAÇÃO EM SANEAMENTO, MEIO AMBIENTE E RECURSOS HÍDRICOS

FOLHA DE APROVAÇÃO

"Evaluation Of Composite From Disposed Ultrafiltration Membranes As Adsorbent For The Removal Of Antibiotics From Water"

ISABEL PEREIRA DA SILVA

Tese defendida e aprovada pela banca examinadora constituída pelos Senhores:

Prof. Eduardo Coutinho de Paula

Prof. Eduardo Henrique Martins Nunes

Profa a. Zuy Maria Magriotis

Prof. Gilberto Alves Romeiro

Profa Luzia Sergina de França Neta

Aprovada pelo Colegiado do PG SMARH Versão Final aprovada por

Profa. Priscilla Macedo Moura

Coordenadora

Prof. Eduardo Coutinho de Paula

Orientador

Belo Horizonte, 29 de fevereiro de 2024.

Documento assinado eletronicamente por **Eduardo Coutinho de Paula**, **Professor do Magistério Superior**, em 04/03/2024, às 12:14, conforme horário oficial de Brasília, com fundamento no art. 5º do Decreto nº 10.543, de 13 de novembro de 2020.

Documento assinado eletronicamente por **Eduardo Henrique Martins Nunes**, **Professor do Magistério Superior**, em 04/03/2024, às 14:03, conforme horário oficial de Brasília, com fundamento no art. 5º do Decreto nº 10.543, de 13 de novembro de 2020.

Documento assinado eletronicamente por **Gilbeto Alves Romeiro**, **Usuário Externo**, em 04/03/2024, às 14:15, conforme horário oficial de Brasília, com fundamento no art. 5º do Decreto nº 10.543, de 13 de novembro de 2020.

Documento assinado eletronicamente por **Luzia Sergina de França Neta**, **Usuário Externo**, em 05/03/2024, às 07:13, conforme horário oficial de Brasília, com fundamento no art. 5º do Decreto nº 10.543, de 13 de novembro de 2020.

Documento assinado eletronicamente por **Zuy Maria Magriotis**, **Usuária Externa**, em 05/03/2024, às 09:41, conforme horário oficial de Brasília, com fundamento no art. 5º do Decreto nº 10.543, de 13 de novembro de 2020.

A autenticidade deste documento pode ser conferida no site https://sei.ufmg.br/sei/controlador_externo.php?acao=documento_conferir&id_orgao_acesso_externo=0, informando o código verificador **3075339** e o código CRC **646F250B**.

Referência: Processo nº 23072.212601/2024-09 SEI nº 3075339

Com amor, dedico essa tese aos meus orientadores na vida: meus pais !

AGRADECIMENTOS

Ao Divino Espírito Santo e ao meu Anjo da Guarda, por me guardar e iluminar!

Aos meus pais, Valéria e Sávio, por serem meu suporte em mais essa batalha. É por vocês que cada lágrima e cada noite em claro valeu a pena!

Ao meu irmão Rodrigo, minha avó Neuza e toda minha família, pelo apoio e orações!

Ao meu orientador, Prof. Dr. Eduardo Coutinho de Paula, e à minha co-orientadora, Prof.ª Dra. Sônia Denise Ferreira Rocha, exemplos de profissionais, por toda confiança, incentivo e ensinamentos a mim entregues!

Ao meu supervisor, Prof. Dr. Amit Bhatnagar, ao Dr. Ali Maged e aos amigos da LUT University na Finlândia pela parceria iniciada e pelos ensinamentos e momentos compartilhados nos 6 meses de uma experiência da qual me lembrarei eternamente!

À UFMG, através do SMARH, à CAPES, especialmente através do CAPES PRINT, pelo amparo concedido para o desenvolvimento da pesquisa!

Aos laboratórios da UFMG de Água na Mineração, através da Prof.ª Dra. Sônia Rocha, e de Processos Industriais, através do Prof. Dr. Daniel Rezende, por viabilizarem equipamentos e espaço físico indispensáveis aos experimentos!

À Petrobrás, através do Rodrigo Suhett de Souza, pela disponibilização das membranas de ultrafiltração descartadas!

Às alunas de IC, Victória e Ana Luísa, e aos companheiros de laboratório, especialmente Giovanni e Cássia, por compartilharem dos mesmos desesperos, porém da mesma determinação!

Às minhas amigas de São João del-Rei e ao meu namorado Frederico, pela torcida e pelos momentos de descontração!

A todos que de alguma maneira se fizeram presentes nessa fase da minha vida, muito obrigada!

RESUMO

Os módulos de membranas de ultrafiltração (UF) utilizados em Estações de Tratamento de Efluentes (ETEs) têm ciclo de vida finito e devem ser substituídos periodicamente, gerando resíduos sólidos inertes. Por outro lado, a presença de produtos farmacêuticos em concentrações crescentes nas águas superficiais, subterrâneas, residuárias e até mesmo na água potável é uma preocupação em todo o mundo. O processo de adsorção emergiu como uma tecnologia operacionalmente simples e eficiente para remover contaminantes refratários, como os fármacos. O desenvolvimento de materiais adsorventes alternativos visa redução de custos, aumento da seletividade, maior capacidade de regeneração, bem como uma alternativa de descarte de subprodutos de outras atividades. Assim, o objetivo geral do estudo foi produzir um carvão de membrana (MC) a partir da pirólise de membranas de ultrafiltração descartadas, feitas de fluoreto de polivinilideno (PVDF), e avaliar o desempenho do compósito carvão de membrana-bentonita (MCBT) sintetizado como adsorvente para a remoção de antibióticos da água. Foram considerados aspectos técnicos e econômicos. A pirólise foi otimizada em relação ao tempo de residência e à temperatura final para produção de MC por meio do planejamento composto central de experimentos, do método de superfície de resposta e do método de otimização do Gradiente Reduzido Generalizado. A pirólise de fibras de PVDF de membranas de UF descartadas em condições otimizadas (584 °C; 111 min) produz um MC com um número de iodo de 242,35 mg/g. Este MC, derivado da remoção de moléculas de flúor ou fluoreto de hidrogênio do PVDF, apresenta estabilidade térmica e domínios grafíticos, com área superficial de 345 m^2/g, volume total de poros de 0,16 cm^3/g e caráter microporoso. Com um baixo custo de produção estimado de 0,14 €/kg, encontra relevância em diversas aplicações industriais, ambientais e de pesquisa. Foi proposta uma metodologia para sintetizar o compósito MCBT combinando MC e argila bentonita na proporção de massa de 3:1. Estudos de caracterização do MCBT revelaram um material homogêneo com área superficial de 398 m^2/g, volume total de poros de 0,18 cm^3/g e diâmetro médio de poros microporosos de 1,8 nm, tornando-o um adsorvente de baixo custo. O MCBT exibiu capacidades máximas de adsorção de 34,0 mg/g para o antibiótico tetraciclina (TC) e 31,3 mg/g para o antibiótico enrofloxacina (ENR) em modo de batelada. Os estudos cinéticos favoreceram o modelo de pseudo-segunda ordem, indicando a quimissorção como mecanismo de adsorção. Estudos isotérmicos demonstraram adsorção em monocamada em regiões específicas da superfície do MCBT. A adsorção em modo contínuo apresentou cinética lenta, necessitando de tempo de contato prolongado. Por fim, testes de regeneração do MCBT utilizando diferentes agentes e concentrações mostraram uma diminuição na sua eficiência de remoção após o terceiro ciclo, possivelmente devido a fortes interações de quimissorção entre moléculas de TC ou ENR e o compósito MCBT. Assim, o MCBT desenvolvido pode ser aplicado para abordar questões em áreas ambientais, promovendo práticas eficientes em termos de recursos e soluções sustentáveis.

Palavras-chave: gestão de resíduos; adsorventes alternativos; pirólise; PVDF; bentonita.

ABSTRACT

Ultrafiltration (UF) membrane modules used in Wastewater Treatment Plants (WWTPs) have a finite life cycle and must be replaced periodically, generating inert solid waste. On the other hand, the presence of pharmaceuticals in increasing concentrations in surface water, groundwater, wastewater and even drinking water is a concern worldwide. The adsorption process has emerged as an operationally simple and efficient technology to remove refractory contaminants such as pharmaceuticals. The development of alternative adsorbent materials aims to reduce costs, increase selectivity, greater regeneration capacity, as well as an alternative for disposing of by-products from other activities. Thus, the general objective of the study was to produce a membrane char (MC) from the pyrolysis of discarded ultrafiltration membranes made from polyvinylidene fluoride (PVDF) and to evaluate the performance of the synthesized membrane char-bentonite composite (MCBT) as an adsorbent for removing antibiotics from water. Technical and economic aspects were considered. Pyrolysis was optimized regarding the residence time and final temperature for MC production via the central composite design of experiments, the response surface method, and the Generalized Reduced Gradient optimization method. Pyrolyzing PVDF fibers from discarded UF membranes at optimized conditions (584 °C; 111 min) yields an MC with an iodine number of 242.35 mg/g. This MC, derived from the removal of fluoride or hydrogen fluoride molecules from PVDF, exhibits thermal stability and graphitic domains, with a surface area of 345 m^2/g, total pore volume of 0.16 cm3/g, and microporous character. With an estimated low production cost of 0.14 €/kg, it finds relevance in various industrial, environmental, and research applications. A methodology to synthesize the MCBT composite by combining MC and bentonite clay in a mass ratio of 3:1 was proposed. Characterization studies of MCBT revealed a homogenous material with a surface area of 398 m^2/g, total pore volume of 0.18 cm^3/g, and microporous average pore diameter of 1.8 nm, making it a cost-effective adsorbent. MCBT exhibited maximum adsorption capacities of 34.0 mg/g for antibiotic tetracycline (TC) and 31.3 mg/g for antibiotic enrofloxacin (ENR) in batch mode. Kinetic studies favored the pseudo-second-order model, indicating chemisorption as the adsorption mechanism. Isotherm studies demonstrated monolayer adsorption on specific regions of the MCBT surface. Continuous mode adsorption showed slow kinetics, requiring prolonged contact time. Finally, MCBT regeneration tests using different agents and concentrations showed a decrease in its removal efficiency after the third cycle, possibly due to strong chemisorption interactions between TC or ENR molecules and the MCBT composite. Thus, the developed MCBT can be applied to address issues in environmental areas, promoting resource-efficient practices and sustainable solutions.

Keywords: waste management; alternative adsorbents; pyrolysis; PVDF; bentonite.

LIST OF FIGURES

LIST OF TABLES

LIST OF CHARTS

LISTA DE ABREVIATURAS E SIGLAS

ABNT– Associação Brasileira de Normas Técnicas

ANOVA – Analysis of variance

ASTM – American Society for Testing and Materials

BC – Breakthrough curve

C_0 – Initial concentration

CA – Cellulose acetate

CAC – Conventional activated carbon

C_B – Breakthrough concentration

CCD – Central composite design

C_E – Exhaustion concentration

D – Dosage

DSC – Differential scanning calorimetry

DTG – Derivative thermogravimetry

DWTP – Drinking Water Treatment Plant

EDS – Energy-dispersive X-ray spectroscopy

ENR – Enrofloxacin

F^- – Fluoride

F – Fluorine

FTIR – Fourier-transform infrared spectroscopy

GAC – Granular activated carbon

GRG - Generalized reduced gradient

H_0 – Null hypothesis

ICP-OES – Inductively coupled plasma optical emission spectrometry

IN – Iodine number

IUPAC – International Union of Pure and Applied Chemistry

MBR – Membrane bioreactor

MC – Membrane char

MCBT – Membrane char-bentonite composite

MTZ – Mass transfer zone

PAC – Powered activated carbon

PAN – Polyacrylonitrile

PES – Polyethersulfone

PhAC – Pharmaceutically active compound

pH_{ZPC} – pH of zero point of charge

PI - Aromatic polyimide

PS – Polysulfone

PTFE – Polytetrafluoroethylene

PVC - Polyvinyl chloride

PVDC - Poly(vinylidene chloride)

PVDF – Polyvinylidene fluoride

q_0 – Adsorption capacity

R% – Removal efficiency

RSM - Response surface method

SAXS - Small angle X-ray scattering

SDG – Sustainable Development Goal

SEM – Scanning electron microscopy

T – Final temperature

t – Residence time

t_B – Breakthrough time

TC – Tetracycline

t_E – Exaushtion time

TEM – Transmission electron microscopy

TG – Thermogravimetry

TGA – Thermogravimetric analysis

UASB – Upflow Anaerobic Sludge Blanket

UF – Ultrafiltration

V – Volume

VDF – Vinylidene fluoride

WAXD – Wide-angle X-ray diffraction

WHO – World Health Organization

WWTP – Wastewater Treatment Plants

XPS – X-ray photoelectron spectroscopy

XRD – X-ray diffraction

SUMÁRIO

CHAPTER 1 - INTRODUCTION

1.1 CONTEXTUALIZATION

Initially, it is important to consider that many operations conducted in Wastewater Treatment Plants (WWTPs), in addition to producing reused water or water that meets the environmental criteria for discharge, also generate solid wastes that require adequate disposal (VON SPERLING, 2005).

Ultrafiltration (UF) membranes are an established technology widely used in water and wastewater treatment systems in several countries, including Brazil. Membranes are synthetic polymeric materials whose permeability and selectivity characteristics are exploited in separation processes. Over time in operation, such membranes suffer a decline in performance, generally due to the occurrence of non-reversible fouling and a consequent reduction in permeate flow, thus being discarded as inert waste in landfills (HABERT, BORGES & NOBREGA, 2006; MATTER, 2018; SHAHID *et al.*, 2020).

In this context, the present study proposed to evaluate the use of UF membranes discarded at the end of their life cycle for char production and its use as an alternative adsorbent material for removing pharmaceuticals from water. The UF membranes evaluated were manufactured in polyvinylidene fluoride (PVDF), in a hollow fiber configuration module, and came from systems with membrane bioreactors (MBR).

Specialized literature reports that pharmaceuticals, as refractory contaminants, are increasingly present in surface water, groundwater, wastewater and even drinking water worldwide (WILKINSON *et al.*, 2022). It occurs because part of the pharmaceuticals consumed is excreted, in addition, the inadequate disposal of these products is a reality, and conventional Wastewater Treatment Plants (WWTPs) are not designed to remove them completely.

Among the most consumed pharmaceutical products in the world are Tetracycline (TC) and Enrofloxacin (ENR), antibiotics used to improve the health and quality of life of humans and animals, respectively (WILKINSON *et al.*, 2022; TROUCHON & LEFEBVRE, 2016; LEICHTWEIS *et al.*, 2022). Even at low concentrations, antibiotics present in aqueous matrices pose risks to environmental compartments and human health, especially concerning bacterial resistance (WILKINSON *et al.*, 2022).

Therefore, removing these pharmaceuticals from water becomes necessary, and among several methods applicable for this purpose, adsorption stands out as a simple, efficient, and economical technology.

Commonly considered a polishing step to remove refractory contaminants, adsorption is also capable of removing pharmaceuticals through the concentration of this adsorbate on the surface of an adsorbent (CAVALCANTI, 2009; COUTO *et al.*, 2020; MANSOURI *et al.*, 2021; METCALF & EDDY, 2014; PHOON *et al.*, 2020). The most used adsorbent, mainly on an industrial scale, is conventional or commercial activated carbon (CAC) and its production is done through pyrolysis of the chosen raw material, followed by an activation step, the objective of which is to increase the concentration of pores and, consequently, the surface area of the adsorbent. However, after the adsorption-desorption cycles, the adsorption capacity of CAC is reduced and its useful life ends, making its disposal in landfills or incineration inevitable (CAVALCANTI, 2009; METCALF & EDDY, 2014). Therefore, the development of alternative adsorbents, replacing CAC, mainly aims to reduce costs and increase the selectivity of the product for specific contaminants, in addition to being an alternative for waste disposal from other activities (DE GISI *et al.*, 2016).

The basic research question in the present study can be summarized as follows: is it possible to take advantage of discarded UF membranes as a by-product of wastewater treatment and use them as raw material to produce alternative adsorbents for the removal of pharmaceuticals?

The work covered char and composite production and characterization, batch and continuous antibiotics adsorption tests, as well as the regeneration of the saturated composite, and additionally preliminary cost evaluations.

1.2 JUSTIFICATION

The activities of waste management, including reduction, reuse, and recycling, along with the concept of the circular economy, aim at both economic prosperity and environmental quality. These activities, combined with the integration of technologies proposed in this work, align with the current discussion of the Sustainable Development Goals (SDGs).

Using by-products to produce alternative adsorbents brings environmental benefits, allowing for the reduction of both solid waste and contaminants in water. Additionally, the cost associated with waste management, including that from water and wastewater treatment, such as ultrafiltration (UF) membranes, poses one of the obstacles to realizing many ideal systems.

In the context of water and wastewater treatment processes, the global expansion of membrane systems is evident, and an increasing number of UF membrane modules will need to be periodically replaced and discarded.

Understanding the various technical and operational aspects that commonly reduce the useful life of membranes, and considering the relevance of adsorption in pollution control, especially for pharmaceuticals, it is pertinent to assess the technical and economic feasibility of using discarded UF membranes to produce alternative adsorbents.

Based on exploratory research, it is important to note that the production of char from discarded UF membranes for use as an adsorbent is unprecedented to date and has not been identified in relevant literature. In light of the above, this research brings originality and aims to contribute to reducing adverse environmental and economic impacts at the end of the useful life of UF membrane modules, as well as to the suitability of water by removing pharmaceuticals.

1.3 PREMISES

- The development of alternative adsorbents, replacing conventional activated carbon (CAC), is an alternative disposal for waste from other activities, such as ultrafiltration membranes (UF).
- Even in low concentrations, antibiotics pose risks to human and animal health, and adsorption is a simple, efficient, and economical technology for removing this contaminant.

1.4 HYPOTHESES

- The pyrolysis of polyvinylidene fluoride (PVDF) fibers from discarded ultrafiltration (UF) membranes, under appropriate operational conditions of final temperature (T) and residence time (t), results in the production of a membrane char (MC).
- The modified MC in the form of MC-bentonite (MCBT) composite possesses relevant porosity, surface area, and surface chemistry for its application as an adsorbent of pharmaceuticals.

1.5 GENERAL OBJECTIVE

Produce char from discarded polymeric ultrafiltration membranes and evaluate a membrane char-bentonite composite synthetized as an adsorbent in the removal of antibiotics from water in both technical and economic aspects.

1.6 SPECIFIC OBJECTIVES

- Identify the appropriate operational conditions of final temperature (T) and residence time (t) for producing char from discarded UF membranes via pyrolysis, the membrane char (MC).
- Propose a methodology for producing MC-bentonite (MCBT) composite.
- Characterize the products MC and MCBT.
- Describe the performance of MCBT as an adsorbent for removing Tetracycline (TC) and Enrofloxacin (ENR) from water in batch and continuous processes.
- Propose a methodology for the regeneration of MCBT used in removing TC and ENR.
- Conduct a preliminary economic assessment of the proposed products MC and MCBT.

1.7 WORK STRUCTURE

To develop the research, four stages were structured to achieve the proposed objectives, as shown in Figure 1.1.

Figure 1.1 - Flowchart of the research stages with the breakdown of objectives

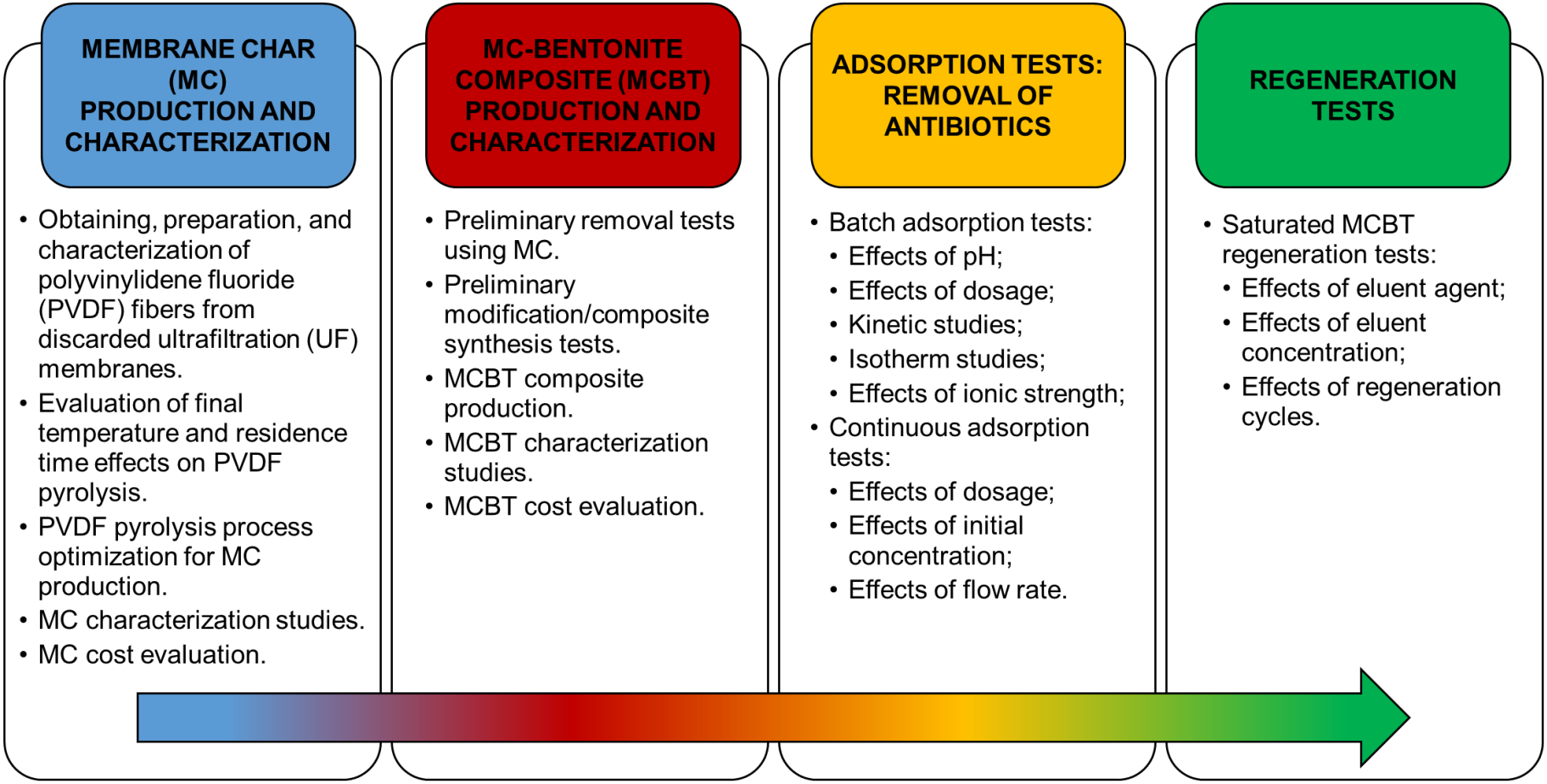

Source: The author herself

This document, in addition to this introductory chapter, is organized into 6 more chapters.

Chapter 2 presents a literature review to provide context regarding ultrafiltration (UF) membranes as by-products of wastewater treatment and polyvinylidene fluoride (PVDF) characteristics. The need for the removal of pharmaceuticals, such as the antibiotics Tetracycline (TC) and Enrofloxacin (ENR) from water, the adsorption process, the alternative adsorbents, and the commonly used techniques in the characterization of char for use as an adsorbent are also presented in this chapter.

In chapters 3 to 6, the Material and Methods section provides information on the methodology applied in each stage from planning and conducting experiments to analyzing results.

Studies on pyrolysis, including PVDF pyrolysis, and the results of the membrane char (MC) production stage, with optimization of the final temperature (T) and residence time (t), are presented in Chapter 3. This chapter also presents the characterization studies and cost evaluation of the MC produced in this work.

Char activation and modification techniques, composite production studies described in the literature, and the methodology applied in the MC-bentonite (MCBT) composite production are described in Chapter 4. Preliminary tests for fluoride (F^-) removal using MC, preliminary modification/composite synthesis tests, MCBT characterization studies, and cost evaluation of the MCBT are also presented.

Concepts regarding equilibrium, kinetics, and dynamics studies of adsorption systems are addressed in Chapter 5. Batch and continuous adsorption tests were carried out to evaluate the effects of many operating parameters on adsorption capacity and removal efficiency. Equilibrium times and removal efficiencies were determined, and adsorption isotherm and kinetic models were evaluated to propose possible adsorption mechanisms and describe the adsorption system.

Chapter 6 covers regeneration techniques of adsorbents described in the literature and the regeneration tests applied to the MCBT used to remove antibiotics.

Finally, Chapter 7 presents the conclusions and the original scientific contributions to knowledge that resulted from the present research.

REFERENCES

CAVALCANTI, J. E. W. A. *Manual de Tratamento de Efluentes Industriais*. 3 ed., [s.l.], Engenho Editora Técnica Ltda, 2009.

COUTO, C. F.; LANGE, L. C.; AMARAL, M. C. Occurrence, fate and removal of pharmaceutically active compounds (PhACs) in water and wastewater treatment plants - A review. *Journal of Water Process Engineering*, v. 32, p. 100927, 2019.

DE GISI, S.; LOFRANO, G.; GRASSI, M.; NOTARNICOLA, M. An overview of low-cost adsorbents for wastewater treatment. *Sustainable Materials and Technologies*, v. 9, p. 10, 2016.

HABERT, A. C.; BORGES, C. P.; NOBREGA, R. *Processos de separação por membranas*. Editora E-papers, Rio de Janeiro, 2006.

LEICHTWEIS, J.; VIEIRA, Y.; WELTER, N.; SILVESTRI, S.; DOTTO, G. L.; CARISSIMI, E. L. A review of the occurrence, disposal, determination, toxicity and remediation technologies of the tetracycline antibiotic. *Process Safety and Environmental Protection*, v. 160, p. 25-40, 2022.

MANSOURI, F.; CHOUCHENE, K.; ROCHE, N.; KSIBI, M. Removal of Pharmaceuticals from water by adsorption and advanced oxidation processes: State of the art and trends. *Applied Sciences*, v. 11, n. 14, p. 6659, 2021.

MATTER, C. G. Membrane filtration (micro and ultrafiltration) in water purification. In: *Handbook Water Used Water Purification*, Springer, p. 1-17, 2018.

METCALF, L.; EDDY, H. P., *Wastewater engineering: treatment and reuse.* 5 ed., McGraw-Hill Education, Nova Iorque, 2014.

PHOON, B. L.; ONG, C. C.; SAHEED, M. S. M.; SHOW, P. L.; CHANG, J. S.; LING, T. C.; LAM, S. S.; JUAN, J. C. Conventional and emerging technologies for removal of antibiotics from wastewater. *Journal of Hazardous Materials*, v. 400, p. 122961, 2020.

SHAHID, M. K.; KASHIF, A.; ROUT, P. R.; ASLAM, M.; FUWAD, A.; CHOI, Y.; BANU J, R.; PARK, J. H.; KUMAR, G. A brief review of anaerobic membrane bioreactors emphasizing recent advancements, fouling issues and future perspectives. *Journal of Environmental Management*, v. 270, p. 110909, 2020.

TROUCHON, T. LEFEBVRE, S. A review of enrofloxacin for veterinary use. *Open Journal of Veterinary Medicine*, 6 (2), p. 40-58, 2016.

VON SPERLING, M. *Introdução à qualidade das águas e ao tratamento de esgotos.* Universidade Federal de Minas Gerais, Belo Horizonte, 2005.

WILKINSON, J. L.; BOXALL, A. B.; KOLPIN, D. W.; LEUNG, K. M.; LAI, R. W.; GALBÁN-MALAGÓN, C.; ...; TETA, C. Pharmaceutical pollution of the world's rivers. *Proceedings of the National Academy of Sciences*, v. 119, n. 8, p. e2113947119, 2022.

CHAPTER 2 - LITERATURE REVIEW

This chapter seeks to objectively present the main themes and concepts addressed during the conception and development of the thesis.

2.1 BY-PRODUCTS OF WASTEWATER TREATMENT

Wastewater treatment takes place in Wastewater Treatment Plants (WWTPs) in stages typically defined as preliminary, primary, secondary, and tertiary treatment. In each of these stages, one or more physical-chemical operations or biological processes are carried out, removing or transforming components such as suspended solids, oils and greases, toxic metals, organic compounds, and pathogenic microorganisms (CAMMAROTA, 2013; VON SPERLING, 2005).

The preliminary treatment is responsible for removing coarse solids and sand from the raw effluent and measuring the feed flow. Grids are the first physical equipment applied in preliminary treatment, with openings between 1 and 10 cm preventing the passage of solids that could cause damage, such as clogging, to the treatment system. Subsequently, grit chambers separate sand from the effluent through sedimentation, preventing silting and premature wear of subsequent equipment (CAVALCANTI, 2009; METCALF & EDDY, 2014; VON SPERLING, 2005).

Decanters are the main components of primary treatment. They are used to remove suspended, settleable, or floating solids from wastewater, including some of the organic matter. These devices allow wastewater to flow slowly so that there is enough time for solids to settle. Floaters, oil separators, screens, and septic tanks may also be present in the primary treatment of wastewater (CAMMAROTA, 2013).

Also known as biological treatment, the secondary treatment stage utilizes microorganisms to remove biodegradable organic matter from the effluent, both in suspension and primarily dissolved. This process occurs in a controlled manner in various systems, ranging from simpler designs to more complex operations. Aerobic treatment systems include activated sludge systems and high-rate ponds, while Upflow Anaerobic Sludge Blanket (UASB) reactors and anaerobic filters are anaerobic biological processes for organic matter removal. The organic matter in the effluents serves as a source of energy for various organisms, mainly bacteria. These organisms,

in turn, convert organic matter into carbon dioxide, water, and cellular material, along with methane under anaerobic biodegradation conditions (CAMMAROTA, 2013; METCALF & EDDY, 2014; VON SPERLING, 2005).

The last stage of effluent treatment, known as tertiary or advanced treatment, is applied to enhance the efficiency of the previous stages and may not necessarily be present in all WWTPs. Specific contaminants such as refractory organic compounds, inorganics, and nutrients are removed in this stage. This polishing stage may involve biological processes, such as maturation ponds, or physical-chemical operations, such as precipitation, ultrafiltration, reverse osmosis, advanced oxidative processes, and adsorption (CAMMAROTA, 2013; METCALF & EDDY, 2014; VON SPERLING, 2005).

The various operations carried out in WWTPs allow the production of reused water and/or its suitability for discharge into the environment. However, some of these technologies only remove contaminants and do not destroy them, generating waste at the end of the process, such as the sand removed in the grit chambers. Other processes, such as biological treatments, result in byproducts in addition to the treated effluent, such as gases and sewage sludge. Components used in some operations, such as filtration membrane modules, have a finite lifespan and need to be replaced from time to time, producing inert solid waste. The cost associated with managing these wastes can pose a challenge to achieving wastewater treatment systems with better cost-effectiveness (CAMMAROTA, 2013; VON SPERLING, 2005).

The production of adsorbents can be an alternative disposal option for the solid byproducts of WWTPs. Some studies, such as Almajed *et al.* (2021), El Mouhri *et al.* (2020), and Liu *et al.* (2017a), investigated the application of sand for alternative adsorbents production, but using commercial silica sand, glass production sand, and beach sand. On the other hand, 31 original scientific research articles on producing adsorbents from sewage sludge, published in English between 2016 and 2021, can be found in the Google Scholar® scientific articles database (TABLE 2.1). Based on these exploratory searches, no publications were identified on the use of discarded membranes for alternative adsorbent production.

Table 2.1 - Studies on alternative adsorbents produced from sewage sludge published between 2016 and 2021

Pollutants to be removed	Adsorption capacity (mg/g)	References
Synozol Blue and Setapers Yellow-Brown	8.54 and 5.4	Kacan (2016)
Diclofenac and Nimesulide	156.7 and 66.4	Dos Reis *et al.* (2016)
Remazol Brilliant Blue R	33.47	Silva *et al.* (2016)
Tetracycline	40.8	Yang, Xu & Yu (2016)
Lead	42.96	Yang *et al.* (2016)
Cadmium	56.2	Ahsaine, Zbair & El Haouti (2017)
Chromium	94.54	Aliakbari *et al.* (2017)
Cadmium	1.8 - 4.9	Fan *et al.* (2017a)
Methylene blue	16.21	Fan *et al.* (2017b)
Copper and methylene blue	114.94 and 125	Guo *et al.* (2017)
Lead	249	Ifthikar *et al.* (2017)
Phosphate	123.46	Jiang *et al.* (2017)
Acetic acid	18.0	Jin *et al.* (2017)
Orange Acid 7	440.53	Liu *et al.* (2017b)
Phosphorus	10.07	Yao *et al.* (2017)
Cadmium	36.5	Zuo *et al.* (2017)
Methylene blue	149.05	Chen *et al.* (2018)
Cesium	52.36	Khandaker *et al.* (2018)
Tetracycline	286.91	Tang *et al.* (2018)
Phosphate	2.99, 1.48 and 1.05	Zhang, Liu & Guo (2018)
Phosphate	29.18	Li *et al.* (2019)
Lead	887.5	Ngambia *et al.* (2019)
Copper	74.51	Tang *et al.* (2019)
Copper, cadmium, and zinc	8.26, 12.36 and 3.92	Wang, Li & Poon (2019a)
Lead	58.28, 60.06 and 62.42	Wang, Li & Poon (2019b)
Chromium	6.03 and 7.84	Wang *et al.* (2019)
Chromium	7.66 and 15.27	Zhang *et al.* (2019)
Methylene blue	-	Ferrentino *et al.* (2020)
Phosphate	93.9	LI *et al.* (2020a)
Iodine and methylene blue	816.27 and 95.25	LI *et al.* (2020b)
Ciprofloxacin	10.42	LI *et al.* (2021)

Source: The author herself

Those sewage sludge-based adsorbents were primarily designed for the removal of toxic metals. Approximately 43% of the conducted studies assessed the removal of 6

species of toxic metals (cadmium, cesium, lead, copper, chromium, and zinc), followed by 6 types of dyes and 4 pharmaceuticals, totaling 16 out of the 18 pollutants tested.

All reported adsorption tests were conducted in batch mode. However, the operational conditions in which these tests were carried out, such as adsorbent dosage, initial adsorbate concentration, and contact time, are not fully available in most studies. Therefore, although adsorptive capacity has been calculated in most tests, the absence of operational parameters hinders a direct comparison of the results achieved. Furthermore, continuous adsorption tests, not addressed in these previous studies, are crucial for assessing the influence of operational parameters on adsorption dynamics and are particularly relevant when considering future industrial applications and process scaling (CAVALCANTI, 2009; CRUZ *et al.*, 2019; MESQUITA *et al.*, 2017a; MESQUITA *et al.*, 2017b; NIGRI *et al.*, 2017; XAVIER *et al.*, 2018).

2.2 ULTRAFILTRATION MEMBRANES

According to Habert, Borges & Nobrega (2006), “a membrane is a barrier that separates two phases and restricts the total or partial transport of one or more chemical species present in the phases." Based on their permeability and selectivity characteristics, filtration membranes retain species in a concentrate fraction and allow the passage of a permeate fraction. Membrane permeation can occur through simple diffusion, selectivity associated with pore size in porous membranes, membrane material in the case of dense membranes, facilitated diffusion, or active transport by agents that facilitate diffusion. The driving force responsible for membrane permeation can be a gradient of chemical potential, a difference in pressure or concentration, or an electrical potential gradient (HABERT, BORGES & NOBREGA, 2006).

Developed in the 1960s, synthetic filtration membranes were primarily used in seawater desalination operations. Nowadays, the applicability of filtration membranes is much broader, ranging from producing reusable water from domestic and industrial wastewater to ensuring potability. They are present in almost every industrial sector, including environmental, electronic, energy, chemical, and biotechnological areas

(ERSAHIN *et al.*, 2012; GALVÃO & GOMES, 2015; HABERT, BORGES & NOBREGA, 2006; LIU *et al.*, 2011; SCHNEIDER & TSUTIYA, 2001).

The membranes used in ultrafiltration (UF) processes belong to the category of porous membranes, with pore sizes ranging from 3 to 50 nm and surface porosity in the range of 0.1 to 1%. By applying pressure gradients between 1 and 7 atm, these membranes can retain colloids and macromolecules with a molecular weight above 5,000 Da (HABERT, BORGES & NOBREGA, 2006). Most commercially used UF membranes are predominantly made from polymeric materials such as cellulose acetate (CA), polysulfone (PS), polyether sulfone (PES), polyacrylonitrile (PAN), and polyvinylidene fluoride (PVDF). Inorganic materials like metals and ceramics can also be used to produce these membranes. However, despite their longer lifespan and ease of cleaning, inorganic membranes are considerably more expensive than polymeric ones (AHMAD, GURIA & MANDAL, 2020; GALVÃO & GOMES, 2015; MATTER, 2018; SCHNEIDER & TSUTIYA, 2001; SHAHID *et al.*, 2020).

UF membranes are commonly used in concentration, dialysis, and purification processes for macromolecules such as proteins. They are also employed in the production of water for reuse, achieving characteristics suitable for drinking water. Another notable application of UF membranes is in membrane bioreactors (MBR), systems that integrate conventional biological treatments in aerobic or anaerobic reactors with membranes responsible for retaining solids and biomass (AHMAD, GURIA & MANDAL, 2020; BARBOSA, 2017; ERSAHIN *et al.*, 2012; HABERT, BORGES & NOBREGA, 2006; HAI, YAMAMOTO & LEE, 2014; KRZEMINSKI *et al.*, 2017; MATTER, 2018; SHAHID *et al.*, 2020; SUBTIL, HESPANHOL & MIERZWA, 2013; XIAO *et al.*, 2019).

In MBR systems, UF membranes are typically used in the form of modules, consisting of a structural part with pressure support and feed and outlet channels for permeate and concentrate (FIGURE 2.1) (ERSAHIN *et al.*, 2012; GALVÃO & GOMES, 2015; HAI, YAMAMOTO & LEE, 2014; MUTAMIM *et al.*, 2013; SHAHID *et al.*, 2020; XIAO *et al.*, 2019).

Figure 2.1 - Individual module and complete membrane bioreactor system (MBR)

Source: Adapted from Suez (2022)

The ZeeWeed membranes from Suez®, such as the ZW500, are examples of ultrafiltration membranes specifically developed for use in MBR (Membrane Bioreactor) systems. They can be employed for potable water applications or industrial wastewater. These membranes exhibit extremely high permeability, exceeding 900 L.m.h/bar, and a lifespan of over 10 years in most applications. These modules feature PVDF membranes with a cylindrical hollow fiber geometry, a nominal pore size of 40 nm, a non-ionic and hydrophilic surface, and a nominal area of 31.6 m^2. They operate at a maximum temperature of 40 °C and pH values between 5 and 9.5 (SUEZ, 2022).

According to BBC Research & Development (2022a), the global MBR (Membrane Bioreactor) market is expected to grow from 2.5 billion dollars in 2021 to 4.1 billion dollars in 2026, with a compound annual growth rate of 10.5% for the period 2021-2026. The increasing use of MBR systems worldwide can be attributed to more stringent regulations for wastewater discharge into the environment, the growing water scarcity, the emphasis on water reuse practices, and increased confidence in the process. In Brazil, various companies employ MBR systems in their processes across diverse sectors, from food and cosmetics industries to shopping malls and oil refineries, including Chocolate Garoto, Colgate, Natura, Nestlé, Petrobrás, and Barra Shopping, as well as sanitation companies (GALVÃO & GOMES, 2015; KRZEMINSKI *et al.*, 2017; LOPES JR & MIERZWA, 2015; SUBTIL, HESPANHOL & MIERZWA, 2013).

The Aquapolo Project, located in the Nova Heliópolis neighborhood of São Paulo, Brazil, for example, is the fifth-largest facility in the world dedicated to producing water of reuse from domestic effluent and utilizes MBR systems in its process. As a Special Purpose Company, Aquapolo is a venture of the São Paulo State sanitation company, Sabesp, and Foz do Brasil, an entity of Odebrecht Ambiental. It has been under operation since 2012, with a contract in place until 2053. The project was designed to supply reclaimed water, primarily for cooling processes, steam production, and the cleaning of cooling towers and boilers, to industries in the Capuava Petrochemical Complex, one of the largest industrial hubs in Brazil and the largest consumer of drinking water in the region. As a result, billions of liters of fresh water are redirected to about 600,000 residents, and client industries can pay approximately 10 times less per cubic meter of water (BARBOSA, 2017; LOPES JR & MIERZWA, 2015; MELO & RODRIGUEZ, 2017; SILVA, 2019).

With 15,000 m^2 of built area, a reservoir of 70,000 m^3 for reclaimed water, and a 17 km pipeline, Aquapolo delivers treated water with the flow and quality specified in the contract to the Petrochemical Complex client. Fed with 650 L/s of treated sewage from the ABC Wastewater Treatment Plant, Aquapolo uses MBR systems with UF membranes to retain solids and produces up to 1,000 L/s of reclaimed water, with the assistance of reverse osmosis membrane systems for polishing treatment when necessary. Aquapolo's MBR systems have a total area of 67,000 m^2 and a project flow of 15 L.h/m^2 (BARBOSA, 2017; LOPES JR & MIERZWA, 2015; MELO & RODRIGUEZ, 2017; SILVA, 2019).

As the use of UF membrane technologies, such as MBR systems, expands, the global market for these membranes is expected to grow from 4.4 billion dollars in 2021 to 5.9 billion dollars in 2026, with a compound annual growth rate of 5.9% for the period 2021-2026 (BBC RESEARCH & DEVELOPMENT, 2022b). However, despite efforts to improve the anti-scaling properties of membranes and develop cleaning techniques, membrane separation systems have a finite lifespan due to reduced permeate flow. UF membranes, for example, with acquisition costs ranging between 50 and 200 dollars per square meter, need to be replaced periodically (LIU *et al.*, 2011; MATTER, 2018; MUTAMIM *et al.*, 2013; SHAHID *et al.*, 2020). Therefore, it can be estimated that an increasing number of membrane modules need to be replaced and periodically

discarded in Brazil and worldwide, typically disposed of in landfills, with few reuse alternatives.

2.3 POLYVINYLIDENE FLUORIDE (PVDF)

Polymers, from the Greek "many repetitive units", are macromolecules formed by covalent bonds between smaller units called monomers and typically composed of carbon, hydrogen, nitrogen, and oxygen atoms (CANEVAROLO JR & SEBASTIÃO, 2010; MANO & MENDES, 2001). Through the polymerization process, monomeric units bond to form linear or cross-linked polymeric chains provided that reactive groups are present in these basic structural units. Polymerization can be natural or synthetic and occurs through addition or condensation reactions (CALLISTER, 2008; ODIAN, 2004).

According to the characteristics of the chain, polymers are classified as homopolymers, if consisting of only one type of monomer, or copolymers, where two or more different monomers are present. Concerning the mechanical behavior exhibited, polymers are divided into three groups: rubbers, plastics, and fibers. The classification of polymers as thermoplastics or thermosetting depends on criteria such as molecular and chemical structures, the average number of monomeric units, and the types of covalent bonds present (AKCELRUD, 2007; CANEVAROLO JR & SEBASTIÃO, 2010; MANO & MENDES, 2001).

Polyvinylidene fluoride or poly(vinylidene fluoride) (FIGURE 2.2), commonly known as PVDF, is a linear chain homopolymer with an average of 2000 monomers and a molecular weight of about 105 g/mol. It is formed from vinylidene fluoride (VDF) monomers, which, due to their carbon-carbon double bond, categorize it into the vinyl polymer family. PVDF polymerization is synthetic and involves addition reactions of fluorine (F) monomers (ABREU, 2012; DROBNY, 2009; ESTERLY, 2002; HARPER, 2000; MARK, 2014; SAXENA & SHUKLA, 2021).

Figure 2.2 - Polyvinylidene fluoride (PVDF) repeating unit

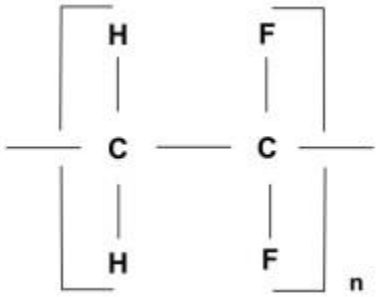

Source: Abreu (2012)

PVDF has thermoplastic properties, semi-crystallinity that reduces the loss of mechanical properties with an increase in temperature, and high chemical resistance. The mechanical strength of PVDF is considered high compared to other thermoplastics such as polyethylene, polypropylene, and polystyrene. As a fluoropolymer, PVDF has higher thermal stability than polymers derived from hydrocarbons due to the high electronegativity of fluorine atoms and the high energy of the C-F bond. Also, due to the presence of fluorine, whose molecular size is small, PVDF has very narrow ultramicro pores of about 1.0 nm (ABREU, 2012; ALCHIKH, FOND & FRÈRE, 2010; CAPITÃO, 2002; DROBNY, 2009; ESTERLY, 2002; FREIRE, 2007; HARPER, 2000; LEE & PARK, 2014; MANO *et al.*, 2003; MARK, 2014; MARTINS, 2010; ODIAN, 2004; SAXENA & SHUKLA, 2021; SILVA, 2009).

Unlike most synthetic polymers, PVDF is a polymorphic polymer with four distinct crystalline structures: alpha (α), beta (β), gamma (γ), and delta (δ). The proportions of these four crystalline phases vary according to the polymerization method used, with the prevalence of the α and β forms in conventional synthesis methods. Many properties of PVDF, such as crystallinity (between 45 and 65%), melting temperature (between 165 and 189 °C), and solubility, depend on the crystalline structure of the polymer chain and can be specifically obtained through the conditions applied during polymerization. The crystalline phases and polymorphic form also impart piezoelectric, pyroelectric, and ferroelectric properties to PVDF, related to the polarization of the material, which, in turn, is due to the symmetrical spatial arrangement of hydrogen and fluorine atoms in the chain (ALCHIKH, FOND & FRÈRE, 2010; CAPITÃO, 2002; DROBNY, 2009; ESTERLY, 2002; FREIRE, 2007; HARPER, 2000; MANO *et al.*, 2003; MARK, 2014; MARTINS, 2010; SAXENA & SHUKLA, 2021; SILVA, 2009).

Given these and other characteristics, PVDF has been applied, especially in the manufacturing of pipelines for transporting more complex fluids, whether at high temperatures, under pressure, or containing concentrated acids, for example. Industries involved in oil and gas extraction are significant consumers of these pipes. The use of PVDF is also common in the production of semiconductors and lithium-ion batteries, primarily for wire insulation. Another equally important application of PVDF is the manufacturing of filtration membranes, which is the focus of this work (ABREU, 2012; CORDEIRO, 2010; LIU *et al.*, 2011; MARK, 2014; SAXENA & SHUKLA, 2021; SOLVAY, 2022).

2.4 PRESENCE OF PHARMACEUTICALS IN AQUEOUS MATRICES

Pharmaceutically active compounds (PhACs), or simply pharmaceuticals, are products used to enhance the health and quality of life of humans and animals, whether in the prevention or treatment of diseases (PHOON *et al.*, 2020; REIS, SANTOS & LANGE, 2021). The increase in the population's life expectancy and the increase in chronic diseases exacerbated by sedentary habits are the main drivers of the global pharmaceutical market. As a paradigm, the dissemination of pharmaceuticals has further favored global life expectancy in recent decades (COOK & WRIGHT, 2022; PEÑA, ZAVALA & RUELAS, 2021).

The presence of pharmaceuticals in aqueous matrices is becoming a worldwide concern due to their adverse effects, even at very low concentrations. These emerging pollutants can cause damage to environmental compartments and human health, such as increased bacterial resistance (DOS SANTOS *et al.*, 2021; REIS, SANTOS & LANGE, 2021; WILKINSON *et al.*, 2022). Bacterial genes that confer resistance to fluoroquinolones detected in drinking water distribution systems in Finland (TIWARI *et al.*, 2021) and bacteria *Salmonella* spp. with resistance to TC found in Brazil (PAVELQUESI *et al.*, 2021) are examples of it.

Excessive consumption of pharmaceuticals and their excretion, inadequate disposal of pharmaceuticals in landfills and their leaching, and the low efficiency of conventional treatment methods generally utilized in Wastewater Treatment Plants (WWTPs) are

the major contributors to the presence of pharmaceuticals in increasing concentrations in surface water, groundwater, wastewater and even drinking water worldwide (FIGURE 2.3) (BÖGER *et al.*, 2021; COUTO, LANGE & AMARAL, 2019; LINDHOLM-LEHTO *et al.*, 2016; REIS *et al.*, 2019; SANTOS *et al.*, 2020; SCARIA, ANUPAMA & NIDHEESH, 2021; WILKINSON *et al.*, 2022).

Figure 2.3 - Transport and degradation flow of antibiotics in environmental systems

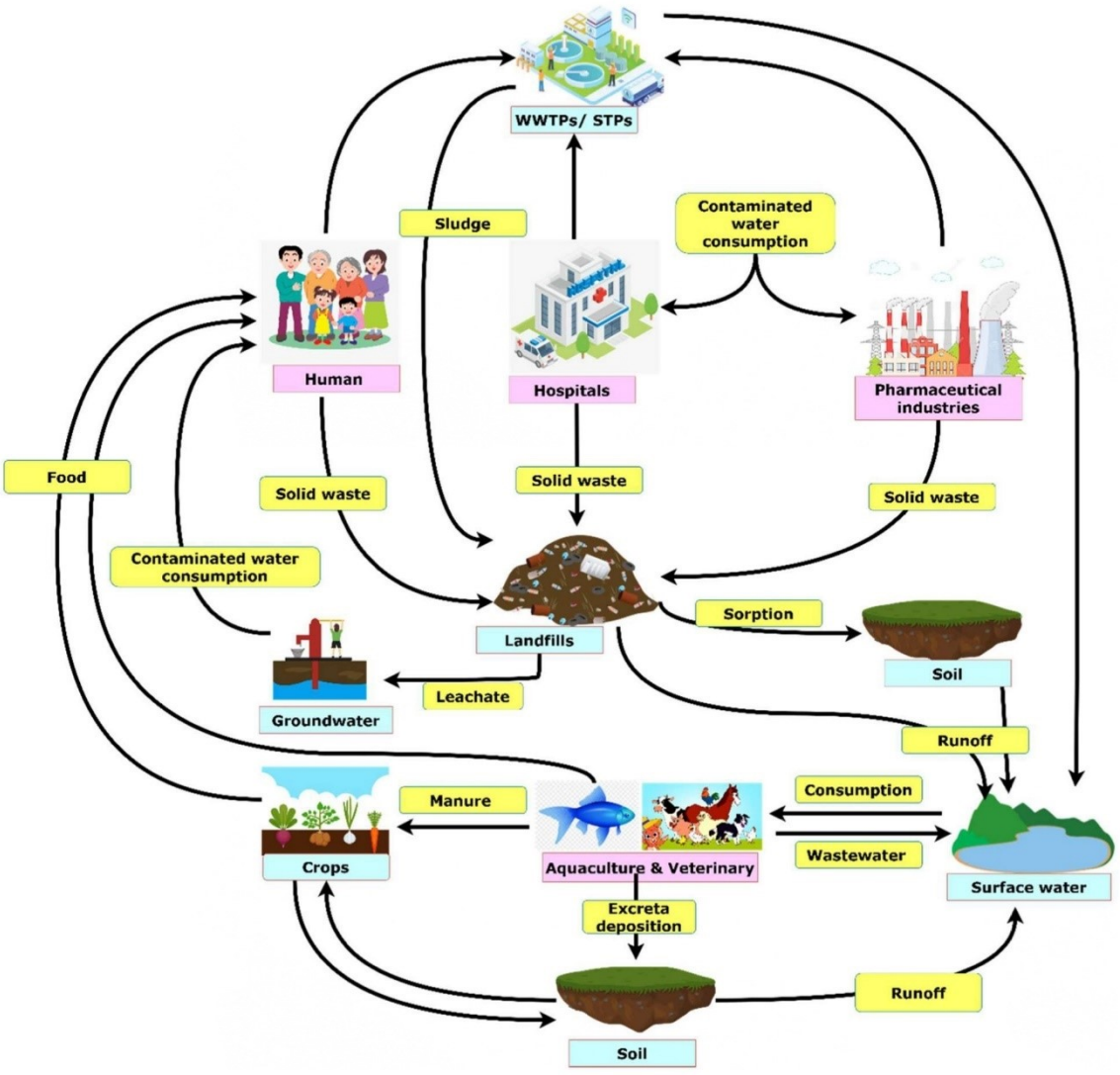

Source: Scaria, Anupama & Nidheesh (2021)

Characterized as refractory contaminants, pharmaceuticals are usually partially removed by the conventional treatment processes used in WWTPs and remain in the effluents at concentration levels of ng/L and µg/L, as micropollutants (COUTO, LANGE & AMARAL, 2019; LINDHOLM-LEHTO *et al.*, 2016; SANTOS *et al.*, 2020; SCARIA, ANUPAMA & NIDHEESH, 2021; WILKINSON *et al.*, 2022). Reis *et al.* (2019) evaluated

the presence of 28 pharmaceuticals from different classes in surface water sources and drinking water samples from six Drinking Water Treatment Plants (DWTPs) in the state of Minas Gerais in Brazil. Even after several steps of conventional treatments, 11 of the 18 pharmaceuticals detected in surface water remained in drinking water.

2.5 ANTIBIOTICS

Antibiotics are groups of pharmaceuticals that destroy or delay the growth of microorganisms and have been part of human history since the discovery of penicillin by Alexander Fleming in 1928. The development of these pharmaceuticals went through the golden age of discoveries between the 50s and 60s and nowadays faces the challenges of microbial resistance, with an increasingly smaller number of new antibiotics reaching the market (KHARDORI, STEVAUX & RIPLEY, 2019). They are extensively aimed at combating bacterial infections in human and veterinary treatments, as well as in cattle breeding (POLIANCIUC *et al.*, 2020).

The pharmacodynamics or mode of action of antibiotics is often used to divide them into classes. By interfering with the synthesis of the cell wall, proteins, nucleic acids, or folate (vitamin B9) or by disrupting the cell membrane, the antibiotics interact with microorganisms to combat infections (GALLAGHER & MACDOUGALL, 2022). The molecular structure, activity spectrum, and administration route can also be used as criteria in this classification of antibiotics. Thus, the most common classes of antibiotics are Beta-lactams, Macrolides, Tetracyclines, Quinolones, Aminoglycosides, Sulphonamides, Glycopeptides, and Oxazolidinones (ETEBU & ARIKEKPAR, 2016).

2.5.1 TETRACYCLINE

The pharmaceuticals from the tetracyclines class are yellow crystals discovered around the 40s and grouped because of their similar molecular structure and mode of action. The molecule of these antibiotics always has four fused hydrocarbon rings (A, B, C, and D) (FIGURE 2.4), which justify the suffix “cyclin” in their nomenclature. They act on the ribosome of microbial cells, inhibiting the addition of amino acids to the

polypeptide chains and, consequently, the synthesis of proteins (ETEBU & ARIKEKPAR, 2016; SCARIA, ANUPAMA & NIDHEESH, 2021).

Figure 2.4 - General molecular structure of tetracycline class

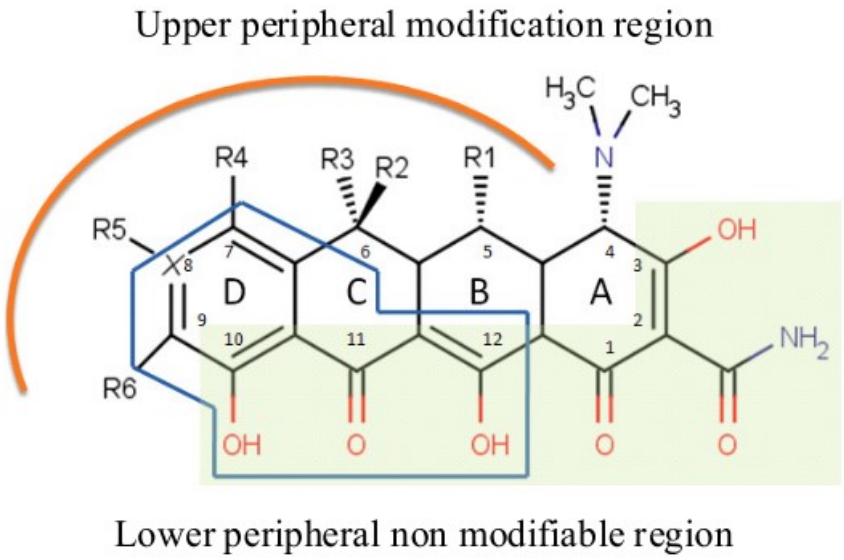

Source: Fuoco (2012)

Tetracyclines are placed among the first three classes of antibiotics produced and consumed worldwide due to their broad spectrum of activity and few side effects. They act on several Gram-positive and negative bacteria, in addition to protozoan parasites. Infectious diseases of the respiratory, digestive, and excretory systems are usually combated using this class of antibiotics (GROSSMAN, 2016; LEICHTWEIS *et al.*, 2022; SCARIA, ANUPAMA & NIDHEESH, 2021).

According to the production technique, tetracyclines with different substitutions on the upper peripheral modifiable region (FIGURE 2.4) are divided into groups. First-generation tetracyclines, such as Tetracycline, Chlortetracycline, Oxytetracycline, and Demeclocycline, are those obtained from a natural source, such as actinomycetes and streptomycetes. Antibiotics produced semi-synthetically are called second-generation tetracyclines, with Doxycycline, Limecycline, Metacycline, Minocycline, and Rolitetracycline being some examples. The Tigecycline is a tetracycline from the third-generation group, manufactured completely synthetically (ETEBU & ARIKEKPAR, 2016; GROSSMAN, 2016; SCARIA, ANUPAMA & NIDHEESH, 2021).

The Tetracycline (TC) ($C_{22}H_{24}N_2O_8$) is an antibiotic belonging to the class with the same name, in the first-generation group, and whose modifications in the general structure (FIGURE 2.4) are R_1: H, R_2: CH_3, R_3: OH and R_4: H, resulting in the molecule shown in Figure 2.5. With a polar character, strong interaction with water, and relatively stable under acidic conditions (TABLE 2.2), it is extensively used in human and veterinary treatments, as feed additives for cattle breeding (LEICHTWEIS *et al.*, 2022).

Figure 2.5 - Molecular structure of Tetracycline (TC)

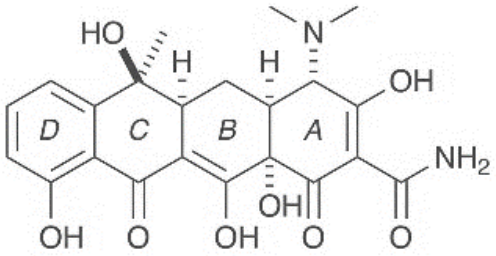

Source: Fuoco (2012)

Table 2.2 - Physicochemical properties of Tetracycline (TC)

Proprieties	Values
Molecular mass	444.4
Log k_{ow}	−1.25
pKa_1	3.3
pKa_2	7.7
pKa_3	9.7
Solubility (mg L^{-1})	231

Source: Adapted from LEICHTWEIS *et al.* (2022)

2.5.2 ENROFLOXACIN

The quinolones constitute an antibiotic class produced synthetically and discovered accidentally as a by-product of obtaining pharmaceutical chloroquine. Nalidixic acid (FIGURE 2.6) is the main example of a first-generation quinolone, also called non-fluorinated quinolone, and has the typical two fused hydrocarbon rings. This pharmaceutical is used in the clinic, administered parenterally or orally, and regarding tissue distribution, it tends to concentrate in the human excretory system, where it is used to combat infections (MILLANAO *et al.*, 2021; SANTOS *et al.*, 2021).

Figure 2.6 - Molecular structure of nalidixic acid

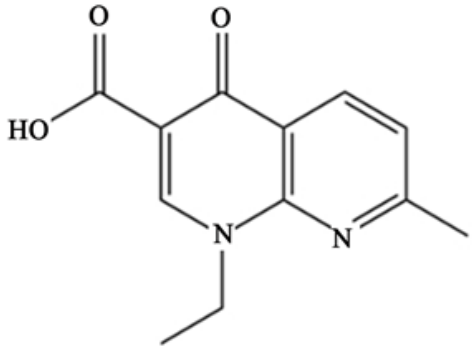

Source: Trouchon & Lefebvre (2016)

When a fluorine atom is added to nalidixic acid in position 6, we have the class of antibiotics called fluoroquinolones or second-generation quinolones (SANTOS *et al.*, 2021). Fluoroquinolones also have a broad spectrum, acting on both Gram-positive and negative bacteria. The mode of action of fluoroquinolones consists of preventing the replication and transcription of the DNA of the target bacteria by inhibiting the enzymes DNA gyrase and topoisomerase IV (BRAR *et al.*, 2020).

An example of fluoroquinolone is Enrofloxacin (ENR) ($C_{19}H_{22}FN_3O_3$), a nalidixic acid molecule added with a piperazine ring at carbon 7 and cyclopropyl at N1 (FIGURE 2.7). The ENR molecule has high lipophilicity and at pH close to neutrality, it appears in the amphoteric form (TABLE 2.3) (PEI *et al.*, 2020; TEIXIDÓ *et al.*, 2014; TROUCHON & LEFEBVRE, 2016).

Figure 2.7 - Molecular structure of Enrofloxacin (ENR)

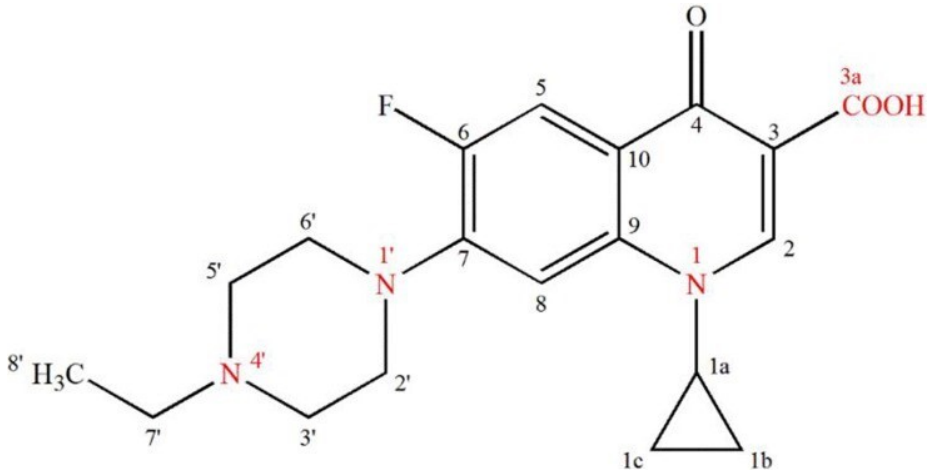

Source: Trouchon & Lefebvre (2016)

Table 2.3 - Physicochemical properties of Enrofloxacin (ENR)

Proprieties	Values
Molecular mass (g/mol)	359.4
Log k_{ow}	1.1
pKa_1	6.3
pKa_2	8.3
Solubility (g/L)	0.23

Source: Adapted from Grabowski *et al.* (2022), Pei *et al.* (2020) and Teixidó *et al.* (2014)

In 1983, ENR was synthesized, but its commercialization as an antibiotic only occurred in 1991. It is a pharmaceutical used only in veterinary medicine, mainly for the treatment of respiratory diseases caused by bacteria in cattle and pigs. However, its release for use in poultry and aquaculture has controversies associated with bacterial resistance and infectious diseases in humans, with several countries not being released for these purposes. For small animals, such as dogs and cats, ENR can treat urinary tract skin infections (GRABOWSKI *et al.*, 2022; MILLANAO *et al.*, 2021; SANTOS *et al.*, 2021).

2.6 ADSORPTION

Among the advanced treatment techniques applicable to the removal of TC, ENR, and other PhACs from aqueous matrices, such as advanced oxidative processes and membrane separation processes (ALVIM *et al.*, 2020; COUTO *et al.*, 2020; DE SOUZA *et al.*, 2018; FOUREAUX *et al.*, 2019; MANSOURI *et al.*, 2021; PHOON *et al.*, 2020; SANTOS, MEIRELES & LANGE, 2015), the adsorption has emerged as an operationally simple and efficient technology, whose performance has been evaluated by researchers in worldwide as a polishing step in wastewater treatment, commonly utilized for the removal of refractory contaminants (AGUSTIN *et al.*, 2022; ASHIQ *et al.*, 2021; DARWEESH & AHMED, 2017; DE ANDRADE *et al.*, 2018; MAGED *et al.*, 2021; MOREIRA *et al.*, 2020; NAKARMI *et al.*, 2022; PENG *et al.*, 2018; PHOON *et al.*, 2020; SEKULIC *et al.*, 2019; TAOUFIK *et al.*, 2020).

The term "sorption" refers to four transport phenomena responsible for retaining substances from one liquid or gaseous phase in another suitable phase, whether it be

solid, liquid, or gaseous. This second phase is called suitable because it must tend to attract and retain the substance dissolved in the fluid phase (METCALF & EDDY, 2014). The phenomena covered by sorption are diffusion, absorption, adsorption, and partition. As paronyms, it is important to highlight the difference between absorption and adsorption, processes that occur in different regions, in the interior and on the surface of the second phase, respectively (METCALF & EDDY, 2014; NIGRI *et al.*, 2017; WORCH, 2012).

Adsorption is a surface phenomenon described as a mass transfer unit operation, in which one or more constituents dissolved in a fluid phase are concentrated on the adsorptive surface due to the action of surface forces. The molecules, ions, or atoms retained at the adsorbent interface are called adsorbates, and the reverse operation is called desorption (FIGURE 2.8) (CAVALCANTI, 2009; MCNAUGHT & WILKINSON, 1997; MESQUITA *et al.*, 2017a; METCALF & EDDY, 2014; WORCH, 2012).

Figure 2.8 - Constituents of adsorption and desorption

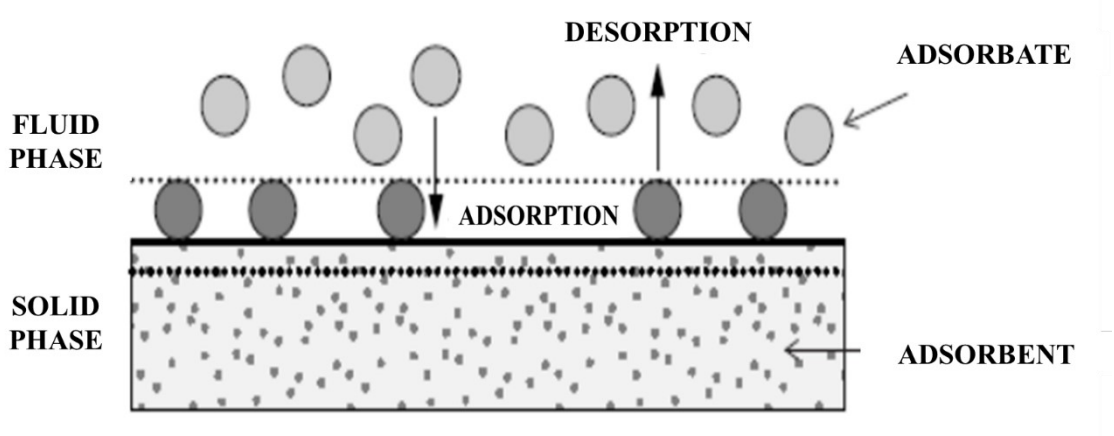

Source: Adapted from Worch (2012)

The adsorbate, adsorbent, and fluid interactions culminate in adsorption, which can be divided into three consecutive steps. The first step is external diffusion, which involves moving the adsorbate from the fluid phase's interior to the adsorbent's surface. It can be further divided into two sub-steps: diffusion from the fluid interior to the boundary layer and diffusion from the boundary layer to the adsorption on the active sites of the external adsorptive surface. Subsequently, internal diffusion of the adsorbate that remains free occurs, transferring from the external surface to the active sites in the internal region of the adsorbent. Finally, diffusion into the active sites takes place for

the adsorbate's actual adsorption on the adsorbent's internal surface (ALVES, 2017; CAVALCANTI, 2009; MESQUITA, 2016).

Factors related to the adsorbate (such as concentration, molar mass, solubility, and polarity), the fluid phase (including the presence of other substances, pH, and temperature), and the operating conditions of the system (such as pressure, stirring speed, and contact time) directly interfere with the results of adsorption (CAVALCANTI, 2009; CRUZ *et al.*, 2019; MESQUITA *et al.*, 2017a; MESQUITA *et al.*, 2017b; NIGRI *et al.*, 2017).

Adsorption can occur either physically or chemically, and the term sorption is often used when it is not possible to distinguish between these two types of adsorption (CAVALCANTI, 2009). In physisorption, or Van der Waals adsorption, there is no transfer of electrons between the adsorbate and the surface groups of the adsorbent. In this case, adsorption occurs due to weak electrostatic interactions, with intermolecular forces greater than intramolecular forces. It is a spontaneous, exothermic process and generally reversible, with the possibility of forming multiple layers, and the adsorption force tends to decrease (CAVALCANTI, 2009; DE GISI *et al.* 2016a; NIGRI *et al.*, 2017). Chemical adsorption, also called chemisorption, is characterized by the sharing of electrons between the adsorbate and the molecules on the surface of the adsorbent, forming covalent bonds. This type of adsorption is strong, often irreversible, and forms a single layer of adsorbates, with an increase in coverage associated with a decrease in the adsorption force (CAVALCANTI, 2009; DE GISI *et al.*, 2016a).

The adsorption operation can occur in batch or continuous mode. In batch mode, there is no mass crossing the system boundaries, meaning that the adsorbent and adsorbate are kept in contact without a variation in the volume of the fluid phase over time. This mode of operation is limited to small volumes but is useful for a preliminary assessment of parameters such as pH, contact time, and adsorbent dosage (CAVALCANTI, 2009; LARGITTE & PASQUIER, 2016; MESQUITA *et al.*, 2017a; NIGRI *et al.*, 2017; QIU *et al.*, 2009).

Continuous operation occurs in a non-stationary state, with the volume of the fluid phase in contact with the adsorbent varying over time. In continuous mode, mass

transfer resistance and the contact time between adsorbate and adsorbent are crucial. The breakthrough curve of the system can be constructed, and dynamic parameters of the process, such as the adsorptive capacity of the bed and efficiency, can be calculated (CAVALCANTI, 2009; MESQUITA *et al.*, 2017b; XAVIER *et al.*, 2018).

Adsorption has emerged as a simple, efficient, and economical technology for industrial separation and water and wastewater treatment processes. It is applicable for gas dehydration, bleaching, fluid fractionation, deodorization, and removal of organic and inorganic contaminants from effluents, among others. The separation of constituents by adsorption occurs through three distinct mechanisms. The pores of the adsorbents, with varying sizes, allow the separation of molecules through steric mechanisms. The selectivity of the adsorbent separates substances using equilibrium mechanisms. Finally, the nature of the adsorbate is involved in the kinetic separation mechanism, and species are separated based on differences in diffusivity (CAVALCANTI, 2009; LARGITTE & PASQUIER, 2016; MESQUITA, 2016; ALVES, 2017). In the treatment of water and wastewater, adsorption is generally a polishing step used for the removal of refractory contaminants that persist after biological treatment. Trihalomethanes, nitrogen, sulfides, dyes, and toxic metals are examples of compounds removable by adsorption, and their processes are increasingly being discussed (CAVALCANTI, 2009; METCALF & EDDY, 2014; DE GISI *et al.*, 2016a; MESQUITA, 2016).

2.7 ADSORBENTS

Solid adsorbents are primarily porous materials because the pores, with specific shapes and sizes, allow the adsorbate to access the internal surface with active sites available for adsorption (ALCANTARA, IZIDORO & FUNGARO, 2015; METCALF & EDDY, 2014; NIGRI *et al.*, 2017). In addition to factors related to the adsorbate, fluid phase, and system operating mode, the characteristics of the adsorbents typically determine the efficiency of adsorption (ALVES, 2017).

The porosity of an adsorbent contributes positively to another important condition, a high surface area. The combination of a high surface area and pores of sufficient

dimensions gives the adsorbent good adsorption kinetics and adsorptive capacity. The tendency of the adsorbent to attract and retain dissolved substances, known as solute affinity, should also be considered when choosing the adsorbent to favor high efficiency. Together, porosity, surface area, and affinity are the most important factors in selecting the adsorbent material. However, other properties such as selectivity, mechanical and chemical resistance, regenerative capacity, durability, and low cost are also desirable. In this way, the adsorption of specific solutes is ensured, along with satisfactory tolerance to handling, the possibility of reusing the adsorbent, and a good cost-benefit ratio (ALCANTARA, IZIDORO & FUNGARO, 2015; CAVALCANTI, 2009; MESQUITA *et al.*, 2017a; METCALF & EDDY, 2014).

Activated carbon, alumina, silica gel, polymers, clays, and zeolites stand out among the most common adsorbents. Activated carbon is the generic term used to designate materials with a high carbon content transformed into char (ALVES, 2017; QIU *et al.*, 2009). They are the most well-known and widely used adsorbents in the industry due to their unparalleled adsorptive capacity associated with their high internal surface area, which ranges between 500 and 1500 m^2/g (ALVES, 2017; DE GISI *et al.*, 2016a). Activated carbons are produced through a combination of pyrolysis and activation processes, with commonly used raw materials being of plant origin. However, materials of animal and mineral origin are also possibilities (ALVES, 2017; QIU *et al.*, 2009). Activated carbons are marketed in granular (GAC) and powdered (PAC) forms, recommended for continuous and batch processes, respectively (CAVALCANTI, 2009; MESQUITA, 2016).

During adsorption, the pores of activated carbon are occupied by the adsorbate and become saturated. After the depletion of these pores, activated carbon loses its applicability as an adsorbent and needs to be regenerated or appropriately disposed of and replaced. The cost of replacing the adsorbent is a drawback for large-scale adsorption processes (CAVALCANTI, 2009; CAZETTA *et al.*, 2013; COSTA *et al.*, 2020; METCALF & EDDY, 2014; ZANELLA, TESSARO & FÉRIS, 2014).

In recent years, various studies on alternative adsorbent materials, especially as a replacement for conventional activated carbon, have been published with the aim of cost reduction, increased selectivity, enhanced regeneration capacity, and as an

alternative for the final disposal of waste/by-products from other activities, as exemplified in the Chart 2.1 (DE GISI *et al.*, 2016b).

Chart 2.1 – Some studies on alternative adsorbents to conventional activated carbon published between 2016 and 2021

Raw Material	Objectives	References
Soybean husk	Use of soybean husk as an adsorbent for the removal of industrial textile dyes Reactive Blue 21 and Reactive Yellow 145.	Giordano *et al.* (2021)
Mollusk shell	Testing the use of shells from the mollusk *Mytella falcata*, both raw and pyrolyzed, for the removal of the antibiotic rifampicin from water.	Henrique *et al.* (2020)
Coffee grounds	Evaluation of the applicability of coffee grounds as an adsorbent for the removal of cadmium from aqueous solutions.	Kim & Kim (2020)
Fish scales	Utilization of modified scales from *Sardinella brasiliensis* as an adsorbent for the removal of dyes from textile effluents.	Niero *et al.* (2019)
Sisal fibers	Use of sisal fibers as an adsorbent material to remove methylene blue and Reactive Black 5 dyes from aqueous solutions.	Vargas *et al.* (2019)
Eggshells	Study of the removal efficiency and adsorption capacity of phosphorus by eggshell adsorbents, including salted eggshell and common eggshell, in effluents with low phosphorus content.	Yirong & Vaurs (2019)
Pumice stone	Evaluation of the performance of natural pumice stone for the removal of aluminum from groundwater through a fixed-bed column.	Indah, Helard & Hudawaty (2018)
Parsley, coriander, and chicory	Observation of the use of adsorbents prepared from three selected plants of the Apiaceae family to remove lead from aqueous solutions.	Boontham & Babel (2017)
Papaya, corn cob, soybean oil cake, banana peel, walnut shell, among others	Critical examination of the removal of toxic metals from wastewater by low-cost agricultural residues as adsorbents.	Habineza *et al.* (2017)
Red mud	Use of raw red mud and red mud modified with hydrochloric acid as adsorbents for the removal of chromium, copper, and lead from aqueous solution.	Tsamo *et al.* (2017)
Pecan nutshell	Preparation, characterization, and application of biochar derived from pecan nutshell as an adsorbent for the removal of Reactive Red 141 dye.	Zazycki *et al.* (2017)
Residual aluminum sulfate and ferric sulfate, and fine and coarse concrete	Evaluation of the long-term performance of low-cost adsorbents in the removal of phosphorus from large-scale adsorption filters.	Callery *et al.* (2016)

Source: The author herself

A variety of raw materials, ranging from agricultural, household, and industrial by-products, such as pecan nut shells, corn cobs, soybean husks, and coffee grounds, to

sludges and marine and soil materials, such as red mud, fish scales, mollusk shells, concrete, and pumice stone, have been studied (DE GISI *et al.*, 2016b).

2.8 ACTIVATED CARBON CHARACTERIZATION TECHNIQUES

Physical-chemical characterization of activated carbon provides information that aids in the selection of the adsorbent material and in understanding the adsorption mechanisms to which it will be subjected. It is known that surface area, porosity, and affinity for the adsorbate are important characteristics of an adsorbent. These and other properties of activated carbons are often analyzed when the goal is their application as an adsorbent (ALCANTARA, IZIDORO & FUNGARO, 2015; CAVALCANTI, 2009; MESQUITA *et al.*, 2017; METCALF & EDDY, 2014).

- *Surface Area and Porosity*

A high surface area combined with pores of sufficient dimensions provides activated carbon with good adsorption kinetics and adsorptive capacity (CAVALCANTI, 2009; METCALF & EDDY, 2014). The multiple-point methodology, proposed by Brunauer, Emmett, and Teller, and hence known as BET, is a mathematical theory aimed at describing the adsorption process and, consequently, enabling the determination of specific surface area. The procedure for analyzing the surface area by the BET method involves determining the volume of inert gas, usually nitrogen, physically adsorbed on the sample's surface using an automatic analyzer containing a thermal conductivity detector and a potentiometric recorder (BRUNAUER, EMMETT & TELLER, 1938). The analysis proposed by Barrett-Joyner-Halenda, known as BJH, is used to determine pore volume and meso- and micropore distribution. Applying the modified Kelvin equation, BJH relates the amount of adsorbate removed from the adsorbent pores with the decrease in relative pressure to the pore size (BARRETT, JOYNER & HALENDA, 1951).

- *Iodine Number*

The adsorption capacity of iodine from an aqueous solution, given in terms of iodine number is used as a relative indicator of the porosity of activated carbon and can be a non-generalized approximation of its surface area and values obtained by the BET method. Due to its diameter smaller than 2 nm, iodine molecules can access the

micropores of activated carbon, and its adsorption can predict the distribution of micropores in activated carbon. The iodine number is given by the amount of iodine adsorbed per gram of powdered activated carbon (mg/g) (ABNT, 1991a; ASTM, 1994).

- *Surface Groups*

Surface groups are the functional groups present on the surface of a substance and, in the case of activated carbon used as an adsorbent, can influence its affinity for the adsorbate. The presence of these surface groups can be detected by applying Fourier-transform infrared spectroscopy (FTIR), a technique that assesses the interaction of samples with infrared radiation. At different frequencies, the molecular structure of the sample undergoes vibrations when absorbing part of the radiation. Thus, based on the transmitted radiation at a specific frequency, it is possible to identify the functional groups present in the analyzed material (O'REILLY & MOSHER; 1983; ŢUCUREANU, MATEI & AVRAM, 2016).

- *pH of zero point of charge*

The pH of zero point of charge (pH_{ZPC}) is the pH value at which the surface of the material has a neutral charge, that is, it is the balance point of the charges present on the surface. In pH_{ZPC}, the surface of the activated carbon acts as a buffer and this is another characteristic that may influence its affinity for the adsorbate, which may help in the correct choice of adsorbent (FIOL & VILLAESCUSA, 2008; KOSMULSKI, 2011).

- *Crystalline Structures*

The analysis of the crystal structures of activated carbon allows the characterization of the material as crystalline or amorphous. X-ray diffraction (XRD) is the technique applied to analyze the crystal structures of materials and involves the incidence of X-rays on the sample, followed by the diffraction of these rays depending on the crystallinity of the material (IWASHITA *et al.*, 2004; LIMA, 2006; NAPOLITANO *et al.*, 2007).

- *Particle size*

As a relevant factor in the efficiency of the adsorption process, the particle size of activated carbon directly influences its contact with the adsorbate. The analysis of the

distribution of carbon particles according to their size can be performed through sieve granulometry. Using sieves with different openings, defined as mesh numbers and standardized internationally, the carbon sample is classified in sizes inversely proportional to the mesh numbers of the sieves (CORREIA & COUTO, 2018).

- *Morphology*

Information regarding the morphology of activated carbon particles can be obtained through the scanning electron microscopy (SEM) technique. The principle of the SEM microscope involves the interaction of a small-diameter, monochromatic electron beam with the surface of the material under vacuum conditions, making microscopic information of the sample visible to the human eye at magnifications of up to 300,000 times (DEDAVID, GOMES & MACHADO, 2007; VERNON-PARRY, 2000; ZHOU *et al.*, 2006).

When energy-dispersive X-ray spectroscopy (EDS or EDX) is coupled with scanning electron microscopy, forming the system known as SEM/EDS, it is possible to perform a semi-quantitative chemical analysis of the material, restricted to the surface of the particles, thus providing an estimate of the concentration of the present chemical elements (MESQUITA, 2016; SAMPAIO, 2010; VIEIRA *et al.*, 2021).

- *Bulk Density*

Commonly used in fluid characterization, bulk density or apparent specific mass applied to activated carbon can be inversely related to its porosity. In the case of activated carbon applications in continuous adsorption beds, bulk density is associated with the mass of the adsorbent and the bed volume (WORCH, 2012). The determination of bulk density can be performed in the laboratory according to technical standards such as NBR 12076/1991 - Powdered activated carbon: determination of bulk density (ABNT,1991b).

- *Moisture Content*

The moisture content of activated carbon is essentially the amount of water present in the material. This property is critical when it comes to the use of activated carbon as an adsorbent, as water can occupy the pores of the material and impair the efficiency

of adsorption. The technical standard NBR 12077/1991 - Powdered activated carbon: determination of moisture content from the Brazilian Association of Technical Standards is an example of a procedure for determining the moisture content of activated carbons in the laboratory using an oven and analytical balance (ABNT, 1991c).

- *Volatile Materials Content*

Volatile materials constitute the mass fraction of the material subject to volatilization under heating. It is expected that the volatile materials content of activated carbon produced via pyrolysis is minimal, as the raw material of the carbon has been previously subjected to high temperatures, and these volatile compounds have been expelled. The technical standard NBR 16587/2017 - Determination of volatile materials content from the Brazilian Association of Technical Standards proposes the use of a muffle furnace and analytical balance for the determination of volatile materials content in carbon (ABNT, 2017a).

- *Ash Content*

Ash is the inorganic compound remaining from the burning of the material at high temperatures, between 500 and 700 °C. In the laboratory, the ash content of activated carbon can be obtained by following procedures described in technical standards, such as NBR 16586/2017 - Test method for determining ash content from the Brazilian Association of Technical Standards, in which organic compounds undergo combustion in a muffle furnace, and inorganic compounds are oxidized (ABNT, 2017b).

- *Fixed Carbon Content*

In contrast to moisture and volatile materials, fixed carbon is not expelled from the material upon heating in an inert atmosphere, as in pyrolysis. Quantifying the carbon content of activated carbon is simple and is based on the difference between the total mass and the sum of the masses relating to moisture, volatile materials, and ash in a sample.

- *Mass Loss as a Function of Temperature*

The variation in the mass of a material as a function of temperature is directly related to its thermal stability. The thermogram, a graph consisting of the mass loss of the material as a function of temperature and the derivative of this variation, obtained from thermogravimetric analysis (TGA) of the sample under an inert atmosphere, makes it possible to evaluate the thermal degradation process of activated carbon, as well as validate the moisture, volatile materials, and fixed carbon contents obtained from bench tests. Replacing the inert gas in the final stage of TGA with oxygen allows the combustion of the sample and, thus, the ash content of the activated carbon can also be determined (DENARI & CAVALHEIRO, 2012).

REFERENCES

ABNT. *NBR 12073/1991 – Carvão ativado pulverizado: Determinação do número de iodo.* Associação Brasileira de Normas Técnicas, Rio de Janeiro, 1991a.

ABNT. *NBR 12076/1991 – Carvão ativado pulverizado: Determinação da massa especifica aparente*. Associação Brasileira de Normas Técnicas, Rio de Janeiro, 1991b.

ABNT. *NBR 12077/1991 – Carvão ativado pulverizado: Determinação da umidade*. Associação Brasileira de Normas Técnicas, Rio de Janeiro, 1991c.

ABNT. *NBR 16586/2017 – Carvão mineral: Método de ensaio para determinação do teor de cinzas*. Associação Brasileira de Normas Técnicas, Rio de Janeiro, 2017b.

ABNT. *NBR 16587/2017 – Carvão mineral: Determinação do teor de materiais voláteis*. Associação Brasileira de Normas Técnicas, Rio de Janeiro, 2017a.

ABREU, F. G. *Análise de polifluoreto de vinilideno (PVDF) sob carregamento cíclico.* Dissertação (Mestrado) - Engenharia Metalúrgica e de Materiais, Universidade Federal do Rio de Janeiro, Rio de Janeiro, 2012.

AGUSTIN, M. B.; MIKKONEN, K. S.; KEMELL, M.; LAHTINEN, P.; LEHTONEN, M. Systematic investigation of the adsorption potential of lignin-and cellulose-based nanomaterials towards pharmaceuticals. *Environmental Science: Nano*, 2022.

AHMAD, T.; GURIA, C.; MANDAL, A. A review of oily wastewater treatment using ultrafiltration membrane: A parametric study to enhance the membrane performance. *Journal of Water Process Engineering*, v. 36, p. 101289, 2020.

AHSAINE, H. A.; ZBAIR, M.; EL HAOUTI, R. Mesoporous treated sewage sludge as outstanding low-cost adsorbent for cadmium removal. *Desalination and Water Treatment*, v. 85, p. 330-338, 2017.

AKCELRUD, L. *Fundamentos da ciência dos polímeros.* Editora Manole Ltda, São Paulo, 2007.

ALCANTARA, R. R.; IZIDORO, J. C.; FUNGARO, D. A. *Adsorção do corante Rodamina B de solução aquosa sobre zeólita de cinzas pesadas de carvão modificada por surfactante.* In: 5º Workshop Internacional | Avanços em Produção Mais Limpa, 20 a 22 de maio, São Paulo, 2015.

ALCHIKH, M.; FOND, C.; FRÈRE, Y. Discontinuous crack growth in poly (vinyl fluoride) by mechanochemical ageing in sodium hydroxide. *Polymer Degradation and Stability*, v. 95, n. 4, p. 440-444, 2010.

ALIAKBARI, Z.; YOUNESI, H.; GHOREYSHI, A. A.; BAHRAMIFAR, N.; HEIDARI, A. Production and characterization of sewage-sludge based activated carbons under different post-activation conditions. *Waste and Biomass Valorization*, v. 9, n. 3, p. 451-463, 2017.

ALMAJED, A.; AHMAD, M.; USMAN, A. R.; AL-WABEL, M. I. Fabrication of sand-based novel adsorbents embedded with biochar or binding agents via calcite precipitation for sulfathiazole scavenging. *Journal of Hazardous Materials,* v. 405, p. 124249, 2021.

ALVES A. P. *Purificação de glicerol usando diferentes adsorventes: análise técnica e termodinâmica.* Dissertação (Mestrado) - Engenharia Química, Universidade Federal Rural do Rio de Janeiro, Seropédica, 2017.

ALVIM, C. B.; MOREIRA, V. R.; LEBRON, Y. A. R.; SANTOS, A. V.; LANGE, L. C.; MOREIRA, R. P.; SANTOS, L. V. S.; AMARAL, M. C. S. Comparison of UV, UV/H_2O_2 and ozonation processes for the treatment of membrane distillation concentrate from surface water treatment: PhACs removal and environmental and human health risk assessment. *Chemical Engineering Journal*, v. 397, p. 125482, 2020.

ASHIQ, A.; VITHANAGE, M.; SARKAR, B.; KUMAR, M.; BHATNAGAR, A.; KHAN, E.; XI, F.; OK, Y. S. Carbon-based adsorbents for fluoroquinolone removal from water and wastewater: a critical review. *Environmental Research*, v. 197, p. 111091, 2021.

ASTM. *ASTM D4607-94 - Standard test method for determination of iodine number of activated carbon.* American Society for Testing and Materials, 1994.

BARBOSA, I. M. *Avaliação do uso de membranas de ultrafiltração modificadas com nanopartículas de argila para tratamento de esgotos*. Tese (Doutorado) - Engenharia Civil, Universidade de São Paulo, São Paulo, 2017.

BARRETT, E. P.; JOYNER, L. G.; HALENDA, P. P. The determination of pore volume and area distributions in porous substances. I. Computations from nitrogen isotherms. *Journal of the American Chemical Society*, v. 73, n. 1, p. 373-380, 1951.

BBC RESEARCH & DEVELOPMENT. *Membrane Bioreactors: Global Markets.* BBC Research & Development, Londres, 2022a. Disponível em: <https://www.bccresearch.com/market-research/membrane-and-separation-technology/membrane-bioreactors.html>. Acesso em: 07 junho 2022.

BBC RESEARCH & DEVELOPMENT. *Ultrafiltration Membranes: Technologies and Global Markets.* BBC Research & Development, Londres, 2022b. Disponível em: <https://www.bccresearch.com/market-research/membrane-and-separation-technology/ultrafiltration-membranes-techs-markets-report.html>. Acesso em: 07 junho 2022.

BÖGER, B.; SUREK, M.; DE O VILHENA, R.; FACHI, M. M.; JUNKERT, A. M.; SANTOS, J. M.; DOMINGOS, E. L.; COBRE, A. F.; MOMADE, D. R.; PONTAROLO, R. Occurrence of antibiotics and antibiotic resistant bacteria in subtropical urban rivers in Brazil. *Journal of Hazardous Materials*, v. 402, p. 123448, 2021.

BOONTHAM, W.; BABEL, S. *Apiaceae family plants as low-cost adsorbents for the removal of lead ion from water environment.* In: IOP Conference Series: Materials Science and Engineering, junho, IOP Publishing, 2017.

BRAR, R. K.; JYOTI, U.; PATIL, R. K.; PATIL, H. C. Fluoroquinolone antibiotics: An overview. *Adesh University Journal of Medical Sciences & Research*, v. 2, n. 1, p. 26-30, 2020.

BRUNAUER, S.; EMMETT, P. H.; TELLER, E. Adsorption of gases in multimolecular layers. *Journal of the American Chemical Society*, v. 60, n. 2, p. 309-319, 1938.

CALLERY, O.; HEALY, M. G.; ROGNARD, F.; BARTHELEMY, L.; BRENNAN, R. B. Evaluating the long-term performance of low-cost adsorbents using small-scale adsorption column experiments. *Water Research*, v. 101, p. 429-440, 2016.

CALLISTER, W. *Ciência e Engenharia de Materiais: Uma Introdução*. 7 ed., Editora LTC, Rio de Janeiro, 2008.

CAMMAROTA, M. C. *Biotecnologia Ambiental*. Universidade Federal do Rio de Janeiro - Escola de Química, Rio de Janeiro, 2013.

CANEVAROLO JR.; SEBASTIÃO V. *Ciência dos polímeros: um texto básico para tecnólogos e engenheiros.* 3 ed., Artliber Editora, São Paulo, 2010.

CAPITÃO, R. C. *Estudo morfológico do PVDF e de blendas PVDF/P (VDF-TrFE).* Tese (Doutorado) - Universidade de São Paulo, São Paulo, 2002.

CAVALCANTI J. E. W. A. *Manual de Tratamento de Efluentes Industriais*. 3 ed., [s.l.], Engenho Editora Técnica Ltda, São Paulo, 2009.

CAZETTA, A. L.; JUNIOR, O. P.; VARGAS, A. M.; DA SILVA, A. P.; ZOU, X.; ASEFA, T.; ALMEIDA, V. C. Thermal regeneration study of high surface area activated carbon obtained from coconut shell: Characterization and application of response surface methodology. *Journal of Analytical and Applied Pyrolysis*, v. 101, p. 53-60, 2013.

CHEN, T.; YAN, B.; XU, D. M.; LI, L. L. Enhanced adsorption performance of methylene blue from aqueous solutions onto modified adsorbents prepared from sewage sludge. *Water Science and Technology*, v. 78, n. 4, p. 803-813, 2018.

COOK, M. A.; WRIGHT, G. D. The past, present, and future of antibiotics. *Science Translational Medicine*, v. 14, n. 657, p. eabo7793, 2022.

CORDEIRO, R. P. *Avaliação do processamento de PVDF homopolímero via moldagem por compressão para diferentes condições de resfriamento.* Trabalho de Conclusão de Curso (Engenharia de Materiais), Universidade Federal do Rio de Janeiro, Rio de Janeiro, 2010.

CORREIA, J. C. G.; COUTO, H. J. B. Classificação e peneiramento. In: *Tratamento de minérios*, 6 ed., CETEM/MCT, p. 223-272, Rio de Janeiro, 2018.

COSTA, L. R. C.; RIBEIRO, L. M.; HIDALGO, G. E. N.; FÉRIS, L. A. Evaluation of efficiency and capacity of thermal, chemical and ultrasonic regeneration of tetracycline exhausted activated carbon. *Environmental Technology*, v. 43, n. 6, p. 907-917, 2020.

COUTO, C. F.; LANGE, L. C.; AMARAL, M. C. Occurrence, fate and removal of pharmaceutically active compounds (PhACs) in water and wastewater treatment plants - A review. *Journal of Water Process Engineering*, v. 32, p. 100927, 2019.

COUTO, C. F.; SANTOS, A. V.; AMARAL, M. C. S.; LANGE, L. C.; DE ANDRADE, L. H.; FOUREAUX, A. F. S.; FERNANDES, B. S. Assessing potential of nanofiltration, reverse osmosis and membrane distillation drinking water treatment for pharmaceutically active compounds (PhACs) removal. *Journal of Water Process Engineering*, v. 33, p. 101029, 2020.

CRUZ, M. A. P.; GUIMARÃES, L. C. M.; DA COSTA JÚNIOR, E. F.; ROCHA, S. D. F.; MESQUITA, P. D. L. Adsorption of crystal violet from aqueous solution in continuous flow system using bone char. *Chemical Engineering Communications*, v. 207, n. 3, p. 372-381, 2019.

DARWEESH, T. M.; AHMED, M. J. Adsorption of ciprofloxacin and norfloxacin from aqueous solution onto granular activated carbon in fixed bed column. *Ecotoxicology and Environmental Safety*, v. 138, p. 139-145, 2017.

DE ANDRADE, J. R.; OLIVEIRA, M. F.; DA SILVA, M. G.; VIEIRA, M. G. Adsorption of pharmaceuticals from water and wastewater using nonconventional low-cost

materials: a review. *Industrial & Engineering Chemistry Research,* v. 57, n. 9, p. 3103-3127, 2018.

DE GISI, S.; LOFRANO, G.; GRASSI, M.; NOTARNICOLA, M. An overview of low-cost adsorbents for wastewater treatment. *Sustainable Materials and Technologies*, v. 9, p. 10, 2016b.

DE GISI, S.; LOFRANO, G.; GRASSI, M.; NOTARNICOLA, M. Characteristics and adsorption capacities of low-cost sorbents for wastewater treatment: a review. *Sustainable Materials and Technologies*, v. 9, p. 10-40, 2016a.

DE SOUZA, D. I.; DOTTEIN, E. M.; GIACOBBO, A.; RODRIGUES, M. A. S.; DE PINHO, M. N.; BERNARDES, A. M. Nanofiltration for the removal of norfloxacin from pharmaceutical effluent. *Journal of Environmental Chemical Engineering*, v. 6, n. 5, p. 6147-6153, 2018.

DEDAVID, B. A.; GOMES, C. I.; MACHADO, G. *Microscopia eletrônica de varredura: aplicações e preparação de amostras: materiais poliméricos, metálicos e semicondutores.* EdiPUCRS, Porto Alegre, 2007.

DENARI, G. B.; CAVALHEIRO, É. T. G. *Princípios e aplicações de análise térmica.* Material de Apoio – Instituto de Química de São Carlos, Universidade de São Paulo, São Carlos, 2012.

DOS REIS, G. S.; BIN MAHBUB, M. K.; WILHELM, M.; LIMA, E. C.; SAMPAIO, C. H.; SAUCIER, C.; PEREIRA DIAS, S. L. Activated carbon from sewage sludge for removal of sodium diclofenac and nimesulide from aqueous solutions. *Korean Journal of Chemical Engineering*, v. 33, n. 11, p. 3149-3161, 2016.

DOS SANTOS, C. R.; ARCANJO, G. S.; DE SOUZA SANTOS, L. V.; KOCH, K.; AMARAL, M. C. S. Aquatic concentration and risk assessment of pharmaceutically active compounds in the environment. *Environmental Pollution*, v. 290, p. 118049, 2021.

DROBNY, J. G. *Technology of fluoropolymers.* 2 ed., CRC Press, Boca Raton, 2009.

EL MOUHRI, G.; MERZOUKI, M.; BELHASSAN, H.; MIYAH, Y.; AMAKDOUF, H.; ELMOUNTASSIR, R.; LAHRICHI, A. Continuous adsorption modeling and fixed bed column studies: adsorption of tannery wastewater pollutants using beach sand. *Journal of Chemistry*, v. 2020, 2020.

ERSAHIN, M. E.; OZGUN, H.; DERELI, R. K.; OZTURK, I.; ROEST, K.; VAN LIER, J. B. A review on dynamic membrane filtration: materials, applications and future perspectives. *Bioresource Technology*, v. 122, p. 196-206, 2012.

ESTERLY, D. M. *Manufacturing of Poly (vinylidene fluoride) and evaluation of its mechanical properties.* Dissertação (Mestrado) - Ciência e Engenharia de Materiais, Virginia Polytechnic Institute and State University, Blacksburg, 2002.

ETEBU, E.; ARIKEKPAR, I. Antibiotics: Classification and mechanisms of action with emphasis on molecular perspectives. *Int. J. Appl. Microbiol. Biotechnol. Res*, v. 4, n. 2016, p. 90-101, 2016.

FAN, S.; LI, H.; WANG, Y.; WANG, Z.; TANG, J.; TANG, J.; LI, X. Cadmium removal from aqueous solution by biochar obtained by co-pyrolysis of sewage sludge with tea waste. *Research on Chemical Intermediates*, v. 44, n. 1, p. 135-154, 2017a.

FAN, S.; WANG, Y.; WANG, Z.; TANG, J.; TANG, J.; LI, X. Removal of methylene blue from aqueous solution by sewage sludge-derived biochar: Adsorption kinetics, equilibrium, thermodynamics and mechanism. *Journal of Environmental Chemical Engineering*, v. 5, n. 1, p. 601-611, 2017b.

FERRENTINO, R.; CECCATO, R.; MARCHETTI, V.; ANDREOTTOLA, G.; FIORI, L. Sewage sludge hydrochar: an option for removal of methylene blue from wastewater. *Applied Sciences*, v. 10, n. 10, p. 3445, 2020.

FIOL, N.; VILLAESCUSA, I. Determination of sorbent point zero charge: usefulness in sorption studies. *Environmental Chemistry Letters*, v. 7, n. 1, p. 79-84, 2009.

FOUREAUX, A. F. S.; REIS, E. O.; LEBRON, Y.; MOREIRA, V.; SANTOS, L. V.; AMARAL, M. S.; LANGE, L. C. Rejection of pharmaceutical compounds from surface water by nanofiltration and reverse osmosis. *Separation and Purification Technology*, v. 212, p. 171-179, 2019.

FREIRE, E. *Estudo de misturas de poli (fluoreto de vinilideno)/poli (metacrilato de metila) processadas em condições de baixo e alto cisalhamento.* Tese (Doutorado) - Programa de Pós-graduação em Engenharia de Minas, Metalúrgica e de Materiais, Universidade Federal do Rio Grande do Sul, Porto Alegre, 2007.

FUOCO, D. Classification framework and chemical biology of tetracycline-structure-based drugs. *Antibiotics*, v. 1, n. 1, p. 1, 2012.

GALLAGHER, J. C.; MACDOUGALL, C. *Antibiotics simplified*. Jones & Bartlett Learning, 2022.

GALVÃO, D. F.; GOMES, E. R. S. Os processos de separação por membranas e sua utilizaão no tratamento de efluentes industriais da indústria de laticínios: revisão bibliográfica. *Revista do Instituto de Laticínios Cândido Tostes*, v. 70, n. 6, p. 349-360, 2015.

GIORDANO, E. D. V.; BRASSESCO, M. E.; CAMISCIA, P., PICÓ; G. A.; VALETTI, N. W. A new alternative and efficient low-cost process for the removal of reactive dyes in textile wastewater by using soybean hull as adsorbent. *Water, Air, & Soil Pollution*, v. 232, n. 5, p. 1-25, 2021.

GRABOWSKI, Ł.; GAFFKE, L.; PIERZYNOWSKA, K.; CYSKE, Z.; CHOSZCZ, M.; WĘGRZYN, G.; WĘGRZYN, A. Enrofloxacin - the ruthless killer of eukaryotic cells or the last hope in the fight against bacterial infections?. *International Journal of Molecular Sciences*, v. 23, n. 7, p. 3648, 2022.

GROSSMAN, T. H. Tetracycline antibiotics and resistance. *Cold Spring Harbor Perspectives in Medicine*, v. 6, n. 4, 2016.

GUO, T.; YAO, S.; CHEN, H.; YU, X.; WANG, M.; CHEN, Y. Characteristics and adsorption study of the activated carbon derived from municipal sewage sludge. *Water Science and Technology*, v. 76, n. 7, p. 1697-1705, 2017.

HABERT, A. C.; BORGES, C. P.; NOBREGA, R. *Processos de separação por membranas*. Editora E-papers, Rio de Janeiro, 2006.

HABINEZA, A.; ZHAI, J.; NTAKIRUTIMANA, T.; QIU, F.; LI, X.; WANG, Q.. Heavy metal removal from wastewaters by agricultural waste low-cost adsorbents: hindrances of adsorption technology to the large scale industrial application-a review. *Desalination and Water Treatment*, v. 78, p. 192-214, 2017.

HAI, F. I.; YAMAMOTO, K.; LEE, C. H. *Membrane biological reactors: theory, modeling, design, management and applications to wastewater reuse.* IWA Publishing, Londres, 2014.

HARPER, C. A. *Modern plastics handbook.* McGraw-Hill Education, Hightstown, 2000.

HENRIQUE, D. C.; QUINTELA, D. U.; IDE, A. H.; ERTO, A.; DA SILVA DUARTE, J. L.; MEILI, L. Calcined *Mytella falcata* shells as alternative adsorbent for efficient removal of rifampicin antibiotic from aqueous solutions. *Journal of Environmental Chemical Engineering*, v. 8, n. 3, p. 103782, 2020.

IFTHIKAR, J.; WANG, J.; WANG, Q.; WANG, T.; WANG, H.; KHAN, A.; JAWAD, A.; SUN, T.; JIAO, X.; CHEN, Z. Highly efficient lead distribution by magnetic sewage sludge biochar: sorption mechanisms and bench applications. *Bioresource Technology*, v. 238, p. 399-406, 2017.

INDAH, S.; HELARD, D.; HUDAWATY, F. *Column study of aluminum adsorption from groundwater by natural pumice.* In: Conference on Innovation in Technology and Engineering Science, novembro, 2018.

IWASHITA, N.; PARK, C. R.; FUJIMOTO, H.; SHIRAISHI, M.; INAGAKI, M. Specification for a standard procedure of X-ray diffraction measurements on carbon materials. *Carbon*, v. 42, n. 4, p. 701-714, 2004.

JIANG, Y.; DENG, T.; YANG, K.; WANG, H. Removal performance of phosphate from aqueous solution using a high-capacity sewage sludge-based adsorbent. *Journal of the Taiwan Institute of Chemical Engineers*, v. 76, p. 59-64, 2017.

JIN, Z.; CHANG, F.; MENG, F.; WANG, C.; MENG, Y.; LIU, X.; WU, J.; ZUO, J.; WANG, K. Sustainable pyrolytic sludge-char preparation on improvement of closed-loop sewage sludge treatment: Characterization and combined in-situ application. *Chemosphere*, v. 184, p. 1043-1053, 2017.

KACAN, E. Optimum BET surface areas for activated carbon produced from textile sewage sludges and its application as dye removal. *Journal of Environmental Management*, v. 166, p. 116-123, 2016.

KHANDAKER, S.; TOYOHARA, Y.; KAMIDA, S.; KUBA, T. Effective removal of cesium from wastewater solutions using an innovative low-cost adsorbent developed from sewage sludge molten slag. *Journal of Environmental Management*, v. 222, p. 304-315, 2018.

KHARDORI, N.; STEVAUX, C.; RIPLEY, K. Antibiotics: from the beginning to the future: Part 1. *The Indian Journal of Pediatrics,* v. 87, p. 39-42, 2020.

KIM, M. S.; KIM, J. G. Adsorption characteristics of spent coffee grounds as an alternative adsorbent for cadmium in solution. *Environments*, v. 7, n. 4, p. 24, 2020.

KOSMULSKI, M. The pH-dependent surface charging and points of zero charge: V. Update. *Journal of Colloid and Interface Science*, v. 353, n. 1, p. 1-15, 2011.

KRZEMINSKI, P.; LEVERETTE, L.; MALAMIS, S.; KATSOU, E. Membrane bioreactors - a review on recent developments in energy reduction, fouling control, novel configurations, LCA and market prospects. *Journal of Membrane Science*, v. 527, p. 207-227, 2017.

LARGITTE, L.; PASQUIER, R. A review of the kinetics adsorption models and their application to the adsorption of lead by an activated carbon. *Chemical Engineering Research and Design*, v. 109, p. 495-504, 2016.

LEE, S. Y.; PARK, S. J. Carbon dioxide adsorption performance of ultramicroporous carbon derived from poly (vinylidene fluoride). *Journal of Analytical and Applied Pyrolysis*, v. 106, p. 147-151, 2014.

LEICHTWEIS, J.; VIEIRA, Y.; WELTER, N.; SILVESTRI, S.; DOTTO, G. L.; CARISSIMI, E. A review of the occurrence, disposal, determination, toxicity and remediation technologies of the tetracycline antibiotic. *Process Safety and Environmental Protection*, v. 160, p. 25-40, 2022.

LI, J.; LI, B.; HUANG, H.; LV, X.; ZHAO, N.; GUO, G.; ZHANG, D. Removal of phosphate from aqueous solution by dolomite-modified biochar derived from urban dewatered sewage sludge. *Science of the Total Environment*, v. 687, p. 460-469, 2019.

LI, J.; LI, B.; HUANG, H.; ZHAO, N.; ZHANG, M.; CAO, L. Investigation into lanthanum-coated biochar obtained from urban dewatered sewage sludge for enhanced phosphate adsorption. *Science of the Total Environment*, v. 714, p. 136839, 2020a.

LI, J.; PAN, L.; YU, G.; LI, C.; XIE, S.; WANG, Y. Synthesis of an easily recyclable and safe adsorbent from sludge pyrochar for ciprofloxacin adsorption. *Environmental Research*, v. 192, p. 110258, 2021.

LI, Y. H.; CHANG, F. M.; HUANG, B.; SONG, Y. P.; ZHAO, H. Y.; WANG, K. J. Activated carbon preparation from pyrolysis char of sewage sludge and its adsorption performance for organic compounds in sewage. *Fuel*, v. 266, p. 117053, 2020b.

LIMA, S. C. *Estudo da técnica de difração de raios X.* Trabalho de Conclusão de Curso (Bacharelado em Física), Universidade Estadual de Feira de Santana, Feira de Santana, 2006.

LINDHOLM-LEHTO, P. C.; AHKOLA, H. S.; KNUUTINEN, J. S.; HERVE, S. H. Widespread occurrence and seasonal variation of pharmaceuticals in surface waters and municipal wastewater treatment plants in central Finland. *Environmental Science and Pollution Research*, v. 23, n. 8, p. 7985-7997, 2016.

LIU, F.; HASHIM, N. A.; LIU, Y.; ABED, M. M.; LI, K. Progress in the production and modification of PVDF membranes. *Journal of Membrane Science*, v. 375, n. 1-2, p. 1-27, 2011.

LIU, S.; MISHRA, S. B.; ZHANG, Y.; QI, L. Uptake of hexavalent chromium in electroplating wastewater by hydrothermally treated and functionalized sand and its sustainable reutilization for glass production. *ACS Sustainable Chemistry & Engineering*, v. 5, n. 2, p. 1509-1516, 2017a.

LIU, T.; LI, Y.; PENG, N.; LANG, Q.; XIA, Y.; GAI, C.; ZHENG, Q.; LIU, Z. Heteroatoms doped porous carbon derived from hydrothermally treated sewage sludge: Structural characterization and environmental application. *Journal of Environmental Management*, v. 197, p. 151-158, 2017b.

LOPES JR, L. A. C.; MIERZWA, J. C. *Influência de variáveis climáticas no desempenho do sistema aquapolo de produção de água de reúso.* In: 2º Congresso Internacional Rede de Saneamento e Abastecimento de Água - Resag, 09 a 11 de dezembro, Aracaju, 2015.

MAGED, A.; DISSANAYAKE, P. D.; YANG, X.; PATHIRANNAHALAGE, C.; BHATNAGAR, A.; OK, Y. S. New mechanistic insight into rapid adsorption of pharmaceuticals from water utilizing activated biochar. *Environmental Research*, v. 202, p. 111693, 2021.

MANO, E. B.; MENDES, L. C. *Introdução a polímeros.* 2 ed., Editora Edgard Blücher Ltda, São Paulo, 2001.

MANO, J. F.; LOPES, J. L.; SILVA, R. A.; BROSTOW, W. Creep of PVDF monofilament sutures: service performance prediction from short-term tests. *Polymer*, v. 44, n. 15, p. 4293-4300, 2003.

MANSOURI, F.; CHOUCHENE, K.; ROCHE, N.; KSIBI, M. Removal of Pharmaceuticals from water by adsorption and advanced oxidation processes: State of the art and trends. *Applied Sciences*, v. 11, n. 14, p. 6659, 2021.

MARK, H. F. *Encyclopedia of polymer science and technology*. John Wiley & Sons, vol. 4, pp. 510-532, Nova Iorque, 2014.

MARTINS, J. D. N. *Preparação e caracterização de nanocompósitos de poli (fluoreto de vinilideno) com poss e nanotubos de carbono.* Dissertação (Mestrado) – Programa de Pós-graduação em Ciência dos Materiais, Universidade Federal do Rio Grande do Sul, Porto Alegre, 2010.

MATTER, C. G. Membrane filtration (micro and ultrafiltration) in water purification. In: *Handbook Water Used Water Purification*, Springer, p. 1-17, 2018.

MCNAUGHT A. D.; WILKINSON A. *Compendium of Chemical Terminology*. Blackwell Science, Oxford, 1997.

MELO, R. D. O. C.; RODRIGUEZ, J. *Envision sustainability assessment of Aquapolo Ambiental, an urban water reuse infrastructure in São Paulo.* In: International Conference on Sustainable Infrastructure 2017, 26 a 28 de outubro, Nova Iorque, 2017.

MESQUITA, P. L. *Uso de carvão de ossos bovinos na remoção de contaminantes orgânicos de concentrados de eletrodiálise e sua contribuição ao reuso de água na indústria de petróleo*. Tese (Doutorado) - Engenharia Metalúrgica, Materiais e de Minas, Universidade Federal de Minas Gerais, Belo Horizonte, 2016.

MESQUITA, P. L.; PIRES, M. A.; SOUZA, C. R.; SANTOS, N. T. G.; NUCCI, E. R.; ROCHA, S. D. F. Removal of refractory organics from saline concentrate produced by electrodialysis in petroleum industry using bone char. *Adsorption*, v. 23, n. 7, p. 983-997, 2017a.

MESQUITA, P. L.; SOUZA, C. R.; SANTOS, N. T. G.; ROCHA, S. D. F. Fixed-bed study for bone char adsorptive removal of refractory organics from electrodialysis concentrate produced by petroleum refinery. *Environmental technology*, v. 39, n. 12, p. 1544-1556, 2017b.

METCALF, L.; EDDY, H. P. *Wastewater engineering: treatment and reuse.* 5 ed., McGraw-Hill Education, Nova Iorque, 2014.

MILLANAO, A. R.; MORA, A. Y.; VILLAGRA, N. A.; BUCAREY, S. A.; HIDALGO, A. A. Biological effects of quinolones: A family of broad-spectrum antimicrobial agents. *Molecules*, v. 26, n. 23, p. 7153, 2021.

MOREIRA, V. R.; LEBRON, Y. A. R.; DA SILVA, M. M.; DE SOUZA SANTOS, L. V.; JACOB, R. S.; DE VASCONCELOS, C. K. B.; VIANA, M. M. Graphene oxide in the remediation of norfloxacin from aqueous matrix: simultaneous adsorption and degradation process. *Environmental Science and Pollution Research*, v. 27, n. 27, p. 34513-34528, 2020.

MUTAMIM, N. S. A.; NOOR, Z. Z.; HASSAN, M. A. A.; YUNIARTO, A.; OLSSON, G. Membrane bioreactor: applications and limitations in treating high strength industrial wastewater. *Chemical Engineering Journal*, v. 225, p. 109-119, 2013.

NAKARMI, K. J.; DANESHVAR, E.; ESHAQ, G.; PURO, L.; MAITI, A.; NIDHEESH, P. V.; WANG, H; BHATNAGAR, A. Synthesis of biochar from iron-free and iron-containing microalgal biomass for the removal of pharmaceuticals from water. *Environmental Research*, p. 114041, 2022.

NAPOLITANO, H. B.; CAMARGO, A. J.; MASCARENHAS, Y. P.; VENCATO, I.; LARIUCCI, C. Análise da difração dos Raios X. *Revista Processos Químicos*, v. 1, n. 1, p. 35-45, 2007.

NGAMBIA, A.; IFTHIKAR, J.; SHAHIB, I. I.; JAWAD, A.; SHAHZAD, A.; ZHAO, M., WANG, J.; CHEN, Z.; CHEN, Z. Adsorptive purification of heavy metal contaminated wastewater with sewage sludge derived carbon-supported Mg (II) composite. *Science of the Total Environment*, v. 691, p. 306-321, 2019.

NIERO, G.; CORRÊA, A. X. R.; TRIERWEILER, G.; MATOS, A. F.; CORRÊA, R.; BAZANI, H. A. G.; RADETSKI, C. M. Using modified fish scale waste from *Sardinella brasiliensis* as a low-cost adsorbent to remove dyes from textile effluents. *Journal of Environmental Science and Health, Part A*, v. 54, n. 11, p. 1083-1090, 2019.

NIGRI, E. M.; CECHINEL, M. A. P.; MAYER, D. A.; MAZUR, L. P.; LOUREIRO, J. M.; ROCHA, S. D. F.; VILAR, V. J. P. Cow bones char as a green sorbent for fluorides removal from aqueous solutions: batch and fixed-bed studies. *Environmental Science and Pollution Research*, v. 24, n. 3, p. 2364-2380, 2017.

ODIAN, G. *Principles of polymerization.* 4 ed., John Wiley & Sons, Nova Iorque, 2004.

O'REILLY, J. M.; MOSHER, R. A. Functional groups in carbon black by FTIR spectroscopy. *Carbon*, v. 21, n. 1, p. 47-51, 1983.

PAVELQUESI, S. L. S.; FERREIRA, A. C. A. O.; RODRIGUES, A. R. M.; SILVA, C. M. S.; ORSI, D. C.; DA SILVA, I. C. R. Presence of tetracycline and sulfonamide resistance genes in Salmonella spp.: literature review. *Antibiotics*, v. 10, n. 11, p. 1314, 2021.

PEI, L. L.; YANG, W. Z.; FU, J. Y.; LIU, M. X.; ZHANG, T. T.; LI, D. B.; ...; FU, H. L. Synthesis, characterization, and pharmacodynamics study of enrofloxacin mesylate. *Drug Design, Development and Therapy*, p. 715-730, 2020.

PEÑA, O. I. G.; ZAVALA, M. A. L.; RUELAS, H. C. Pharmaceuticals market, consumption trends and disease incidence are not driving the pharmaceutical research on water and wastewater. *International Journal of Environmental Research and Public Health*, v. 18, n. 5, p. 2532, 2021.

PENG, X.; HU, F.; ZHANG, T.; QIU, F.; DAI, H. Amine-functionalized magnetic bamboo-based activated carbon adsorptive removal of ciprofloxacin and norfloxacin: A batch and fixed-bed column study. *Bioresource Technology*, v. 249, p. 924-934, 2018.

PHOON, B. L.; ONG, C. C.; SAHEED, M. S. M.; SHOW, P. L.; CHANG, J. S.; LING, T. C.; LAM, S. S.; JUAN, J. C. Conventional and emerging technologies for removal of antibiotics from wastewater. *Journal of Hazardous Materials*, v. 400, p. 122961, 2020.

POLIANCIUC, S. I.; GURZĂU, A. E.; KISS, B.; ŞTEFAN, M. G.; LOGHIN, F. Antibiotics in the environment: causes and consequences. *Medicine and Pharmacy Reports*, v. 93, n. 3, p. 231, 2020.

QIU, H.; LV, L.; PAN, B. C.; ZHANG, Q. J.; ZHANG, W. M.; ZHANG, Q. X. Critical review in adsorption kinetic models. *Journal of Zhejiang University-Science A*, v. 10, n. 5, p. 716-724, 2009.

REIS, E. O.; FOUREAUX, A. F. S.; RODRIGUES, J. S.; MOREIRA, V. R.; LEBRON, Y. A.; SANTOS, L. V.; AMARAL, M. C. S.; LANGE, L. C. Occurrence, removal and seasonal variation of pharmaceuticals in Brazilian drinking water treatment plants. *Environmental Pollution*, v. 250, p. 773-781, 2019.

REIS, E. O.; SANTOS, L. V.; LANGE, L. Prioritization and environmental risk assessment of pharmaceuticals mixtures from Brazilian surface waters. *Environmental Pollution*, v. 288, p. 117803, 2021.

SAMPAIO, M. F. *Fundamentos e roteiro da caracterização de materiais por DRX/MEV-EDS e aplicação destas técnicas em um estudo de caso: finos de uma liga FeCrAC e os produtos do seu processamento químico.* Dissertação (Mestrado) - Engenharia Mecânica, Universidade do Estado do Rio de Janeiro, Rio de Janeiro, 2015.

SANTOS, A. V.; COUTO, C. F.; LEBRON, Y. A. R.; MOREIRA, V. R.; FOUREAUX, A. F. S.; REIS, E. O.; ...; LANGE, L. C. Occurrence and risk assessment of pharmaceutically active compounds in water supply systems in Brazil. *Science of the Total Environment*, v. 746, p. 141011, 2020.

SANTOS, L. V. S.; MEIRELES, A. M.; LANGE, L. C. Degradation of antibiotics norfloxacin by Fenton, UV and UV/H_2O_2. *Journal of Environmental Management*, v. 154, p. 8-12, 2015.

SANTOS, M. F; MARIOTTO, I. F.; MASSITEL, I. L.; RUBIM, F. M.; DE ALMEIDA, J. V. F. C.; FELIX, L. A.; ...; FERRANTE, M. Uso das fluoroquinolonas em cães e gatos domésticos. *Research, Society and Development*, v. 10, n. 9, p. e25110917858-e25110917858, 2021.

SAXENA, P.; SHUKLA, P. A. comprehensive review on fundamental properties and applications of poly (vinylidene fluoride) (PVDF). *Advanced Composites and Hybrid Materials*, v. 4, n. 1, p. 8-26, 2021.

SCARIA, J.; ANUPAMA, K. V.; NIDHEESH, P. V. Tetracyclines in the environment: An overview on the occurrence, fate, toxicity, detection, removal methods, and sludge management. *Science of The Total Environment*, v. 771, p. 145291, 2021.

SCHNEIDER, R. P.; TSUTIYA, M. T. *Membranas filtrantes para o tratamento de água, esgoto e água de reuso.* ABES, São Paulo, 2001.

SEKULIC, M. T.; BOSKOVIC, N.; SLAVKOVIC, A.; GARUNOVIC, J.; KOLAKOVIC, S.; PAP, S. Surface functionalized adsorbent for emerging pharmaceutical removal: adsorption performance and mechanisms. *Process Safety and Environmental Protection*, v. 125, p. 50-63, 2019.

SHAHID, M. K.; KASHIF, A.; ROUT, P. R.; ASLAM, M.; FUWAD, A.; CHOI, Y.; BANU J, R.; PARK, J. H.; KUMAR, G. A brief review of anaerobic membrane bioreactors

emphasizing recent advancements, fouling issues and future perspectives. *Journal of Environmental Management*, v. 270, p. 110909, 2020.

SILVA, A. B. D. *Processamento, caracterização e determinação do perfil de polarização do Poli (fluoreto de vinilideno).* Dissertação (Mestrado) – Programa de Pós-graduação em Ciência e Engenharia de Materiais, Universidade Federal de São Carlos, São Carlos, 2009.

SILVA, C*. Reutilização de águas residuais urbanas pela indústria: um estudo de caso do Aquapolo Ambiental*. Dissertação (Mestrado Profissional) - Escola de Administração de Empresas de São Paulo, Fundação Getulio Vargas, São Paulo, 2019.

SILVA, T. L.; RONIX, A.; PEZOTI, O.; SOUZA, L. S.; LEANDRO, P. K.; BEDIN, K. C.; KARLA K. BELTRAME, K. K.; CAZETTA, A. L.; ALMEIDA, V. C. Mesoporous activated carbon from industrial laundry sewage sludge: Adsorption studies of reactive dye Remazol Brilliant Blue R. *Chemical Engineering Journal*, v. 303, p. 467-476, 2016.

SOLVAY. *Solef® PVDF Applications.* Solvay Group, 2022. Disponível em: <https://www.solvay.com/en/brands/solef-pvdf/applications>. Acesso em: 23 junho 2022.

SUBTIL, E. L.; HESPANHOL, I.; MIERZWA, J. C. Biorreatores com membranas submersas (BRMs): alternativa promissora para o tratamento de esgotos sanitários para reúso. *Revista Ambiente & Água*, v. 8, p. 129-142, 2013.

SUEZ. *Membranas de fibra oca de ultrafiltração ZeeWeed*. SUEZ Water Technology & Solutions, 2022. Disponível em: <https://www.suezwatertechnologies.com.br/products/zeeweed-ultrafiltration>. Acesso em: 17 janeiro 2022.

TANG, L.; YU, J.; PANG, Y.; ZENG, G.; DENG, Y.; WANG, J.; REN, X.; YE, S.; PENG, B.; FENG, H. Sustainable efficient adsorbent: alkali-acid modified magnetic biochar derived from sewage sludge for aqueous organic contaminant removal. *Chemical Engineering Journal*, v. 336, p. 160-169, 2018.

TANG, S.; SHAO, N.; ZHENG, C.; YAN, F.; ZHANG, Z. Amino-functionalized sewage sludge-derived biochar as sustainable efficient adsorbent for Cu (II) removal. *Waste Management*, v. 90, p. 17-28, 2019.

TAOUFIK, N.; BOUMYA, W.; JANANI, F. Z.; ELHALIL, A.; MAHJOUBI, F. Z. Removal of emerging pharmaceutical pollutants: A systematic mapping study review. *Journal of Environmental Chemical Engineering*, v. 8, n. 5, p. 104251, 2020.

TEIXIDÓ, M.; MEDEIROS, J.; BELTRÁN, J. L.; PRAT, M. D.; GRANADOS, M. Sorption of enrofloxacin and ciprofloxacin in agricultural soils: Effect of organic matter. *Adsorption Science & Technology*, v. 32, n. 2-3, p. 153-163, 2014.

TIWARI, A.; GOMEZ-ALVAREZ, V.; SIPONEN, S.; SAREKOSKI, A.; HOKAJÄRVI, A. M.; KAUPPINEN, A.; TORVINEN, E.; MIETTINEN, I. T.; PITKÄNEN, T. Bacterial genes encoding resistance against antibiotics and metals in well-maintained drinking water distribution systems in Finland. *Frontiers in Microbiology*, v. 12, 2021.

TROUCHON, T. LEFEBVRE, S. A review of enrofloxacin for veterinary use. *Open Journal of Veterinary Medicine*, 6 (2), p. 40-58, 2016.

TSAMO, C.; DJOMOU DJONGA, P. N.; DANGWANG DIKDIM, J. M.; KAMGA, R. Kinetic and equilibrium studies of Cr (VI), Cu (II) and Pb (II) removal from aqueous

solution using red mud, a low-cost adsorbent. *Arabian Journal for Science and Engineering*, v. 43, n. 5, p. 2353-2368, 2017.

ŢUCUREANU, V.; MATEI, A.; AVRAM, A. M. FTIR spectroscopy for carbon family study. *Critical Reviews in Analytical Chemistry*, v. 46, n. 6, p. 502-520, 2016.

VARGAS, V. H.; PAVEGLIO, R. R.; PAULETTO, P. D. S.; SALAU, N. P. G.; DOTTO, L. G. Sisal fiber as an alternative and cost-effective adsorbent for the removal of methylene blue and reactive black 5 dyes from aqueous solutions. *Chemical Engineering Communications*, v. 207, n. 4, p. 523-536, 2019.

VERNON-PARRY, K. D. Scanning electron microscopy: an introduction. *III-Vs Review*, v. 13, n. 4, p. 40-44, 2000.

VIEIRA, M. E. M.; SILVA, M. L. S.; OLIVEIRA, L. F. C.; PERRONE, Í. T.; STEPHANI, R. Espectroscopia de energia dispersiva de raios-X (EDS) acoplada ao microscópio eletrônico de varredura (MEV): fundamentos e aplicações em produtos lácteos. *Research, Society and Development*, v. 10, n. 10, p. e262101018622-e262101018622, 2021.

VON SPERLING, M. *Introdução à Qualidade das Águas e ao Tratamento de Esgotos.* Universidade Federal de Minas Gerais, Belo Horizonte, 2005.

WANG, Q.; LI, J. S.; POON, C. S. Recycling of incinerated sewage sludge ash as an adsorbent for heavy metals removal from aqueous solutions. *Journal of Environmental Management*, v. 247, p. 509-517, 2019a.

WANG, Q.; LI, J. S.; POON, C. S. Using incinerated sewage sludge ash as a high-performance adsorbent for lead removal from aqueous solutions: Performances and mechanisms. *Chemosphere*, v. 226, p. 587-596, 2019b.

WANG, Y.; ZHAO, W.; ZHENG, W.; CHEN, S.; ZHAO, J. Preparation of N-doped carbon nanosheets from sewage sludge for adsorption studies of Cr (VI) from aqueous solution. *Nanomaterials*, v. 9, n. 2, p. 265, 2019.

WILKINSON, J. L.; BOXALL, A. B.; KOLPIN, D. W.; LEUNG, K. M.; LAI, R. W.; GALBÁN-MALAGÓN, C.; ...; TETA, C. Pharmaceutical pollution of the world's rivers. *Proceedings of the National Academy of Sciences*, v. 119, n. 8, p. e2113947119, 2022.

WORCH, E. *Adsorption technology in water treatment - Fundamentals, process, and modelling.* Walter de Gruyter GmbH & Co, Dresden, 2012.

XAVIER, A. L. P.; ADARME, O. F. H.; FURTADO, L. M.; FERREIRA, G. M. D.; DA SILVA, L. H. M.; GIL, L. F.; GURGEL, L. V. A.. Modeling adsorption of copper (II), cobalt (II) and nickel (II) metal ions from aqueous solution onto a new carboxylated sugarcane bagasse. Part II: Optimization of monocomponent fixed-bed column adsorption. *Journal of Colloid and Interface Science*, v. 516, p. 431-445, 2018.

XIAO, K.; LIANG, S.; WANG, X.; CHEN, C.; HUANG, X. Current state and challenges of full-scale membrane bioreactor applications: A critical review. *Bioresource Technology*, v. 271, p. 473-481, 2019.

YANG, X.; XU, G.; YU, H. Removal of lead from aqueous solutions by ferric activated sludge-based adsorbent derived from biological sludge. *Arabian Journal of Chemistry,* v. 12, n. 8, p. 4142-4149, 2016.

YANG, X.; XU, G.; YU, H.; ZHANG, Z. Preparation of ferric-activated sludge-based adsorbent from biological sludge for tetracycline removal. *Bioresource Technology,* v. 211, p. 566-573, 2016.

YAO, S.; WANG, M.; LIU, J.; TANG, S.; CHEN, H.; GUO, T.; YANG, G.; CHEN, Y. Removal of phosphate from aqueous solution by sewage sludge-based activated carbon loaded with pyrolusite. *Journal of Water Reuse and Desalination*, v. 8, n. 2, p. 192-201, 2017.

YIRONG, C.; VAURS, L. P. Wasted salted duck eggshells as an alternative adsorbent for phosphorus removal. *Journal of Environmental Chemical Engineering*, v. 7, n. 6, p. 103443, 2019.

ZANELLA, O.; TESSARO, I. C.; FÉRIS, L. A. Desorption-and decomposition-based techniques for the regeneration of activated carbon. *Chemical Engineering & Technology*, v. 37, n. 9, p. 1447-1459, 2014.

ZAZYCKI, M. A.; GODINHO, M.; PERONDI, D.; FOLETTO, E. L.; COLLAZZO, G. C.; DOTTO, G. L. New biochar from pecan nutshells as an alternative adsorbent for removing reactive red 141 from aqueous solutions. *Journal of Cleaner Production*, v. 171, p. 57-65, 2017.

ZHANG, L.; LIU, J.; GUO, X. Investigation on mechanism of phosphate removal on carbonized sludge adsorbent. *Journal of Environmental Sciences*, v. 64, p. 335-344, 2018.

ZHANG, L.; PAN, J.; LIU, L.; SONG, K.; WANG, Q. Combined physical and chemical activation of sludge-based adsorbent enhances Cr (Ⅵ) removal from wastewater. *Journal of Cleaner Production*, v. 238, p. 117904, 2019.

ZHOU, W.; APKARIAN, R.; WANG, Z. L.; JOY, D. Fundamentals of scanning electron microscopy. In: *Scanning microscopy for nanotechnology*, Springer, p. 1-40, Nova Iorque, 2006.

ZUO, W. Q.; CHEN, C.; CUI, H. J.; FU, M. L. Enhanced removal of Cd (II) from aqueous solution using $CaCO_3$ nanoparticle modified sewage sludge biochar. *Rsc Advances*, v. 7, n. 26, p. 16238-16243, 2017.

CHAPTER 3 - MEMBRANE CHAR PRODUCTION AND CHARACTERIZATION

3.1 LITERATURE REVIEW

3.1.1 PYROLYSIS

Pyrolysis, from the Greek *pyrós* and *lýsis* which mean “breaking by fire”, is one of the thermochemical routes for the degradation of organic materials, promoting the cleavage of chemical bonds in organic chains by supplying energy in the form of heat in equal amounts or greater than the energy of such bonds. Different from the thermochemical process of combustion, pyrolysis takes place in an inert gaseous atmosphere, under zero oxygen concentrations or in stoichiometric quantities below what would be necessary for combustion to take place (AMER & ELWARDANY, 2020; BASU, 2010; MOHAN, PITTMAN JR & STEELE, 2006; OLIVEIRA JR, 2016; VIDAL, 2017; ZANARDINI, 2019).

Two main types of reactions can take place during pyrolysis, primary reactions, and secondary reactions. In primary reactions, usually elimination, subtraction, or addition, the volatiles are expelled as phenols, carbohydrates, alcohols, aldehydes, ketones, and carboxylic acids. Secondary reactions take place between the products of primary reactions and produce more complex molecules, such as esters and polymers (AMER & ELWARDANY, 2020; BASU, 2010; CANEVAROLO JR & SEBASTIÃO, 2010; OLIVEIRA JR, 2016; PAPUGA, GVERO & VUKIĆ, 2016; VIDAL, 2017).

Through these reactions, the raw material thermally decomposed by pyrolysis, initially formed by complex hydrocarbons, has its calorific value and energy content enriched, being converted into solid, liquid, and gaseous fractions, in various proportions. The solid products can be given as the fixed carbon content while the sum of the liquid and gas fractions constitute the content of the volatile materials. According to Basu (2010), considering generic biomass as raw material, it is possible to summarize the pyrolysis process according to the following reaction (EQUATION 3.1):

$$C_n H_m O_p \xrightarrow{Heat} \sum_{Solids} C + \sum_{Liquids} C_a H_b O_c + \sum_{Gases} C_x H_y O_z + H_2 O \qquad (3.1)$$

The gaseous fraction produced by pyrolysis is formed, in general, by the non-condensable gases carbon monoxide, carbon dioxide, methane, and hydrogen and, when obtained from biological materials, is called biogas. Due to their calorific value, the main applications of these gases are in the production of thermal energy for the pyrolysis reactor itself and as raw material in electricity-generating plants. The gaseous fraction, consisting mainly of carbon monoxide and hydrogen, widely known as synthesis gas, can also be used in the synthesis of methanol and ammonia (BASU, 2010; HAMAGUCHI, CARDOSO & VAKKILAINEN, 2012; VIDAL, 2017; ZANARDINI, 2019).

The liquid products are a mixture of up to 20% water with hydrocarbons, organic acids, and alcohols derived from homogeneous reactions of condensable gases or vapors produced in pyrolysis. Low molar mass acids and alcohols, such as acetic acid and methanol, constitute the so-called volatile liquids, while low volatility liquids receive different names such as tar, pyroligneous acid, bio-oil, pyrolysis oil, and wood oil, among others. Tar has a dark color, in shades of brown to black, its elemental composition is similar to the pyrolyzed raw material and can be used as an input in the chemical industry, replacing up to 50% by mass of petrochemical phenol in the production of phenolic resins, for example (BASU, 2010; HAMAGUCHI, CARDOSO & VAKKILAINEN, 2012; MOHAN, PITTMAN JR & STEELE, 2006; OLIVEIRA JR, 2016; ZANARDINI, 2019).

Finally, the solid fraction is the rustically porous residue resulting from the raw material not being converted into gases or liquids. Composed mainly of carbon, this porous solid product of pyrolysis is called char. Its applications include energy supply for various industrial sectors, water/nutrient retention, and soil correction for agriculture, contaminant removal as an adsorbent for water and wastewater treatment, and metal extraction for the metallurgical industry. This solid fraction must have different properties and is called charcoal, biochar, activated char, or coke, respectively, in each of these applications (AMER & ELWARDANY, 2020; BASU, 2010; OLIVEIRA JR, 2016; ZANARDINI, 2019).

The relative yields and the characteristics of the pyrolysis products depend on the parameters applied in the process and these operating conditions must be defined to

maximize or minimize the fraction of interest. Several authors agree when pointing out that the main factors that influence pyrolysis are: raw material, final or pyrolysis temperature, heating rate, residence time in the reactor, type and operating pressure of the reactor, use of catalyst and inert gas flow (AMER & ELWARDANY, 2020; BASU, 2010; GARCIA-NUNEZ *et al.*, 2017; HAMAGUCHI, CARDOSO & VAKKILAINEN, 2012; IPPOLITO *et al.*, 2020; LENG & HUANG, 2018; LU *et al.*, 2011; MOHAN, PITTMAN JR & STEELE, 2006; OLIVEIRA JR, 2016; PAPUGA, GVERO & VUKIĆ, 2016; VIDAL, 2017; ZANARDINI, 2019; ZHANG, LIU & LIU, 2015).

The different parameters involved in pyrolysis make the direct application to different raw materials complex, as well as the comparison between processes. The literature even reports disagreements regarding the definitions of the types of pyrolysis, from the nomenclature given to the variant to the ranges of the operational parameters considered in each of them (TABLE 3.1). In general, the final temperature, the heating rate, and the residence time are the parameters used to define the pyrolysis variants.

Table 3.1 - Pyrolysis variants and their operational parameters by different authors

Reference	Pyrolysis			
	Slow	**Conventional**	**Fast**	**Other**
Zanadirni (2019)	**Temperature:** 300 - 500 °C **Rate:** < 4.8 °C/min **Time:** > 60 min	**Temperature:** < 667 °C **Rate:** 6 - 60 °C/min **Time:** 7.5 - 9.5 min	**Temperature:** 577 - 977 °C **Rate:** 600 - 12000 °C/min **Time:** 0.5 - 10 s	Instant or flash **Temperature:** 777 - 1027 °C **Rate:** 60000 °C/min **Time:** < 0.5 s
Oliveira Jr (2016)	**Temperature:** < 600 °C **Rate:** 20 - 100 °C/min **Time: -**		**Temperature:** < 650 °C **Rate:** 100 - 1000 °C/min **Time:** -	Instant or flash **Temperature:** 450 - 1000 °C **Rate:** >1000 °C/min **Time:** seconds
Hamaguchi, Cardoso & Vakkilainen (2012)	**Temperature:** 316 - 510 °C **Rate:** - **Time:** 30 s – 3.3 min	-	**Temperature:** 343 - 510 °C **Rate:** - **Time:** 1 - 5 s	Carbonization **Temperature:** 357 °C **Rate:** - **Time:** days
Basu (2010)	**(a)** Carbonization **Temperature:** 400 °C **Rate:** very low **Time:** days	**(b)** Conventional **Temperature:** 600 °C **Rate:** low **Time:** 5 - 30 min	**Temperature:** 500 °C **Rate:** very high **Time:** < 2 s **(a)** Instant or flash **Temperature:** < 650 °C **Rate:** high **Time:** < 1 s **(b)** Ultrafast **Temperature:** 1000 °C **Rate:** very high **Time:** < 0.5 s	-
Mohan, Pittman Jr & Steele (2006)	Carbonization **Temperature:** 400 °C **Rate:** very low **Time:** days	**Temperature:** 600 °C **Rate:** low **Time:** 5 - 30 min	**Temperature:** 650 °C **Rate:** very high **Time:** 0.5 - 10 s	-

Temperature: final temperature; Rate: heating rate; Time: residence time.

Source: The author herself

Zanadirni (2019), in addition to slow, conventional, and fast pyrolysis, considered instant or flash pyrolysis as another variant. Oliveira Jr (2016) placed slow and conventional pyrolysis as a single variant, without considering residence times, and cited instant pyrolysis as another type of pyrolysis. Hamaguchi, Cardoso & Vakkilainen (2012) classified pyrolysis into slow and fast without considering heating rates and cited carbonization as another variant. Basu (2010) divided slow pyrolysis into carbonization and conventional pyrolysis, and, in addition to considering fast pyrolysis as a variant, he also divided it into instant and ultra-fast. Mohan, Pittman Jr & Steele (2006) associated slow pyrolysis with the term carbonization. Amer & Elwardany (2020) were not included in Table 3.1, as they only mentioned pyrolysis as carbonization, with a final temperature above 300 °C, high heating rate, and residence time between 2 hours and several days.

Regarding the relative yields of the products in each pyrolysis variant, the relevant literature points to the prevalence of solid products in slow pyrolysis and carbonization. Approximate yields among solid, liquid, and gaseous products, of 35, 30 and 35%, respectively, are expected in conventional pyrolysis. In fast and instantaneous pyrolysis, however, liquid products are the majority, around 70%, followed by gases and solids with approximate yields. In ultrafast pyrolysis, in turn, the majority production of gaseous products is expected (AMER & ELWARDANY, 2020; BASU, 2010; HAMAGUCHI, CARDOSO & VAKKILAINEN, 2012; MOHAN, PITTMAN JR & STEELE, 2006; OLIVEIRA JR, 2016; ZANARDINI, 2019).

An analysis of the average values of the operational parameters final temperature, heating rate, and residence time, calculated from Table 3.1, and of the estimated yields of the products (TABLE 3.2), allows raising some relationships between these parameters and the yields in the variants of the pyrolysis process (BASU, 2010; MOHAN, PITTMAN JR & STEELE, 2006; PAPUGA, GVERO & VUKIĆ, 2016; VIDAL, 2017; ZANARDINI, 2019):

- The occurrence of secondary reactions and the conversion of condensable vapors, produced in the primary reactions, into char and non-condensable gases are favored by longer residence times, on the order of hours and days.

- The term carbonization, used for slow pyrolysis, is commonly associated with processes whose objective is the production of char.
- Compared to combustion, conventional pyrolysis takes place at relatively low temperatures, usually below 600 °C.
- Temperatures above 600 °C increase the vibration of the molecules, favor the breaking of chemical bonds in organic chains and, consequently, result in the production of smaller molecules that constitute non-condensable and condensable vapors.
- The heating rate is significantly increased in fast and ultra-fast pyrolysis, from around 40 °C/min to values above 200 °C/min, so that the final temperatures are reached in minimum residence times, of the order of seconds, without the occurrence of secondary reactions.
- At temperatures above 600 °C and lower than the residence time, in the order of seconds, a reduction in solid products and an increase in liquid and gaseous products can be seen in fast and ultra-fast pyrolysis compared to slow and conventional pyrolysis.

Table 3.2 - Main variants of pyrolysis, their average operational parameters, and the yields of solid, liquid, and gaseous products

Variant	Final temperature	Heating rate	Residence time	Yield of products
Slow or Carbonization	~ 423 °C	~ 42 °C/min	Hours – days	Mostly S
Conventional	~ 617 °C	~ 46 °C/min	Minutes	35% S - 30% L - 35% G
Fast or Instant or Flash	~ 676 °C	~ 208 °C/s	Seconds	15% S - 70% L - 15% G
Ultrafast	~ 1000 °C	Very high	< 0.5 s	Mostly G

S: solids; L: liquids; G: gaseous

Source: The author herself

It is important to point out that the results presented in Table 3.2 corroborate the nomenclatures, intervals, and relationships indicated by Basu (2010) for the pyrolysis process.

In addition to the operational parameters of final temperature, heating rate, and residence time, the raw material's inherent characteristics and the pyrolysis reactor's design also influence the pyrolysis products.

When the objective of pyrolysis is the production of char, the raw materials most used are of plant origins, such as wood and agroforestry residues, and are known as lignocellulosic biomass, a complex mixture of cellulose and hemicellulose polymers, as well as lignin and other substances. When this solid is obtained from the pyrolysis of this lignocellulosic biomass it is called just char and when the raw material is any type of biological material, including lignocellulosic biomass, it is commonly called biochar. Sewage sludge from water and effluent treatment and bovine bones from refrigerating activities are other examples of raw materials used in the production of biochar by pyrolysis. The use of industrial and urban solid waste, consisting mostly of synthetic polymer mixtures, as raw material for pyrolysis is also possible, despite adding some complexity to the process (IPPOLITO *et al.*, 2020; LENG & HUANG, 2018).

The size or granulometry of the raw material particles also plays an important role in the distribution of the pyrolysis products and the efficiency of the reaction, mainly due to its influence on the heat transfer and, consequently, on the heating rate. In fast pyrolysis, the raw material used generally has a low granulometry, below 1 mm, since, in this way, the volatiles are expelled with less resistance, without suffering secondary reactions of conversion into char and non-condensable gases, thus resulting in more liquid products. The opposite happens in slow pyrolysis, in which larger particles are usually used and secondary reactions are facilitated (BASU, 2010; HAMAGUCHI, CARDOSO & VAKKILAINEN, 2012; IPPOLITO *et al.*, 2020; LENG & HUANG, 2018; VAN DE VELDEN *et al.*, 2010).

The pyrolysis of wood, in large particles has been recorded in history since ancient times and, initially, its only objective was the production of char, the first synthetic material produced by humans for heating purposes. With the progress of civilization, the other products of pyrolysis began to be collected in brick ovens and the ancient Egyptians, for example, used tar to embalm their dead. In the 19th century, the pyrolysis industry established itself for char and liquids production, and since then

pyrolysis or pyrolytic reactors, or simply pyrolizers, have evolved in the search for better adjustments of the operational parameters to meet the final product of interest and allow increasingly satisfactory yields (AMER & ELWARDANY, 2020).

Inside a pyrolysis reactor chemical, thermodynamic, fluid transport, and heat and mass transfer phenomena govern the decomposition of the raw material. If the pyrolysis process is divided into stages according to the temperature, it is usually said that pyrolytic reactors have zones where each stage takes place. The main stages of pyrolysis are drying, pyrolysis, and cooling, with variable temperature boundaries and the possibility of overlap between them, depending on characteristics such as the granulometry of the raw material used. The reaction zones established along the pyrolysis reactors receive the same nomenclature (AMER & ELWARDANY, 2020; BASU, 2010).

In the drying step, the pyrolysis temperature reaches the evaporation temperature of the water, close to 100 °C, mainly due to the transfer of heat by conduction from the reactor walls to the raw material, and the free moisture present in the raw material is released. Thus, raw materials with high moisture content, such as sewage sludge, require a greater heat supply for converting water in the liquid phase to steam, and pre-drying in the sun, for example, is recommended. Drying can continue up to temperatures close to 200 °C, with heat being conducted into the raw material and releasing bound water molecules and light gases such as CO and CO_2. Some authors even subdivide drying into three stages, pre-drying, drying, and post-drying or initial stage, in which the raw material is kept at a constant temperature and without suffering degradation (AMER & ELWARDANY, 2020; BASU, 2010).

Above 300 °C, the thermal decomposition of the raw material begins, in the pyrolysis itself, through the reactions described above. In primary pyrolysis, between 300 and 600 °C the primary reactions occur, and condensable and non-condensable gases are produced, in addition to char. At temperatures that reach 1000 °C, the final stage of pyrolysis takes place with the conversion of condensable gases produced in the primary reactions into liquids and more char (AMER & ELWARDANY, 2020; BASU, 2010).

Finally, in the cooling stage, it is important that the material produced, overheated, does not get into contact with atmospheric oxygen, to prevent its ignition. Still isolated inside the reactor, the pyrolysis products are cooled down to room temperature. The heat released in this step can be used in the pre-drying process of the raw material (AMER & ELWARDANY, 2020; BASU, 2010).

Pyrolysis reactors are mainly classified according to the equipment operating mode and the raw material availability mode. The method of heat transfer (direct, indirect, or microwave), the heat source (electric, gas, or biomass combustion), the operating pressure, the material of construction (earth, brick, concrete, or steel), and the mobility (stationary or portable) also vary among the different existing pyrolysis reactors (AMER & ELWARDANY, 2020; BASU, 2010; LENG & HUANG, 2018; VAN DE VELDEN *et al.*, 2010).

In terms of the operating mode, the reactors are batch or continuous type. Despite the constructive and operational simplicity, batch reactors usually generate non-homogeneous solids in terms of quality. Precise temperature control can minimize this disadvantage and prevent the occurrence of temperature gradients, irregular gas circulation, and partial combustion, for example, inside batch reactors. On the other hand, continuous reactors are more modern, focused mainly on producing gases and liquids, and use mixing mechanisms, favoring the homogeneity and yield of the produced char. However, these reactors have more complex construction, operation, and maintenance, requiring precise control of the residence time of the raw material and the application of volatiles produced in the heating of the reactor itself, in addition to the burning of part of the raw material to complement the supply of heat and electrical energy to power the equipment's motors. The models of continuous pyrolysis reactors most used are the drum and the rotating screw (AMER & ELWARDANY, 2020; BASU, 2010).

Among the reactors operated in batches, how the raw material is available defines the fixed bed and fluidized bed reactors. Fixed-bed reactors are traditional wood-fired coal-making furnaces, initially made from earth and now improved by using steel and bricks in construction. In these kilns, heat is provided exclusively by the partial burning of the raw material, which is limited by the presence of small openings in the lower part of the

kiln for air to enter and by the way the wood is stacked, thus preventing complete combustion of the material. The control of the residence time in the ovens is based on the color and density of the released gases (AMER & ELWARDANY, 2020; BASU, 2010).

In fluidized or moving bed reactors, heat is provided outside the bed, usually by burning the pyrolysis gas itself, and the entry of inert gas into the reactor is responsible for bed fluidization (FIGURE 3.1). In this type of reactor, there is good mass and heat transfer, with thermal efficiency between 60 and 70%, and the residence times of the gaseous products are shorter than the residence times of char. Fluidized bed reactors are the most commonly chosen due to their versatility and attractive cost of deployment. In fast pyrolysis, particles smaller than 5 mm, commonly used, must be added to fluidized bed reactors, in shallow beds and/or high flows of inert gas, to reach minimum residence times and obtain majority liquid products. The most well-known fluidized bed reactors are the bubbling bed and the circulating bed, which differ especially in terms of the degree of expansion of the bed and the superficial velocity of the inert gas (BASU, 2010; GARCIA-NUNEZ *et al.*, 2017; HAMAGUCHI, CARDOSO & VAKKILAINEN, 2012).

Figure 3.1 - Fluidized bed pyrolysis reactor

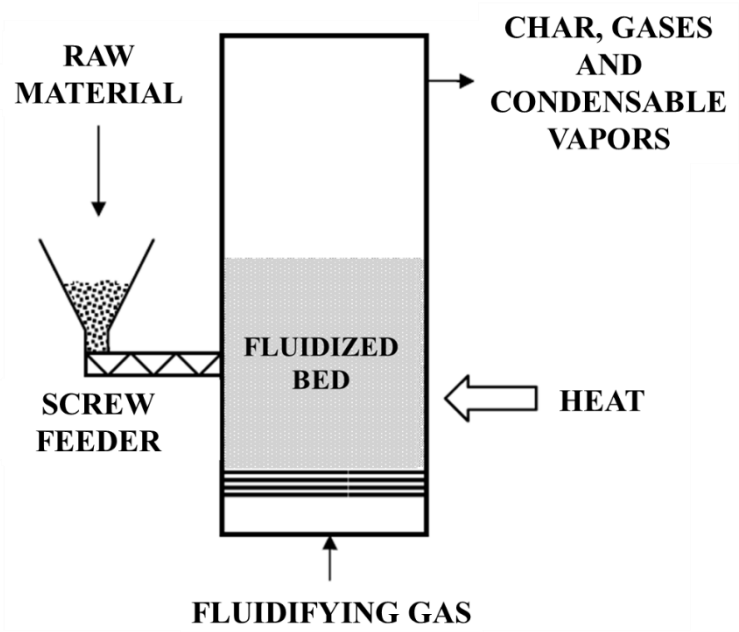

Source: Adapted from Basu (2010)

Ultrafast pyrolysis requires high heat transfer to increase the heating rate, so a solid is used in fluidized bed reactors, such as sand, as a heat carrier. From this, it becomes necessary the existence a gas-solid separator in the reactors used in this type of pyrolysis to separate the heat-carrying solids from the produced vapors. These solids are heated in a separate reactor, where they are returned by the gas-solid separator, and then returned to the pyrolizer carried by the inert gas in use (BASU, 2010; GARCIA-NUNEZ *et al.*, 2017; HAMAGUCHI, CARDOSO & VAKKILAINEN, 2012).

According to Garcia-Nunez *et al.* (2017), the designs and applications of pyrolysis reactors have been rethought due to technical and operational issues, such as difficulties in operating ultrafast pyrolysis reactors that use sand as a solid heat carrier and refining oils produced with high levels of oxygen. Environmental issues involved in the carbonization process, such as the release of pyrolysis gases into the atmosphere, are also a point of attention in the design of pyrolizers. The supply of heat in pyrolysis reactors in a more sustainable way, such as partial combustion of the raw material itself and the use of solar energy, should also be prioritized to the detriment of electrical energy (AMER & ELWARDANY, 2020).

Following the history of the pyrolysis industry, at the beginning of the 20th century, the petroleum industry came up with cheaper products which led to a decline in the application of pyrolysis. Only during the 1970s, with the oil crisis, was pyrolysis reconsidered as a viable technology for reducing dependence on fossil fuels. In Brazil, the main purpose of applying pyrolysis is the degradation of lignocellulosic biomass aiming at producing char to supply energy in several industries, especially pig iron and steel, one of the world's largest producers. The petrochemical industry also applies pyrolysis in the carbonization of wood to obtain coke, in the reuse of shale and waste tires, as well as in the treatment of other residues. The option of pyrolysis for the treatment of industrial and urban solid waste has even been driven by the possibility of using the products obtained in the process in other sectors. (BASU, 2010; GARCIA-NUNEZ *et al.*, 2017).

As a significant fraction of industrial and urban solid waste, polymer pyrolysis has been investigated and can produce various hydrocarbons, with chains between 9 and 50 carbon atoms, since some polymers are cleaved into their monomers, while others

produce random hydrocarbons of different molar masses. These hydrocarbons form liquid and gaseous products of interest to the petrochemical industry, such as olefinic gases, naphtha, fuel gases, oil fractions, coke, paraffin, and even synthetic fuel (PAPUGA, GVERO & VUKIĆ, 2016; VIDAL, 2017; ZANARDINI, 2019). In the thermal degradation of polymers, the supply of heat to equal or exceed the energy of the carbon-carbon bonds of the polymer chain and to break these bonds must be high, since polymers have low thermal conductivity. In this sense, the temperatures applied in the pyrolysis of polymers are usually higher than for other materials (SPINACÉ & DE PAOLI, 2005).

3.1.2 PVDF PYROLYSIS

The pyrolysis mechanism of polyvinylidene fluoride (PVDF) occurs through cross-linking and branching processes of the polymer, which result in the formation of polyunsaturated aliphatic compounds, called polyenes, fluoroaromatic compounds and hydrogen fluoride molecules (FIGURE 3.2) (LEE & PARK, 2014).

Figure 3.2 - Possible mechanism of PVDF pyrolysis

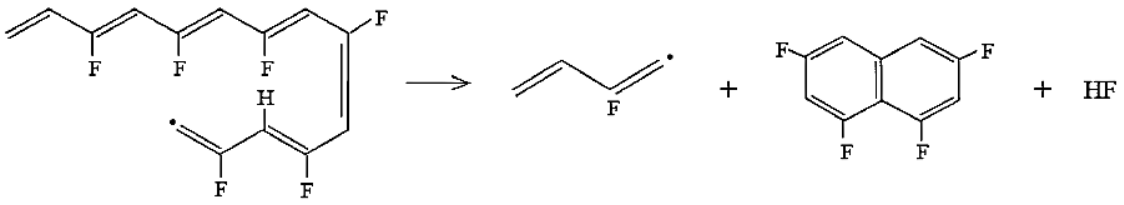

Source: Lee & Park (2014)

The formation of pores in the solid material resulting from the PVDF pyrolysis occurs when there is the release and elimination of the fluorinated functional groups of the polymer carbon chain by thermal degradation (HONG *et al.*, 2016; XU *et al.*, 2010). However, the high electronegativity of the fluorine atoms and the high energy of the C-F bond in the polymeric chain, give PVDF a high thermal stability that implies the need to apply higher pyrolysis temperatures than other polymers (DA COSTA, 2017). According to Lee & Park (2014), the higher the pyrolysis temperature used, the greater the carbonization degree of the PVDF.

As it is a microporous compound, the pyrolyzed PVDF gives rise to microporous chars of up to 1.0 nm. Other surface characteristics of PVDF chars, interfere with the porosity of the material, depending on the amount of fluorinated functional groups remaining in the material structure (LEE & PARK, 2014).

The PVDF pyrolysis process has been investigated especially to produce adsorbents and electrodes for supercapacitors (TABLE 3.3). Using pure PVDF or combined with other compounds as precursors, research carried out from 2001 onwards made use of furnaces with an inert gaseous atmosphere and different heating rates, final temperatures, and residence times. The char activation step has been applied in some works and will be discussed in Chapter 4.

Table 3.3 - Some papers on the pyrolysis of polyvinylidene fluoride (PVDF)

Objective	Precursor	Gaseous atmosphere	Final temperature	Heating rate	Residence time	Activation	Reference
Electrodes for supercapacitors	PVDF and Aromatic polyimide (PI)	Nitrogen	800 °C	-	30 min	-	Lee, Lee & Jung (2021)
Electrodes for supercapacitors	PVDF and Polytetrafluoroethylene (PTFE)	Nitrogen (300 cm^3/min)	900 °C	5 °C/min	2 h	-	Son *et al.* (2020)
Adsorption of CO_2	PVDF e Polyacrylonitrile (PAN)	-	900 °C	-	-	Vapor (5 mL/h) at 900 °C for 1 h	Heo *et al.* (2018)
Adsorption of CO_2	PVDF	Argon	400, 500, 600, and 800 °C	3 °C/min	1 h	-	Hong *et al.* (2016)
Adsorption of CO_2	PVDF	Nitrogen	400, 500, 600, and 700 °C	2 K/min	2 h	-	Lee & Park (2014)
Comparison with poly(vinylidene chloride) (PVDC) char	PVDF	Nitrogen	600, 700, 800 e 900 °C	10 °C/min	1 h	-	Xu *et al.* (2010)
Methylene blue adsorption comparing the use of fibers and films with and without dehydrofluorination	PVDF	Nitrogen (500 cm^3/min)	Several below 1300 °C	2 °C/min	-	CO_2 (500 cm^3/min) at 850 °C	Yamashita *et al.* (2001)

Source: The author herself

Yamashita *et al.* (2001) aimed to evaluate methylene blue adsorption by comparing the use of PVDF fibers and films with and without dehydrofluorination. The authors heated the raw material at a rate of 2 °C/min to the desired temperatures, below 1300 °C, in a nitrogen atmosphere. Finally, CO_2 at 500 cm^3/min and 850 °C was used to activate the pyrolyzed material. The film of activated char produced reached an adsorption capacity of 538 mg/g for methylene blue. The presence of pores was not observed in the chars produced below 300 °C and the increase in pore size with increasing pyrolysis temperature from 400 °C was small. Furthermore, the chars produced from PVDF without dehydrofluorination showed larger pores due to fluorine released during pyrolysis. The degree of dehydrofluorination inversely influenced the pore size, varying between 0.3 and 2.3 nm.

Just like Yamashita *et al.* (2001), Heo *et al.* (2018) activated the pyrolyzed material. However, steam at 900 °C and 5 mL/h for 60 min and a pressure of 1.2 bar was used. The porous char obtained from the polyacrylonitrile (PAN) and PVDF hybrid composite was applied as an adsorbent in CO_2 capture, showing a reversible and satisfactory capture performance of 2.21% by weight.

Hong *et al.* (2016) also pyrolyzed PVDF to produce an adsorbent for CO_2 removal. This work used temperatures of 400, 500, 600, and 800 °C, at a heating rate of 3 °C/min, and an argon atmosphere for 1 hour. Pyrolysis at 800 °C allowed the complete carbonization of the material and the obtainment of a predominantly microporous char, below 0.7 mm, with a surface area of 1011 m^2/g, pore volume of 0.416 cm^3/g and CO_2 adsorption capacity of 3.59 mol/kg at 25 °C. Surface area and total pore volumes increased with pyrolysis temperature up to 600 °C. At 800 °C, a small increase in the surface area and a small reduction in the total pore volume of the produced char were observed.

With a similar objective to Heo *et al.* (2018) and Hong *et al.* (2016), Lee & Park (2014) carried out the pyrolysis of PVDF at various temperatures (400, 500, 600, and 700 °C) maintained for 2 hours. A 2 K/min flow of ultrapure nitrogen gas was applied to obtain the inert atmosphere inside the reactor. In this way, an adsorptive capacity of 155 mg/g for CO_2 was reached by the adsorbent produced at 600 °C. The char produced at 400 °C had a surface area almost four times smaller than the others, possibly because

most fluorine or hydrogen fluoride molecules were not expelled from the carbon chain during pyrolysis at that temperature. With the increase of the pyrolysis temperature up to 600 °C, the release and elimination of these molecules happen completely and the surface area and the total, micro and mesopores volumes of the produced chars increased. However, according to the authors, these properties decreased in pyrolysis at 700 °C, possibly due to the collapse of micropores, by the disorderly release of fluorine and hydrogen fluoride molecules.

Lee, Lee & Jung (2021) and Son *et al.* (2020) aimed to prepare electrodes for supercapacitors with high energy storage performance, differing from each other by the precursors used in combination with PVDF, aromatic polyimide (PI) and polytetrafluoroethylene (PTFE), respectively.

PVDF was also used to prepare char by pyrolysis in the research by Xu *et al.* (2010), to compare it with char produced from poly (vinylidene chloride) (PVDC). Under a nitrogen atmosphere and a heating rate of 10 °C/min, the PVDF was subjected to temperatures between 600 and 900 °C for 1 hour. With a yield of about 35%, the PVDF char had a pore size of 0.55 mm, a pore volume of 0.41 cm^3/g, and a surface area of 1012 m^2/g, comparable to the characteristics of char. commercial activated. All these characteristics were independent of the pyrolysis temperature used.

Knowledge of the material’s inherent characteristics to be subjected to pyrolysis is essential for defining the appropriate operating conditions, directly influencing the properties of the char produced. In this sense, carrying out a stage of characterization of the raw material before pyrolysis is necessary, especially when it comes to waste, since the previous use of the material may have modified its initial characteristics.

3.1.3 POLYMER CHARACTERIZATION TECHNIQUES

For the characterization of polymers, among several techniques reported in the literature, the most common are Fourier-transform Infrared Spectrometry (FTIR), Scanning Electron Microscopy (SEM), and Thermogravimetric Analysis (TGA). Such techniques allow knowing the material's surface constituents, morphology, and mass loss with temperature. Thermogravimetric analysis is essential for pyrolysis planning

as it helps to understand polymer degradation with temperature variation. The infrared analysis indicates, qualitatively estimating, the crystalline structure of polymorphic polymers. In the case of PVDF, the existence of α crystalline phases can be indicated by exclusive absorption bands. In contrast, the γ phases have overlapping bands with the β phases that compromise their distinction (CANEVAROLO JR & SEBASTIÃO, 2004; CUI *et al.*, 2015).

In the studies on PVDF pyrolysis shown in Table 3.3, the raw material characterization stage was carried out in differently by the authors, not being mentioned in the papers for some of them. Xu *et al.* (2010) performed a TGA analysis of PVDF, which showed a dramatic mass loss between 400 and 600 °C and determined the minimum pyrolysis temperature of 600 °C to be used. The decomposition peak of PVDF at 462 °C, much higher than PVDC at 246 °C, corroborates the greater thermal stability of fluorinated polymers.

Yamashita *et al.* (2001) used FT-IR, elemental analysis, X-ray diffraction (XRD), and small angle X-ray scattering (SAXS) to characterize the PVDF used as a precursor. Infrared absorption bands at 490, 610, 760, 840, 970, 1070, and 1400 cm^{-1} were observed in the PVDF sample. The mass fractions of hydrogen, carbon, nitrogen, and fluorine were determined, as well as the crystalline and general structures of the material.

Hong *et al.* (2016) applied TGA and FT-IR analyses in the characterization of PVDF, which showed the occurrence of degradation from 400 to 800 °C, with a considerable decrease in mass at approximately 418 °C, and the existence of α and β crystalline phases in the structure of the PVDF used as a precursor in pyrolysis. X-ray photoelectron spectroscopy (XPS) was also used and allowed the identification and quantification of 60.7% of fluorine among the chemical elements present on the surface of PVDF.

As presented in this theoretical framework, based on exploratory research, the pyrolysis of PVDF fibers originating from discarded ultrafiltration membranes, regardless of the proposed application for the produced char, has not been identified in the relevant literature. Thus, the works discussed above (TABLE 3.2 and TABLE

3.3) were used as a reference for developing the membrane char (MC) production stage of this research.

3.1.4 PVDF CHAR CHARACTERIZATION

The characterization of char produced via the pyrolysis of pure PVDF was conducted by Lee & Park (2014), Hong *et al.* (2016), Yamashita *et al.* (2001), and Xu *et al.* (2010).

Lee & Park (2014) characterized the carbon produced via pyrolysis for CO_2 adsorbent application. X-ray photoelectron spectroscopy (XPS) was used to investigate the chemical elements on the carbon's surface quantitatively. The authors also employed X-ray diffraction (XRD) and BET techniques in the characterization stage.

Also aiming to produce an adsorbent for CO_2 removal, Hong *et al.* (2016) applied two microscopy techniques, scanning electron microscopy (SEM) and transmission electron microscopy (TEM), which allow analysis of the surface and interior of the sample, respectively. The Raman spectroscopy used by the authors allows for checking the existence of surface groups on the activated carbon in more detail than Fourier-transform infrared (FTIR) spectroscopy, which was also performed. The authors further characterized the obtained carbon through XPS, BET, XRD, and TGA.

Yamashita *et al.* (2001), investigating the adsorption of methylene blue using PVDF with and without dehydrofluorination, performed the elemental analysis of the fibers and dehydrofluorinated films produced to determine the mass fractions of hydrogen, carbon, nitrogen, fluorine, and oxygen. In addition to the more common techniques of FTIR and BET, the authors also used techniques such as differential scanning calorimetry (DSC), wide-angle X-ray diffraction (WAXD), and small-angle X-ray scattering (SAXS).

Intending to compare PVDF-derived charcoal with charcoal produced from poly(vinylidene chloride) (PVDC), Xu *et al.* (2010) only applied the BET method for the characterization of the produced char.

3.2 MATERIAL AND METHODS

3.2.1 OBTAINING AND PREPARING PVDF FIBERS

The present study used a Suez® ZW500 ultrafiltration membrane module, in a hollow fiber configuration, discarded by an oil refinery (FIGURE 3.3). At the refinery, the membrane module operated with biological sludge, in a membrane bioreactor (MBR) system, receiving the raw effluent from the refinery after removing oils and grease.

Figure 3.3 - Ultrafiltration (UF) membrane module discarded by the refinery

Source: The author herself

The PVDF fibers were donated by the refinery already separated from the structural part of the membrane module, made of polyvinyl chloride (PVC), totaling about 11.5 kg of material of interest (FIGURE 3.4a). For cleaning, the fibers were washed twice in water and then kept in a 500 ppm sodium hypochlorite solution for 15 minutes (FIGURE 3.4b), following the supplier's guidelines for a maximum temperature of 40 °C, pH between 2 and 10.5 and a maximum Cl_2 concentration of 1000 ppm (SUEZ, 2021). Cleaning is necessary to remove the biomass retained in the fibers during their application in the BRM system. Then, the fibers were rinsed in running water and left at room temperature to dry for 48 hours (FIGURE 3.4c). Finally, the dry fibers' fragmentation into pieces of approximately 3 cm was carried out manually using a cleaver on a rigid surface (FIGURE 3.4d).

Figure 3.4 - Steps for cleaning and fragmenting PVDF fibers

Source: The author herself

Representative samples of the PVDF fibers to be used in the characterization and pyrolysis tests were taken from a larger volume of fibers using quartering on a rigid, clean, and flat surface (FIGURE 3.5) according to the technical standard for reducing the field sample for laboratory tests (ABNT, 2001).

Figure 3.5 - Quartering on a rigid, clean, and flat surface

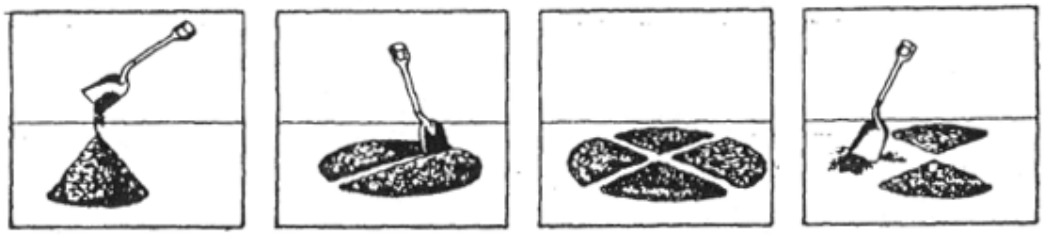

Source: ABNT (2001)

3.2.2 IODINE NUMBER DETERMINATION

The char produced from the pyrolysis of PVDF fibers for use as an adsorbent, called membrane char (MC) was evaluated by the iodine number parameter. The adsorption of iodine from an aqueous solution is used as a relative indicator of the porosity of the char, which may be a non-generalized approximation of the adsorbent surface area, since factors such as the raw material and the pore volume distribution of the char

influence this characteristic. The iodine number is given by the amount of iodine adsorbed per gram of powdered char (mg/g) (ABNT, 1991; ASTM, 1994).

The methodology applied to determine the iodine number of char samples (APPENDIX A) was adapted from the procedures described in NBR 12073/1991 and ASTM D4607/1994 (ABNT, 1991; ASTM, 1994; DE SOUZA, 2022). In the experimental design and validation tests, the iodine number determination methodology described in APPENDIX A was modified for samples of 0.5 g of char and iodine solution and sodium thiosulfate titrant solution with a concentration of 0.05 N to reduce the consumption of reagents in these steps, without damage to the results obtained. The iodine number of CABOT's commercial activated char NORIT® GAC 1240W, a conventional activated char, was also determined to methodology validate and for comparison to membrane char (MC) (CABOT, 2009).

3.2.3 EXPERIMENTAL DESIGN

A central composite design (CCD) of experiments was used to evaluate the effects of the independent variables final temperature (T) and residence time (t) on the iodine number (dependent variable) of the membrane char (MC). The CCD was performed in 2 levels and 2 factors (2^2), generating a total of 13 tests, divided into 5 central points, 4 cubic points, and 4 axial points. The levels to be evaluated for the T and t factors were defined based on:

- The objective of this study is to obtain char as the major product of pyrolysis for use as an adsorbent: slow and conventional pyrolysis (TABLE 3.2).
- In the operational parameters applied in previous works on PVDF pyrolysis (TABLE 3.3).
- In the result of the evaluation of mass loss with the temperature of the PVDF fibers through thermogravimetric analysis (TGA) (SECTION 3.3.5).
- Within the operating limits of the reactor used: maximum final temperature of 600 °C and no heating rate control.

The conditions of the independent variables T and t for the axial (levels $-\sqrt{2}$ and $\sqrt{2}$), cubic (levels -1 and +1), and central (level 0) points of the CCD are shown in Table 3.4.

Table 3.4 - Experimental conditions of final temperature (T) and residence time (t) for the axial, cubic, and central points

Independent variables	Levels				
	$-\sqrt{2}$	-1	0	$+1$	$+\sqrt{2}$
T (°C)	400	429	500	571	600
t (min)	30	52	105	158	180

3.2.4 MEMBRANE CHAR (MC) PREPARATION

The pyrolysis of the previously cleaned and fragmented PVDF fibers was carried out on a laboratory scale using a fluidized bed stainless steel tubular reactor, with an approximate capacity of 750 cm^3 (FIGURE 3.6a). A ceramic crucible was used as a support inside the reactor to avoid dispersion and facilitate material removal after pyrolysis (FIGURE 3.6b). The reactor was placed inside a vertical electric furnace with a stainless-steel outer casing, an insulating and refractory inner lining where the electrical resistances are located, supplied with nitrogen gas, and coupled to an air extractor (FIGURE 3.6c).

Figure 3.6 - Pyrolysis system with the tubular reactor, the ceramic crucible, and the electric furnace

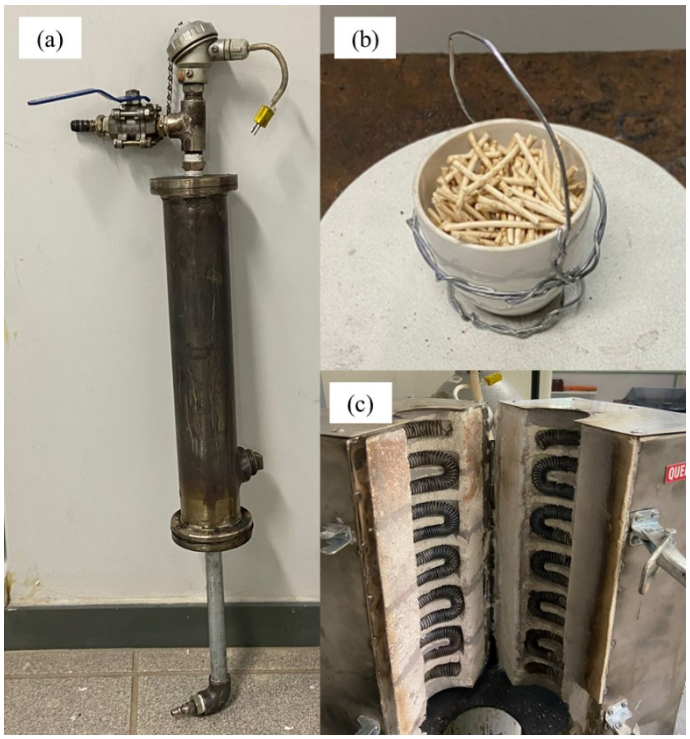

Source: The author herself

In each test, about 8 g of PVDF fibers were added to the pyrolysis reactor, which was heated to the final temperature to be evaluated. After reaching the final temperature, the reactor remained heated during the residence time related to the test condition. Afterward, the furnace was turned off and the tubular reactor was removed to cool naturally to room temperature. After cooling, the reactor was opened and the ceramic crucible containing the char was removed. The membrane char (MC) produced was weighed on a Shimadzu analytical balance (AY220) and reserved for iodine number analysis. Due to control restrictions of the reactor used, the heating rate and the nitrogen flow were only monitored during the tests, with average values of 19.9±3.2 °C/min and 1.0±0.3 L/min, respectively. The volatile products of pyrolysis were not collected, since the object of interest in this work is the solid product, char. However, the fractions of liquids and gases can be obtained by mass balance.

The operating conditions used in each test performed according to the experimental design (SECTION 3.2.3) are presented in Table 3.5.

Table 3.5 - Operating conditions used in pyrolysis tests

Test	Final temperature (°C)	Residence time (min)
1	429	52
2	571	52
3	429	158
4	571	158
5	400	105
6	600	105
7	500	30
8	500	180
9	500	105
10	500	105
11	500	105
12	500	105
13	500	105

The membrane char (MC) yield in each pyrolysis test was calculated by dividing the mass of PVDF fibers placed in the reactor by the mass of char obtained, multiplied by 100.

To remove the fines adhered to the surface of the particles, the samples were washed four times with distilled water, in a 250:1 ratio (grams of char:liters of distilled water). Finally, the adsorbents obtained were dried in a Biobase oven (BJPX - Spring) at 120 °C for 2 hours.

3.2.5 PROCESS OPTIMIZATION

ANOVA analysis was conducted to assess the appropriateness of the obtained model for iodine number, with a 95% confidence interval, and the experimental data were analyzed via the response surface method (RSM) using Minitab 18®. To maximize the response, the Generalized Reduced Gradient (GRG) optimization method was applied by iterative numerical methods on Microsoft Excel Solver®. According to the obtained model, the optimal values of the factors were predicted. The Power and Sample Size tool was used to determine the number of runs needed to validate the optimized conditions, with an acceptable power of 0.8, normally sufficient for engineering

experiments. Validation tests were performed under optimized conditions, and the One-Sample T-Test was applied to compare the iodine number average obtained to the predicted by the optimization. The Power and Sample Size tool and the One-Sample T-Test were performed via Minitab 18®.

3.2.6 MC CHARACTERIZATION STUDIES

Thermogravimetric analysis (TGA) of PVDF fiber and MC was performed on a NETZSCH TG thermal analyzer at a heating rate of 5 °C/min. The functional groups of PVDF and MC samples were studied using Fourier transform infrared spectroscopy (FTIR) on a JASCO FTIR 4600 Japan. The moisture content of the PVDF fibers was determined according to the ASTM D6980/2017 procedure (AHMAD *et al.*, 2023). The surface area, pore size, and pore volume were obtained from the N_2 adsorption-desorption isotherm data obtained by Tristar® II Plus. The crystalline structure of the MC was evaluated using X-ray powder diffraction (XRD) analysis on a diffractometer (Shimadzu, LabX XRD-6100) with Cu-Kα monochromatic radiation wavelength (λ) of 1.5405 Å, accelerating voltage of 40 kV, and 30 mA current, from 3 to 35° on the 2θ angle. The structural features of PVDF and MC samples were characterized by Raman spectroscopy (LabRam ARAMIS IR2). The surface morphology and elemental distribution of the PVDF fiber and MC were studied by scanning electron microscope with integrated energy dispersive X-ray spectroscopy (SEM-EDS) on a Schottky FE-SEM/JEOL 7900 JSM-F.

3.2.7 MC COST EVALUATION

The cost estimation for MC production was determined using Equation 3.2, including the sum of feedstock/reagents expenses ($C_{Materials}$) and the sum of energy consumption costs (C_{Energy}) (MAGED *et al.*, 2023a).

$$Total\ cost = \sum C_{Materials} + \sum C_{Energy} \tag{3.2}$$

The price of the discarded PVDF ultrafiltration membranes is neglected (free) and sodium hypochloride was the only reagent used during the synthesis process. The

energy consumption cost of the MC production was calculated via Equation 3.3 for each electrical equipment used (MAGED *et al.*, 2023b). The energy cost per kilowatt-hour (kWh) was calculated based on the average electricity rate (0.05 €/kWh).

$$C_{Energy} = P_D.L.T.C_C \quad (3.3)$$

where, C_{Energy} is the energy cost (€), P_D is the consumed power by each device (kW), L is the device factor load (0.5 for half-operation mode and 1.0 for full-operation mode), T is the operated time (h), and C_C is the energy price (€/kWh).

3.3 RESULTS AND DISCUSSION

3.3.1 OBTAINMENT AND PREPARATION OF PVDF FIBERS

- *Disassembly of the membrane module*

The initial step of preparing the PVDF fibers was carried out by the oil refinery that provided the material, bringing up a relevant discussion on polymer recycling. The PVDF fibers were donated by the refinery already separated from the structural part of the membrane module. The polyvinyl chloride (PVC) residues from that structural part were sent to landfill by the refinery itself. Sending these residues for recycling, whose conventional processing includes screening, fragmentation, washing, drying, agglutination, and extrusion steps, could be a more sustainable alternative. Recycled PVC, among other applications, could be used in electrical conduits and low-pressure tubes, for example (PIVA, BAHIENSE NETO & WIEBECK, 1999).

The modification of physicochemical properties of the polymeric residues, that is, their recycling, aims at transforming these polymers into inputs or new products, and must be carried out following the definitions of Decree-Law No. 12,305, of August 2, 2010, on the National Solid Waste Policy (DE OLIVEIRA NETO, 2015; BRASIL, 2010).

The polymer recycling process can be classified into four main categories. Primary recycling consists of reintroducing the residue, generally made up of trimmings from the process itself and which are essentially clean, into the extrusion cycle, resulting in products with characteristics similar to those produced from virgin polymers.

Secondary recycling, mechanical as well as primary, applies to homogeneous and clean waste that, after its original application and from an initial shredding stage, originates new polymeric materials, qualitatively inferior. The third category, called tertiary or chemical recycling, provides the production of monomeric molecules, whose application is common in the petrochemical industry, through the depolymerization or degradation of the polymer chains of the waste, including non-homogeneous ones. Finally, quaternary or energy recycling is the process of recovering energy from polymeric waste, homogeneous or mixed, thermally processed, by incineration, pyrolysis, gasification, or catalytic conversion (LAWLER *et al.*, 2012; DE OLIVEIRA NETO, 2015; SPINACÉ & DE PAOLI, 2005).

The present study aims to take advantage of only one of the by-products generated in the disassembly of the ultrafiltration membrane modules, the PVDF fibers, since the applicability of each component of the membrane module to the thermal processing of the quaternary recycling of polymers with the objective of char production must be analyzed separately, mainly about the carbon content of the component (LAWLER *et al.*, 2012; SPINACÉ & DE PAOLI, 2005).

- *Fragmentation of PVDF fibers*

The search for tools capable of performing the fragmentation, or size reduction, of PVDF fibers was a challenge for the sequence of the present work. Fragmentation is essential for pyrolysis to occur homogeneously and efficiently, due to the influence of the particle size of the raw material in the process (GARCIA-NUNEZ *et al.*, 2017). However, recognized for its high mechanical strength compared to other thermoplastics, PVDF as fibers proved to be quite resistant to being fragmented, as reported in the literature (DROBNY, 2009; MANO *et al.*, 2003; ESTERLY, 2002; ALCHIKH, FOND & FRÈRE, 2010).

The fragmentation of materials occurs through the application of brute force, which can be pressure, impact, abrasion, or cutting, depending on the physical properties of the material. The most commercially used equipment, including in recycling processes, for fragmenting polymers are knife and hammer rotor mills (FERNANDES, 2014; RIBEIRO & ABRANTES, 2001).

For the fragmentation step of the PVDF fibers, the present study evaluated different methods. A knife mill was tested for fragmenting the PVDF fibers, but the material was crushed and not cut by the equipment. A paper shredder machine in an association of recyclable collectors was also evaluated. However, as it is a rotating machine, the long PVDF fibers wound around the equipment shaft, and cutting the material was not possible. A paper guillotine for the fragmentation of PVDF fibers showed a good result, however, the large volume of material being processed soon impaired the cutting capacity of the equipment blade. Manual cutting of the PVDF fibers using different types of scissors was also considered, but the material was also crushed by the blades and not cut. Finally, the fragmentation of the PVDF fibers was achieved manually, using a cleaver on a rigid surface and friction movements, requiring physical and repetitive effort.

Therefore, for future scaling of this stage of the PVDF fibers preparation process, a broader investigation of fragmentation techniques would be necessary. The use of cryogenics and a reassessment of the equipment tested in this research may be a viable alternative.

3.3.2 EFFECT OF FINAL TEMPERATURE AND RESIDENCE TIME

The results of the obtained iodine number and MC yield in the experimental design are presented in Table 3.6. The effect of final temperature and residence time, separately, through the median iodine number of the runs carried out at the same level for each factor is represented in Figure 3.7. The highest levels of final temperature (571, 571, and 600 ºC), applied in runs 2, 4, and 6, provided the highest iodine numbers of 88.24, 102.11, and 72.60 mg/g, respectively. These results suggest that higher temperatures produce MC with better iodine adsorption performance. However, the iodine number of 72.60 mg/g obtained at 600 ºC was lower than the one obtained at 571 ºC (88.24 and 102.11 mg/g). A similar observation for the surface area reduction was reported for pure PVDF pyrolysis at 700 ºC (LEE & PARK, 2014). This may be related to a temperature limitation beyond which the pore structure of the char was impaired by the collapse of micropores, which, in turn, occurs due to the disorderly release of fluorine and hydrogen fluoride molecules.

Table 3.6 - Iodine number and process yield in membrane char (MC) production

Test	Final temperature (°C)	Residence time (min)	Iodine number (mg/g)	Yield (%)
1	429	52	0.00	68.7
2	571	52	88.24	28.6
3	429	158	12.70	32.4
4	571	158	102.11	28.4
5	400	105	0.00	53.9
6	600	105	72.60	30.7
7	500	30	7.36	32.2
8	500	180	20.17	30.6
9	500	105	28.75	37.2
10	500	105	26.47	32.2
11	500	105	26.96	32.6
12	500	105	24.16	28.1
13	500	105	25.57	31.0

Figure 3.7 - The median iodine number of the runs carried out under the same level for (a) final temperature (green columns) and (b) residence time (red columns)

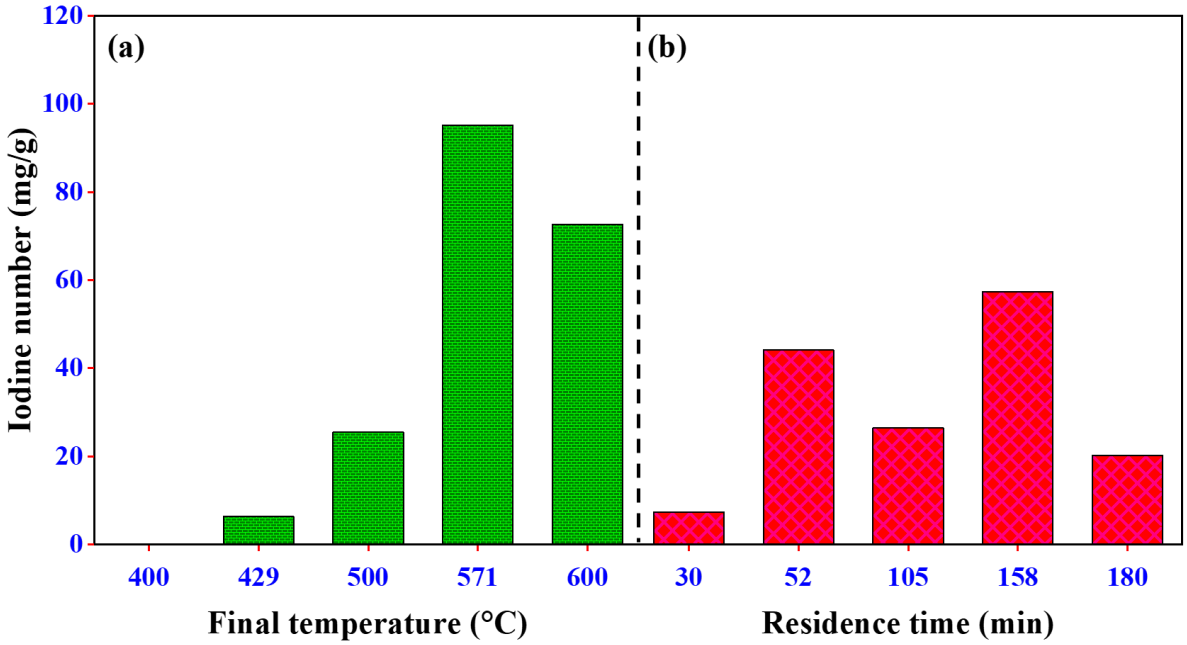

On the other hand, when the lowest levels of final temperature (429 ºC and 400 ºC) were evaluated, in runs 1 and 5, no removal of iodine was noted by the MC produced, with iodine number responses equal to zero mg/g. However, in run 3, under the same final temperature of 429 ºC, the iodine number was 12.70 mg/g, probably due to partial compensation for the longer residence time of 158 min applied. It was not possible to

visualize a relationship between the residence time and the iodine number, pointing to a low influence of this factor on the MC ability for iodine adsorption.

Regarding the MC yield (TABLE 3.6), outliers of 68.7% and 53.9% were observed in run 1 (429 ºC; 52 min) and run 5 (400 ºC; 105 min), respectively. This might be because the applied conditions were insufficient to expel the fluorine/hydrogen fluoride molecules from the carbon chain and, consequently, did not provide porosity to the solid product. Furthermore, the findings were supported by the iodine numbers which were equal to zero mg/g (LEE & PARK, 2014). Excluding these outliers, the average yield in the experimental design runs was 31.3±2.6%. This value meets the expectations due to the theoretical carbon content of 37.5% of the PVDF monomer, the vinylidene fluoride, and the final temperature and residence time applied, which favored approximate yields between solid, liquid, and gaseous products (BASU, 2010; MOHAN, PITTMAN JR & STEELE, 2006).

3.3.3 PROCESS OPTIMIZATION

A factorial analysis, considering the cubic and central levels (-1, 0, and +1), allowed verifying the presence of curvature in the model by the p-value equal to 0.001 for a confidence interval of 95%. Thus, it is suggested that at least one of the factors has a curved relationship with the iodine number, and the RSM is applicable. The Main Effects graph of the factorial analysis (FIGURE 3.8) confirms the presence of curvature through the central point (zero) outside the effect lines drawn by the cubic points (-1 and +1) of final temperature and residence time.

Figure 3.8 - Main effects of final temperature and residence time on iodine number in the factorial analysis

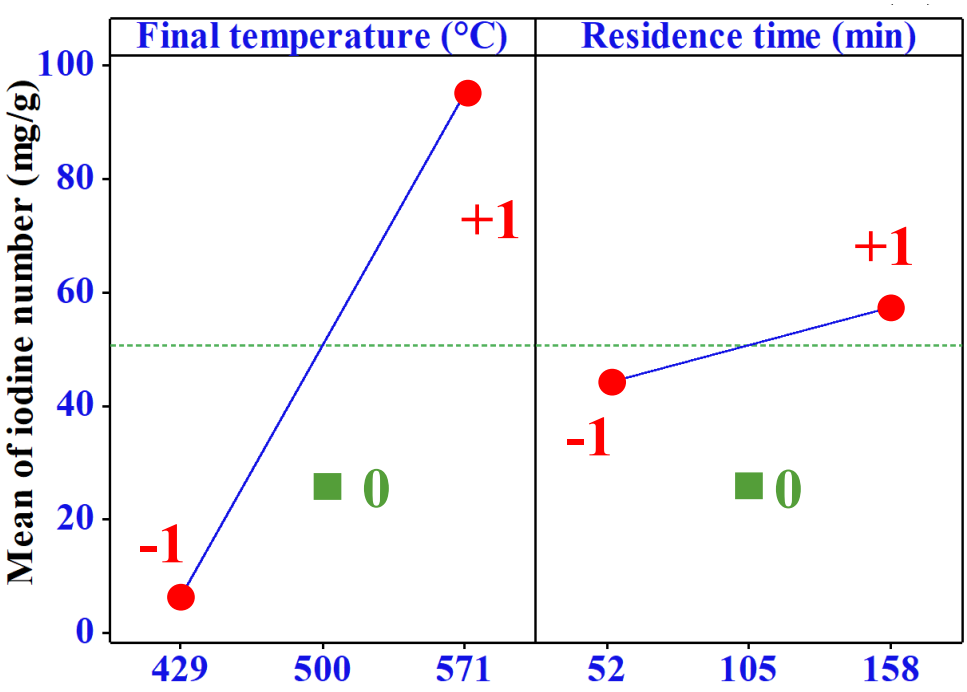

A quadratic model (EQUATION 3.4) was generated by modeling the experimental data with an R-squared of 0.8430, pointing out that the model can explain 84.3% of the iodine number variability.

$$IN = 338 - 1.77 \times T + 0.06 \times t + 0.00226 \times T^2 + 0.00004 \times \mathrm{t}^2 + 0.00008 \times \mathrm{T} \times \mathrm{t} \quad (3.4)$$

where IN is the iodine number (mg/g), *T* is final temperature (ºC), and *t* is residence time (min).

Table 3.7 displays the regression coefficients. By the positive values of regression coefficients, it can be concluded that the iodine number increases when the factors increase. The factor of utmost significance is the final temperature (T), as indicated by its highest regression coefficient value. In contrast, the residence time (t), the quadratic terms (TT and tt), and the interaction between the two factors (Tt) demonstrate weak effects.

Table 3.7 - Coefficients of model terms on the iodine number response

Term	Coefficient
T	35.0397
T	5.5861
T*T	11.3901
t*t	0.1239
T*t	0.2939

Linear factors: final temperature (T) and residence time (t); Quadratic interactions: T*T and t*t; Interaction between 2 factors: T*t.

The analysis of variance (ANOVA) table (TABLE 3.8), generated from the CCD, was used to assess the significance of the independent variables, T and t, for the dependent variable iodine number of MC produced.

Table 3.8 - Analysis of variance (ANOVA) for the iodine number of membrane char (MC) produced

Source	DF	SS (Adj.)	MS (Adj.)	t-value	P-value
Model	5	10987.9	2197.57	7.51	0.010
Linear	2	10071.9	5035.94	17.22	0.002
T	1	9822.2	9822.24	33.59	0.001
T	1	249.6	249.63	0.85	0.386
Quadratic	2	915.6	457.82	1.57	0.274
T * T	1	902.5	902.51	3.09	0.122
t * t	1	0.1	0.11	0.00	0.985
Interaction between 2 factors	1	0.3	0.35	0.00	0.974
T * t	1	0.3	0.35	0.00	0.974
Error	7	2047.1	292.44		
Lack-of-fit	3	2035.5	678.51	235.12	0.000
Pure error	4	11.5	2.89	*	*
Total	12	13034.9			

DF: degrees of freedom; SS (Adj.): adjusted sum of squares; MS (Adj.): adjusted mean square.

To be significant, an independent variable needs to reject the null hypothesis (H_0: p-value > α). Table 3.8 showed that a p-value below 0.05 and a t-value above the calculated critical t-value, represented in the Pareto diagram (FIGURE 3.9), were obtained only for the final temperature (T), indicating that just this term is significant for the iodine number of MC, with a 95% confidence level (α = 0.05). The terms residence time (t), quadratics (TT and tt), and interaction between the two factors (Tt) have no significant effect on the iodine number. These analyses complement the discussion about the impact of the factors, confirming statistically that there is no significant impact of residence time (t) on the iodine number of MC produced under the evaluated conditions.

Figure 3.9 - Pareto diagram of standardized effects of model terms on iodine number

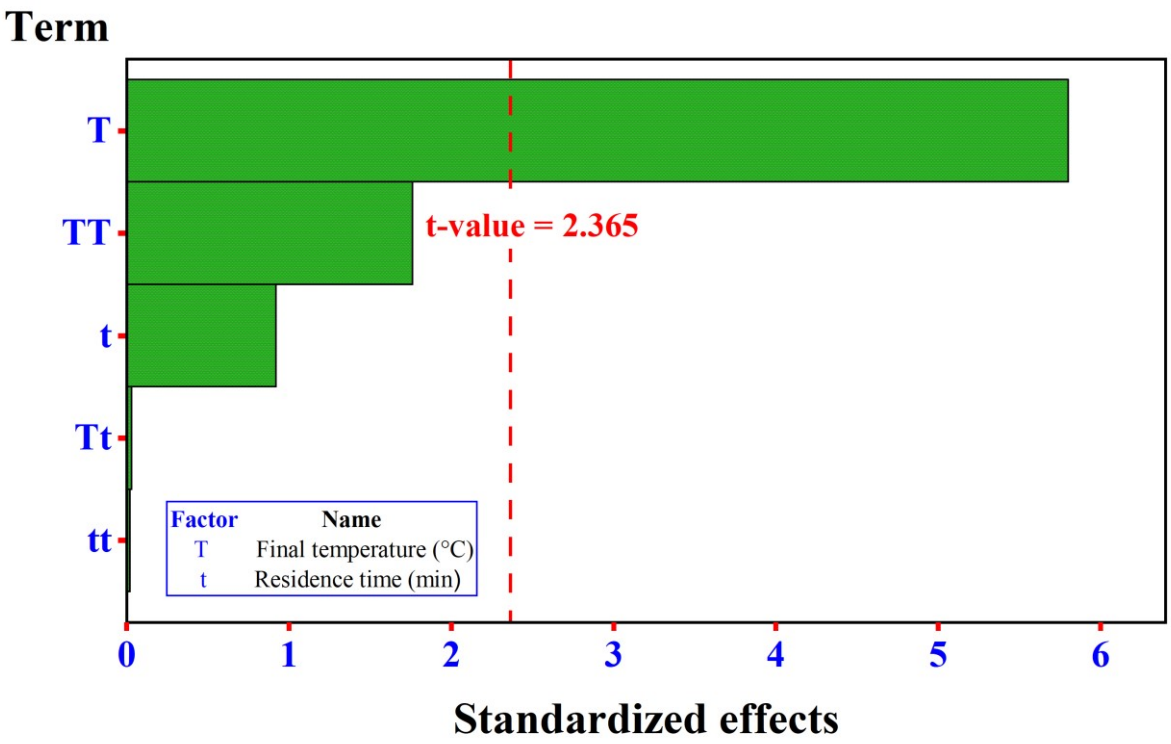

Figure 3.10 exhibits the Response Surface plot of the iodine number by the final temperature and the residence time. The existence of a maximum region of iodine number corroborates with effect analyses (SECTION 3.3.2) that at higher final temperatures, independent of the residence time, was achieved a better performance of PVDF pyrolysis, in terms of the iodine number. Within the evaluated levels, it was not possible to identify a statistically significant effect of the residence time on the iodine number. However, Figure 3.10 illustrates the inclination on the surface on the residence time axis, especially at higher final temperatures, showing that different iodine numbers can be obtained depending on the residence time applied. In this sense, the residence time was maintained in the model to be optimized with the final temperature.

Figure 3.10 - Three-dimensional responses with Overlaid Contour plot of iodine number

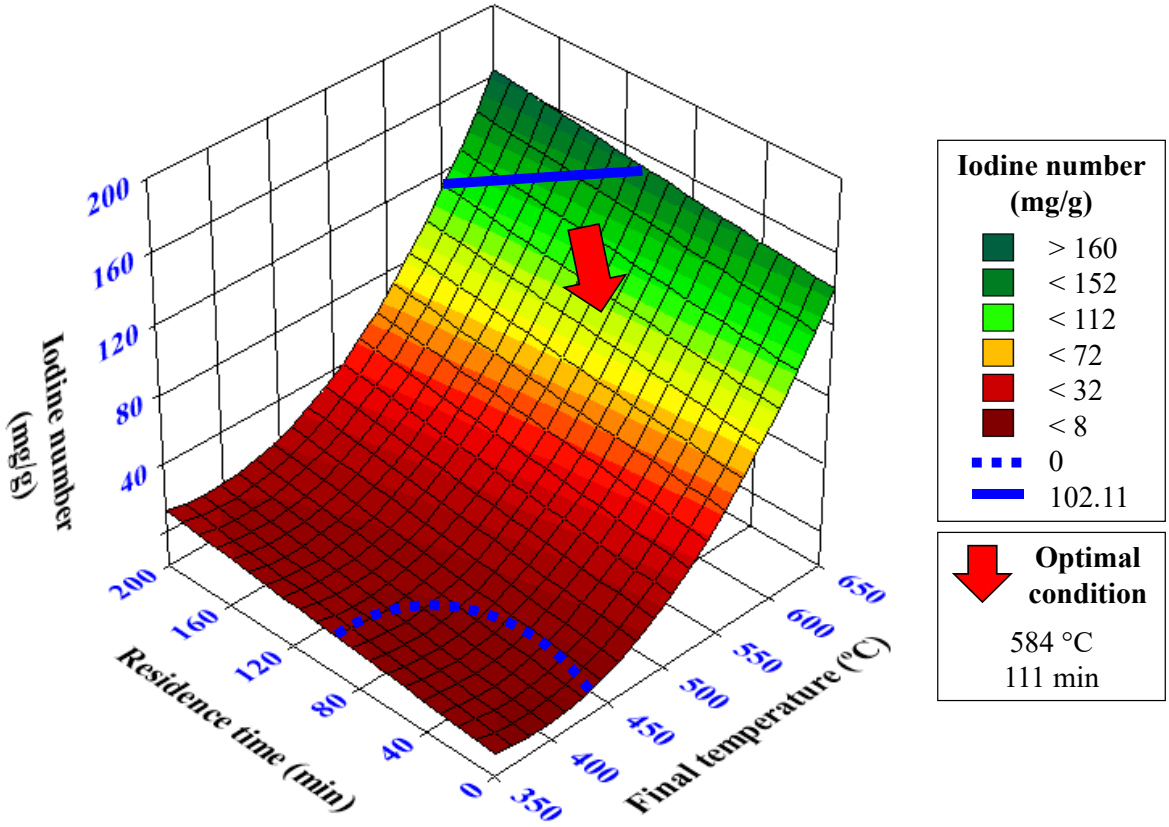

To maximize the iodine number, the Generalized Reduced Gradient (GRG) optimization method generated optimal values of final temperature and residence time. Table 3.9 shows the optimal value of both factors and predicted and obtained responses of iodine number at these conditions. The region between the dashed and solid blue lines in the response surface plot (FIGURE 3.10) shows the viable region represented by the generated model. The optimized pyrolysis conditions are in this region as necessary and feasible. Four repetitions were conducted to confirm the optimization of MC preparation under optimal conditions. The difference between predicted and obtained values of iodine number is negligible (p-value equal to 0.25), indicating the validity of the optimization.

Table 3.9 - Operational conditions and iodine number predicted by optimization and iodine numbers observed in validation tests

Final temperature (°C)	Residence time (min)	Iodine number (mg/g)	
		Predict	Observed
584	111	87.49	94.81
			84.95
			92.32
			89.87

Finally, the operating conditions of T = 584 °C and t = 111 min can be considered optimal for a 95% confidence interval (α = 0.05) with a calculated p-value equal to 0.25, thus rejecting the null hypothesis (H_0: p-value < α), being possible to reach values close to 87.49 mg/g for the iodine number of the MC.

3.3.4 IODINE NUMBER

The methodology applied to determine the iodine number, using 1 g of char and 0.1 N iodine solution and sodium thiosulfate titrant solution, was validated from the value of 928.85 mg/g obtained for the commercial activated carbon NORIT® GAC 1240W from CABOT, a result close to the one reported by the supplier of 950 mg/g (CABOT, 2009). However, it is important to point out that the accuracy of the standard procedures NBR 12073/1991 and ASTM D4607/1994 is attested only for iodine numbers between 600 and 1450 mg/g (ABNT, 1991; ASTM, 1994; ATTRI *et al.*, 2022). Therefore, the iodine number was used in this work as a relative indicator of porosity and as an approximation of the surface area of the MC. Moreover, the obtained MC demonstrated an iodine number of 242.35 mg/g under the optimized conditions. This value can be considered an approximation of the optimal surface area of MC. Being applied the “full” concentrations (1 g of char and 0.1 N iodine solution and sodium thiosulfate titrant solution) to validate the methodology and obtain the “full” iodine number.

3.3.5 MC CHARACTERIZATION STUDIES

- *Thermogravimetric (TG-DTG) analysis*

Figure 3.11 illustrates TG-DTG analysis for the discarded PVDF fibers and obtained char MC to investigate their thermal behavior/stability, degradation kinetics, and decomposition characteristics.

Figure 3.11 - TG/DTG curves of (a) PVDF and (b) MC

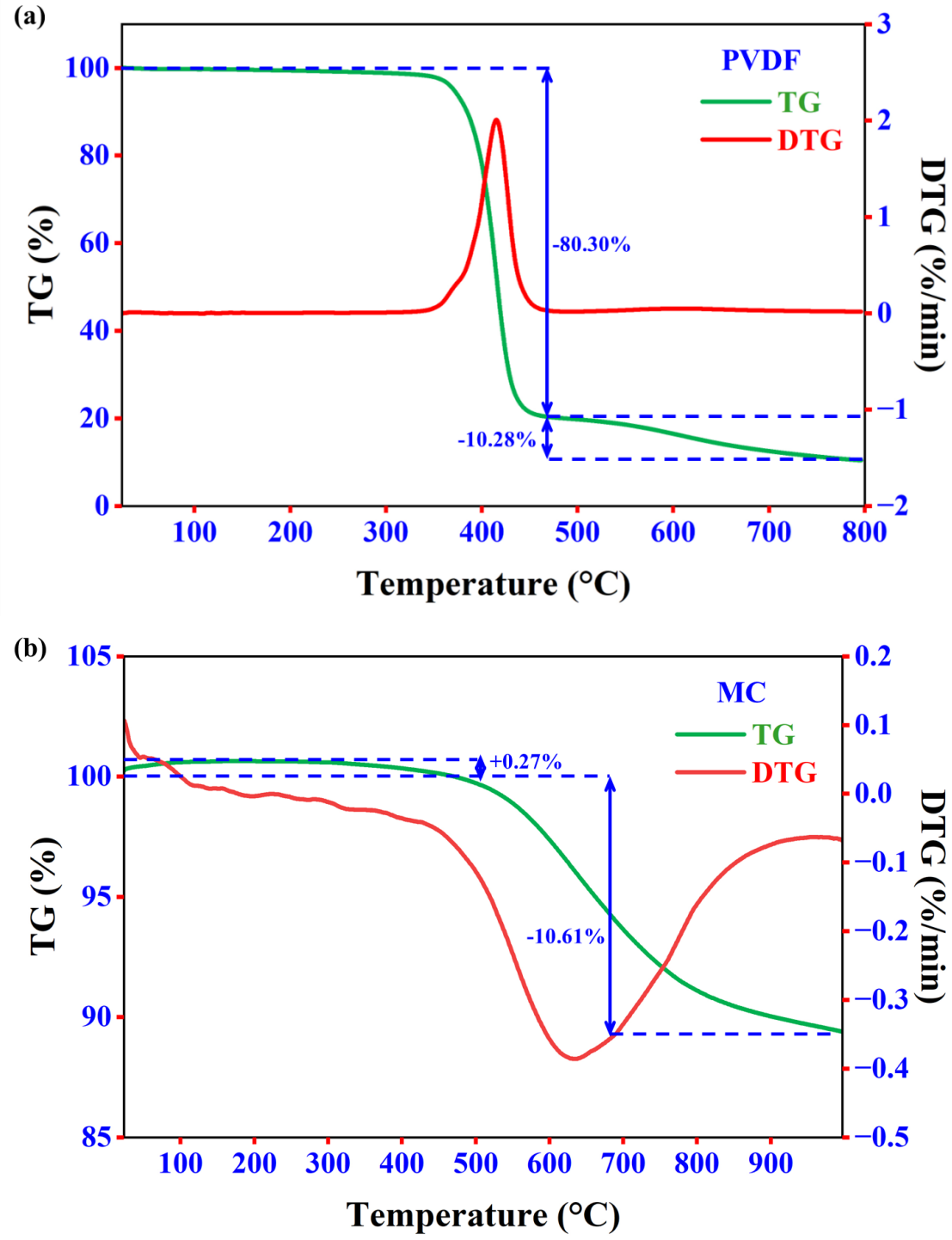

The TGA curve of the discarded PVDF fibers depicts the weight loss as a function of temperature. The initial weight loss (1st stage) observed at 415 ºC in the TGA curve was accompanied by an exothermic peak in the DTA curve (FIGURE 3.11(a)). This weight loss could be attributed to removing various components such as absorbed moisture (EL-QELISH *et al.*, 2024), residual contaminants, and organic or polymeric substances that accumulate on the membrane's surface during previous use. Moreover, the thermal degradation peak could be attributed to releasing and eliminating the fluorinated functional groups of the polymer carbon chain in a single step with a mass loss of 80.30% (FIGURE 3.11(a)). This initial step indicates the membrane's cleanliness and the presence or absence of surface impurities. However, the existence of an exothermic peak observed at 425 ºC in the DTA of PVDF typically implies an exothermic reaction or process occurring within the fibers at the detected temperature. The presence of this exothermic peak can be ascribed to the crystallization or phase transition occurring in the PVDF fibers. This phenomenon can be explained based on three main reasons: (i) Based on the fact that PVDF can exist in different crystalline phases, especially β-phase and γ-phase (indicated by FTIR), therefore, phase transition and/or crystallization from the amorphous state to a more ordered crystalline state often releases energy in the form of heat, resulting in an exothermic peak (GÜMÜŞ, 2020); (ii) The secondary reactions (chemical or structural changes) occurred within the polymer chain or at the polymer's interface with PVDF fibers, leading to the release of energy (PRABAKARAN *et al.*, 2017). The existing impurities can influence this secondary reaction in PVDF fibers from the previous treatment process; (iii) The degradation of the oil refinery residues in the surface and/or within the structure of the PVDF membrane fibers. The degradation of these substances experienced thermal degradation or chemical reactions at around 400-500 ºC (FIGURE 3.11(a)). Consequently, the heat generated by the decomposition of these contaminants can contribute to an exothermic peak in the DTA curve. Moreover, through the TG analysis progress (second stage), further weight loss (10.28%) occurred beyond 425 ºC in the PVDF fibers. This detected loss beyond this temperature revealed that a new decomposition step occurred (HONG *et al.*, 2016; XU *et al.*, 2010). This loss can be attributed to an oxidative breakdown of the fluorinated polymer and the revocation of the C-F bond (ALI *et al.*, 2022). Overall, the information gained from TG-DTA analysis of PVDF membrane fibers is essential for sustainable

waste management and the responsible handling of these fibers for further applications.

Furthermore, the TG-DTA analysis of PVDF-derived char is illustrated in Figure 3.11(b). The initial weight loss observed in the TGA curve typically corresponds to removing volatile components, such as residual or adsorbed moisture, commonly present in carbonaceous materials. Furthermore, the 2nd stage, up to a temperature of ≈ 957 ºC, exhibited the highest reactivity and induced a substantial mass reduction (10.61%) due to the primary decomposition reaction and carbonaceous material decomposition (volatiles) (FIGURE 3.11(b)). This region is also marked by a sharp endothermic peak in the DTA curve, indicating heat absorption during these volatiles' desorption. Thereafter, the TG curve shows a plateau or gradual decline, indicating a reduction in the rate of weight loss (FIGURE 3.11(b)). This region is associated with the thermal stability of the remaining carbonaceous substance and the formation of stable carbon structures like graphitic domains (confirmed in FT-IR and XRD analysis).

- *Fourier-transform infrared (FT-IR) analysis*

Figure 3.12 illustrates the FTIR spectra of the pristine PVDF fibers and MC. The FTIR spectrum of PVDF reveals characteristic peaks associated with various chemical moieties. The main transmittance peaks observed in the FTIR spectra of the PVDF fibers Figure 3.12 were found between 1500 and 600 cm^{-1}, which are characteristics of the PVDF structure. The presence of the C-F (carbon-fluorine) stretching vibration was typically observed as a distinct peak in the FTIR spectrum band at 1131 cm^{-1}. This peak is a hallmark of PVDF and confirms the presence of fluorine atoms in the polymer chain (SAWANT, KALLA & MURTHY, 2023). Generally, the PVDF is a polymorphic polymer exists with four possible crystalline structures (α, β, γ, and δ). The α and δ were not indicated in the obtained FTIR spectrum. However, the β phase of PVDF was indicated by the characteristic peak at 842 cm^{-1}. The β phase exhibits a distinct FTIR signature due to its molecular arrangement. The β-phase is characterized by a well-ordered and symmetrical structure (CAI *et al.*, 2017). Moreover, other bands at 1173 and 876 cm^{-1} were detected, which are characteristic of γ phases Figure 3.12. Therefore, the coexistence of β and γ phases in the discarded PVDF fibers could occur (KASPAR *et al.*, 2020). The low-intensity peaks at 2923 and 1731 cm^{-1} can be attributed to the oil traces in the PVDF fibers, which were accumulated due to the use

of these ultrafiltration membranes in the oil refinery, despite the previous cleaning Figure 3.12. Additionally, the bands at ≈ 3300 and 1700 cm^{-1} can be ascribed to the traces of moisture present in the PVDF fibers. This finding suggests the presence of hydroxyl groups by water stretching and -OH bending vibrations, respectively, even after the previously drying process.

Figure 3.12 - FTIR spectra of PVDF and MC.

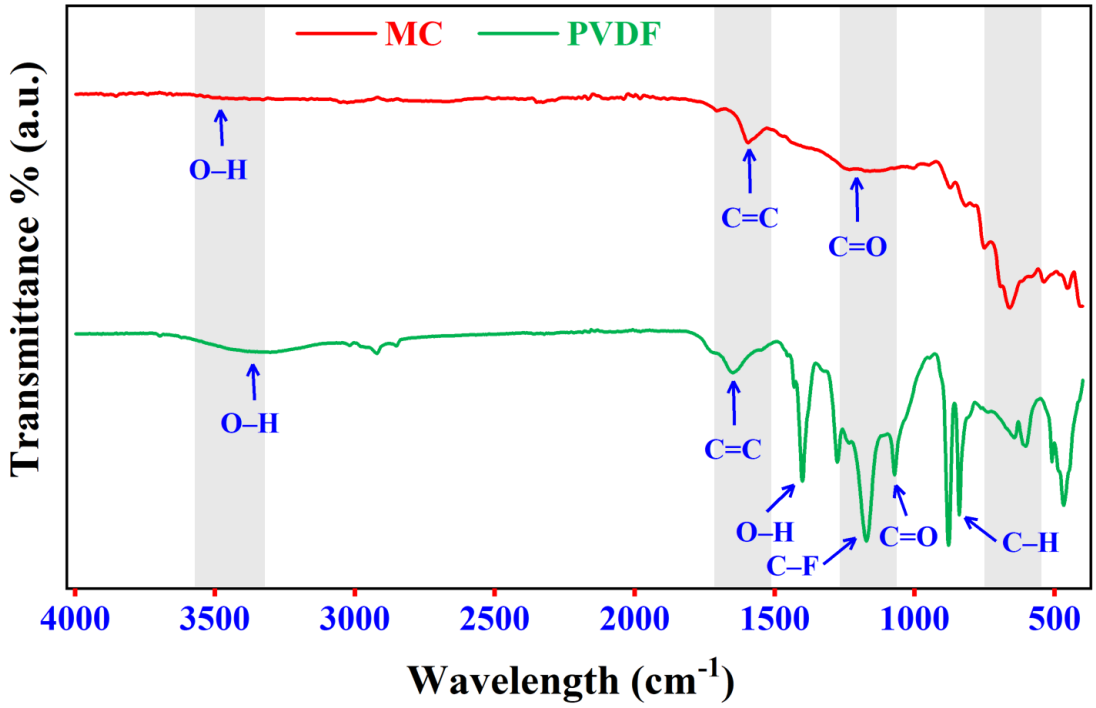

The FTIR analysis of MC presents valuable insights into this carbonaceous material's chemical composition and structural characteristics Figure 3.12. Several significant peaks were detected in the MC spectra. One of the most prominent features in the FTIR spectrum of MC is the absence of characteristic PVDF peaks, such as the C-F stretching vibration around 1200 cm^{-1} (FIGURE 3.12). This absence signifies the successful thermal decomposition of the original PVDF polymer during the pyrolysis process, forming a new carbon-rich material. The presence of absorption peaks in the FTIR spectrum of MC can be attributed to functional groups typically found in carbonaceous materials. The bands in the range of 1600-1700 cm^{-1} indicate the presence of C=C, which can result from the thermal degradation of the PVDF polymer backbone. Moreover, the low-intensity absorption peaks in the range of 2800-3600 cm^{-1} can be associated with O-H and N-H stretching vibrations, signifying the presence of surface functional groups, such as hydroxyl and amino groups (MAGED *et al.*, 2021),

which contribute to the MC surface reactivity and sorption capabilities. Furthermore, the presence of bands in the range of 1300-1600 cm^{-1} could suggest the presence of disordered/amorphous carbon. However, the sharp band at ≈ 1600 cm^{-1} indicated the presence of graphitic carbon. Furthermore, the moisture content of the PVDF fibers was found to be 0.1115±0.0001%, obtained according to the ASTM D6980/2017 standard procedure, which corroborates the results of TGA and FTIR analysis, suggesting the existence of a minimal amount of water in the sample previously dried at room temperature.

- *X-ray powder diffraction (XRD) analysis*

Figure 3.13 demonstrates the XRD analysis of MC produced from PVDF carbonized at 584 ºC to get insights into the structural properties of the resulting carbonaceous material. The MC exhibits distinct peaks at around 26° and 44°, which correspond to the diffraction patterns of the (0 0 2) plane and (1 0 0)/(1 0 1) planes within the graphite structure, respectively. The presence of well-defined intense peaks in the XRD pattern at low angles of the graphitic peak (002) indicates a highly ordered, graphitic carbon structure (MAGED *et al.*, 2023a). The position and intensity of this peak can give information about the degree of graphitization and the crystallite size within the MC. Furthermore, the absence of sharp peaks in the XRD pattern or the presence of broad at the low angle (< 20º), suggests the presence of amorphous carbon structures. The presence of amorphous carbon structures can influence the MC properties, such as electrical conductivity and reactivity.

Figure 3.13 - XRD pattern of MC

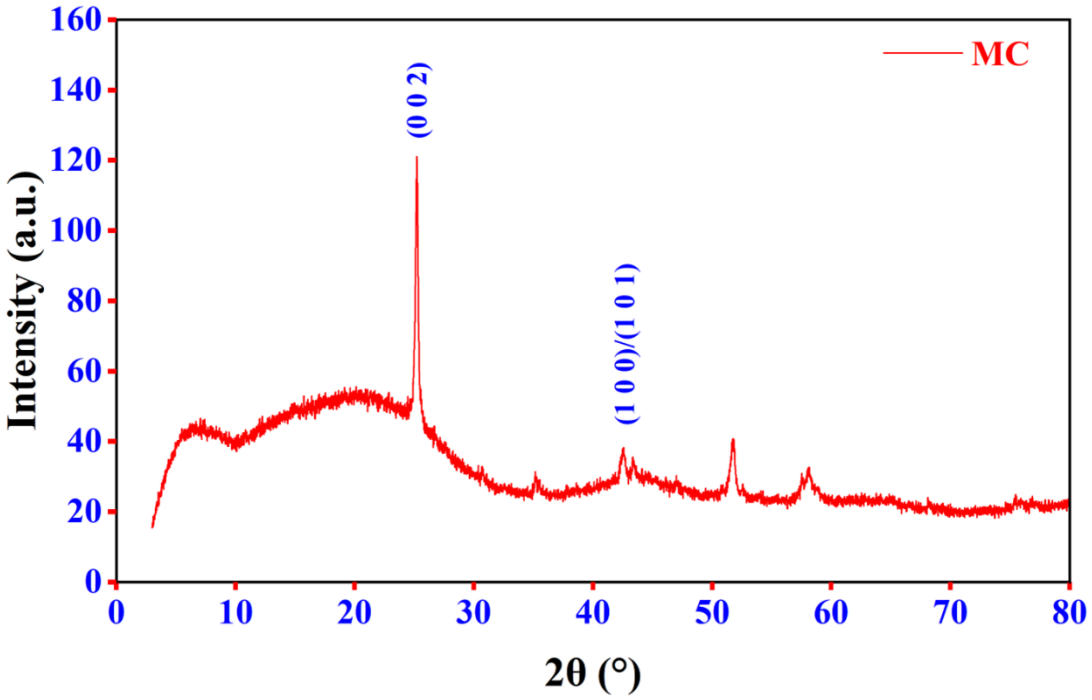

- *Raman analysis*

Raman spectroscopy was used to verify the molecular composition and structural characteristics of PVDF fiber and obtained MC (FIGURE 3.14). The Raman analysis of the discarded PVDF membrane showed two different crystalline phases (γ-phase and β-phase) with distinct Raman spectra. PVDF fiber's peak at 850 cm^{-1} is generally attributed to the β and γ phases. However, the peaks at 1087 and 1284 cm^{-1} are attributed only to the β phase of the crystalline structure (HONG *et al.*, 2016; SOBOLA *et al.*, 2021). The appearance of peaks around 1430 cm^{-1} related to CH_2 bending vibrations may indicate the presence of surface contamination or chemical modification of the membrane from the previous use. Additionally, the peaks at 1606 and 1720 cm^{-1} are water-bending peaks and can be attributed to the traces of moisture in the PVDF fiber even after the previous drying process. In contrast, the characteristic peak of the α phase at 796 cm^{-1} is not observed in the Raman spectrum of the PVDF fiber, reinforcing the absence of this crystalline structure pointed out in the FTIR analysis (SOBOLA *et al.*, 2021).

Figure 3.14 - Raman spectra of PVDF and MC

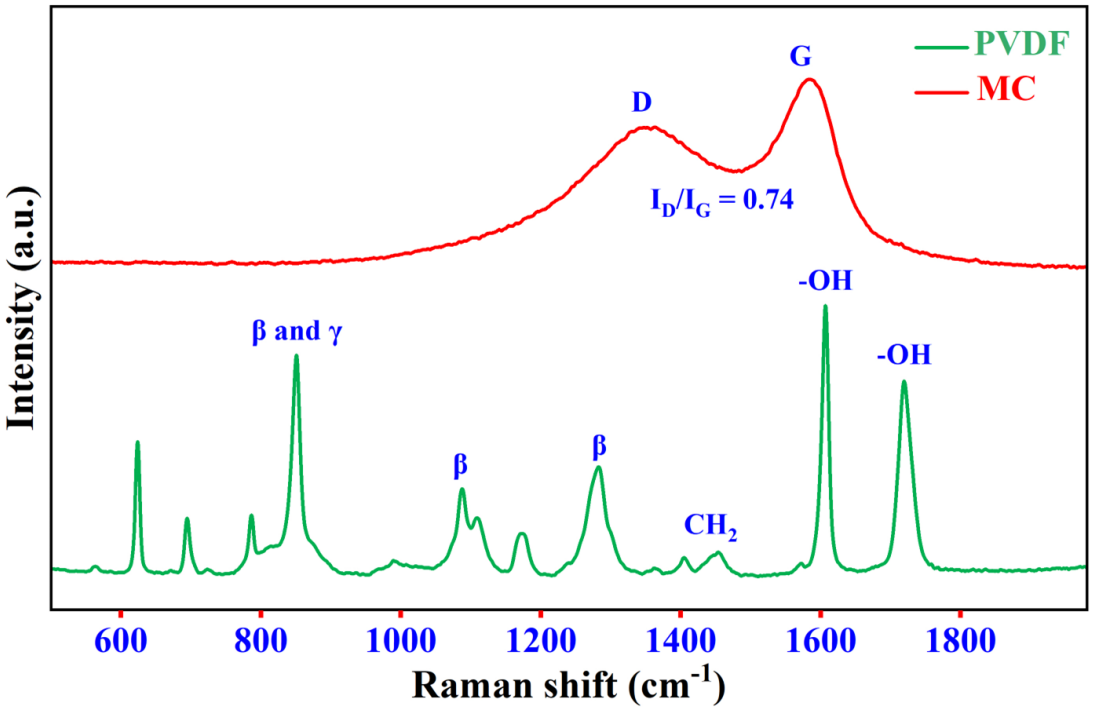

In the case of MC, Raman spectra show the structural changes after pyrolysis at 584 ºC (FIGURE 3.14). The degree of graphitization (G band) and/or the presence of disordered (D band) carbon structures can be assessed through Raman analysis (FIGURE 3.14). The peak at 1346 cm^{-1} (D band) is associated with sp^3-hybridized carbon. The G band was identified at 1584 cm^{-1}, related to the vibration of sp^2-hybridized carbon (HONG *et al.*, 2016). When calculating the ratio between the intensities of the identified bands (I_D/I_G) equal to 0.74, there is a correlation with the degree of development of the pores of the carbonaceous material. The higher the I_D/I_G ratio, the greater the material's porosity, measured in the material's texture analysis. The width of the peaks is associated with the degree of carbon disorder. The greater the width of the peaks, the more amorphous the material's structure, as discussed in the XRD analysis (MAGED *et al.*, 2023a). The obtained Raman analysis of the MC derived from the discarded PVDF membrane is essential for tailoring its properties to specific applications, such as adsorption, catalysis, or energy storage. The degree of graphitization, presence of surface functional groups, and crystalline structure all influence the material's performance. Additionally, this analysis provides valuable information for optimizing the pyrolysis or carbonization process for char production, contributing to sustainable waste management and resource utilization strategies.

- *Surface and textural analysis*

The SEM analysis aiming to investigate the superficial morphology of the PVDF fiber and MC is presented in Figure 3.15(a-b). As expected, the cross-section micrographs of the PVDF fiber can be observed as elongated and compact particles with regular tubular shapes with a diameter of ~15 µm, the polymer chains. In contrast, the MC is flaked with irregular shapes and not compact, typical of porous carbons, making it possible to observe pores on the surface of the particles. The pyrolysis of the PVDF results in the breaking of polymer chains and the release of fluorinated functional groups, consequently replacing the regular tubular shapes of the polymer with irregular porous flakes of the char (LEE & PARK, 2014).

Figure 3.15 - SEM micrographs for (a) PVDF and (b) MC

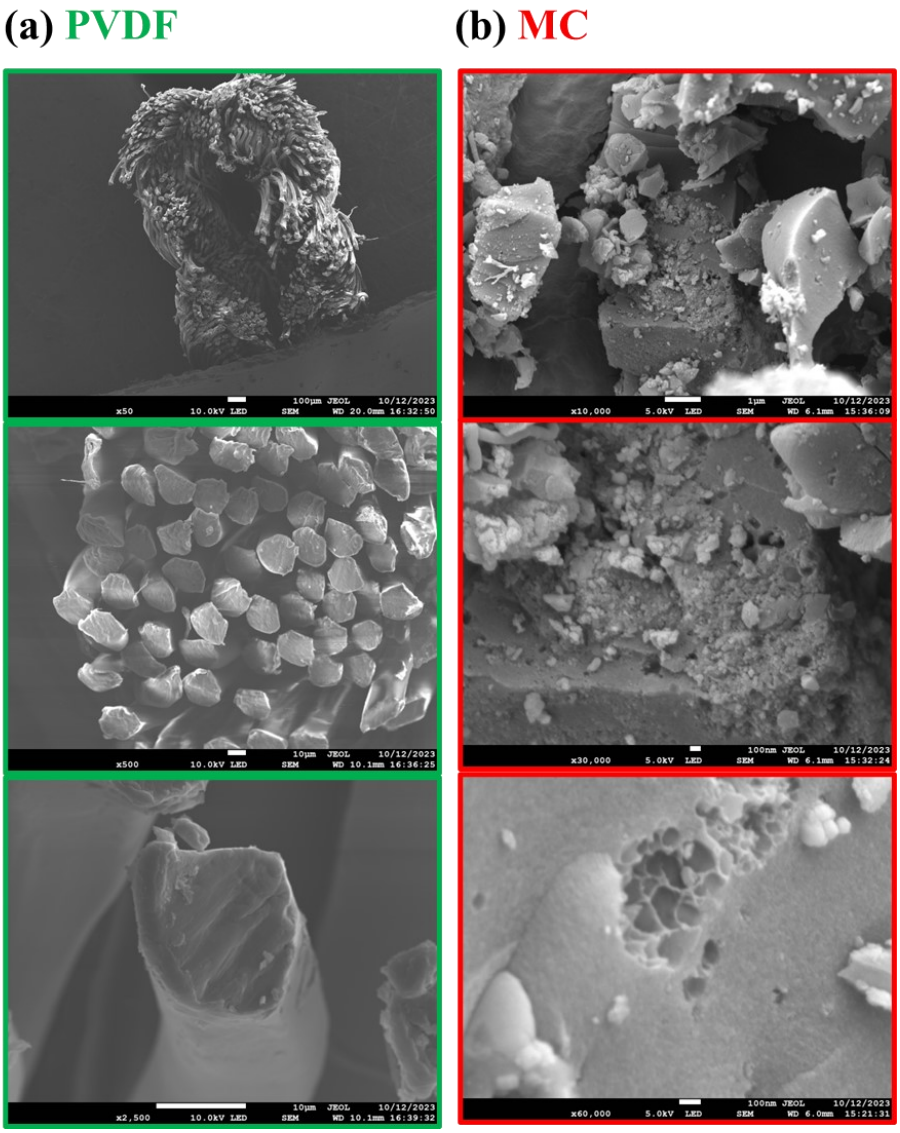

Figure 3.16 shows the EDS elemental analysis of PVDF and MC samples. From these results, C is the most abundant constituent in both samples, as C is the basic element in the PVDF polymer chain and MC. As expected, a noticeable increment in the C content (weight %) was observed after pyrolysis (MC). This increase can be attributed to the increased concentration of C in the sample due to the expulsion of F molecules, leading to a reduction from an initial value of 19.3% to 7.8%. F was released as fluoride or hydrogen fluoride molecules, which is a distinctive characteristic of PVDF, known as a fluorinated polymer. A surface area of 345 m^2/g was determined for MC through BET analysis. The total pore volume was also 0.16 cm^3/g. This high total pore volume is generally advantageous for applications requiring high gas adsorption or liquid infiltration capacity. The average pore diameter was found to be 1.8 nm, which can be categorized as microporous carbon. The surface and textural analysis of MC showed that after optimizing the pyrolysis process, the obtained material has applicability for various industrial and research purposes.

Figure 3.16 - EDS elemental analysis for PVDF and MC

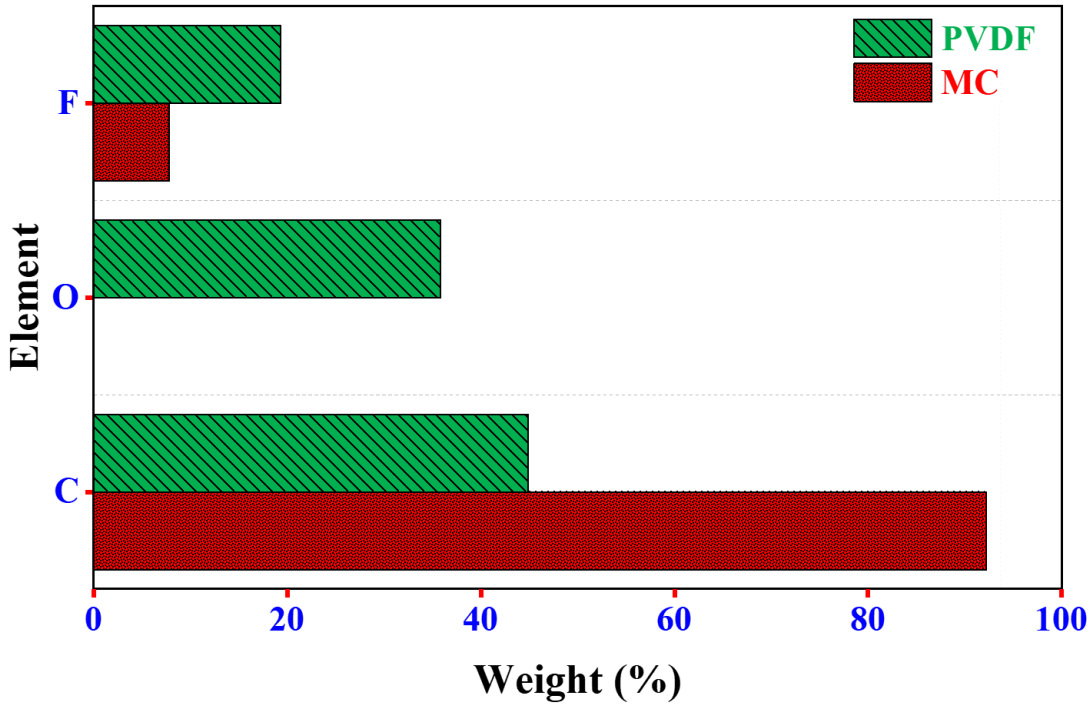

3.3.6 MC COST EVALUATION

The production of the MC by pyrolysis, using discarded PVDF ultrafiltration membranes, is a simple process, dispensing the use of expensive reagents or

sophisticated equipment. According to the results of this study, the production of MC uses moderate temperature and the scale-up of the pyrolysis can be applicable depending on the reactor capacity.

The cost estimation of the char production is an important factor in analyzing its economic viability and potential for large-scale. The cost of char mainly depends on the costs of materials, such as feedstock and reagents, and consumed energy. The detailed production costs of MC are presented in Table 3.10. The total preparation cost of MC was calculated to be 0.14 €/kg, which is a low-cost material compared to commercial chars as CAS nº 7440-44-0 from Sigma Aldrich® that costs 111 €/kg (SIGMA ALDRICH, 2024). The low synthesis cost of MC can be ascribed to the zero or low costs of feedstock and chemicals and the reduced electricity consumption (Table 3.10). Generally, the costs decrease even further when the process is applied on a larger scale to produce a higher amount of char.

Table 3.10 - Cost analysis of producing 1 kg of MC

Items	Consumed amount	Price	Total cost (€)
Materials			
PVDF fibers	3.2 kg*	Free[υ]	0.00
Sodium hypochloride (5.8%)	0.03 L[ϕ]	0.53 €/L	0.02
Energy			
Tube furnace[ϒ] (874 W/h)	1.62 kWh	0.05 €/kWh	0.08
Drying oven (425 W/h)	0.85 kWh	0.05 €/kWh	0.04
Total			0.14

(*) Calculated based on the average pyrolysis yield of 31.3%.
(υ) Collected by the authors without cost.
(ϕ) Calculated based on a 500 ppm solution.
(ϒ) Presence of nitrogen gas from the laboratory source.

3.4 CONCLUSIONS

Pyrolysis of PVDF fiber from discarded ultrafiltration membranes was studied to evaluate its potential for char production. The final temperature and residence time were optimized to enhance the adsorptive efficiency of the obtained membrane char (MC) towards iodine removal. The maximum iodine number of MC was 242.35 mg/g

under the optimized conditions of 584 ºC and 111 min. PVDF fiber and MC were extensively characterized to comprehend the polymer pyrolysis process and char properties for future applications. The TG-DTA analysis for the PVDF fiber indicated that the releasing and elimination of the fluorinated functional groups of the polymer carbon chain occur in a single step at 415 ºC with a mass loss of 80.30%. The second stage of weight loss (10.28%) in the PVDF fiber occurred after 425 ºC, attributed to an oxidative breakdown of the fluorinated polymer and the revocation of the C-F bond. The FT-IR results indicated the coexistence of β and γ phases in the crystalline structure of the PVDF fibers, reinforced by the peaks identified on Raman analysis. For the MC, the TG-DTA analysis showed the thermal stability of the carbonaceous substance and the formation of stable carbon structures like graphitic domains, confirmed by FT-IR, XRD, and Raman analyses. By the surface and textural analysis, it was possible to ensure the removal of fluoride or hydrogen fluoride molecules from the PVDF fiber and, consequently, the carbon concentration increasing on the obtained MC during the pyrolysis process. The determined MC properties of the surface area of 345 m^2/g, total pore volume of 0.16 cm^3/g, microporous character, and an estimated low cost of 0.14 €/kg are relevant to its applicability in various industrial, environmental, and research purposes.

REFERENCES

ABNT. *NBR 12073/1991 – Carvão ativado pulverizado – Determinação do número de iodo.* Associação Brasileira de Normas Técnicas, Rio de Janeiro, 1991.

ABNT. *NBR NM27/2001 - Agregados - Redução da amostra de campo para ensaios de laboratório.* Associação Brasileira de Normas Técnicas, Rio de Janeiro, 2001.

AHMAD, M. N.; ISHAK, M. R.; TAHA, M. M.; MUSTAPHA, F.; LEMAN, Z. Mechanical, thermal and physical characteristics of oil palm (Elaeis Guineensis) fiber reinforced thermoplastic composites for FDM–Type 3D printer. *Polymer Testing*, v. 120, p. 107972, 2023.

ALCHIKH, M.; FOND, C.; FRÈRE, Y. Discontinuous crack growth in poly (vinyl fluoride) by mechanochemical ageing in sodium hydroxide. *Polymer Degradation and Stability*, v. 95, n. 4, p. 440-444, 2010.

ALI, M. E.; ZAGHLOOL, E.; KHALIL, M.; KOTP, Y. H. Surface and internal modification of composite ion exchange membranes for removal of molybdate, phosphate, and nitrate from polluted groundwater. *Arabian Journal of Chemistry*, v. 15, n. 4, p. 103747, 2022.

AMER, M.; ELWARDANY, A. Biomass Carbonization. In: *Renewable Energy - Resources, Challenges and Applications.* IntechOpen, p. 211-232, 2020.

ASTM. *ASTM D4607-94 - Standard test method for determination of iodine number of activated carbon.* American Society for Testing and Materials, 1994.

ATTRI, P.; GARG, S.; RATAN, J. K.; GIRI, A. S. Comparative study using advanced oxidation processes for the degradation of model dyes mixture: Reaction kinetics and biodegradability assay. *Materials Today: Proceedings*, v. 57, p. 1533-1538, 2022.

BASU, P. *Biomass gasification and pyrolysis: practical design and* theory. Academic press, Oxford, 2010.

BRASIL. *Lei nº 12.305 de 2 de agosto de 2010.* Institui a Política Nacional de Resíduos Sólidos. Presidência da República, Brasília, 2010.

CABOT. *Norit® GAC 1240W.* In: Norit Digital Library, n. 124WD, Cabot Corporation, 2009.

CAI, X.; LEI, T.; SUN, D.; LIN, L. A critical analysis of the α, β and γ phases in poly (vinylidene fluoride) using FTIR. *RSC Advances*, v. 7, n. 25, p. 15382-15389, 2017.

CANEVAROLO JR.; SEBASTIÃO V. *Ciência dos polímeros: um texto básico para tecnólogos e engenheiros.* 3 ed., Artliber Editora, São Paulo, 2010.

CANEVAROLO JR.; SEBASTIÃO V. *Técnicas de caracterização de polímeros.* Artliber Editora, São Paulo, 2004.

CUI, Z.; HASSANKIADEH, N. T.; ZHUANG, Y.; DRIOLI, E.; LEE, Y. M. Crystalline polymorphism in poly (vinylidenefluoride) membranes. *Progress in Polymer Science*, v. 51, p. 94-126, 2015.

DA COSTA, J. S. *Cinética da degradação de PVDF reciclado por análise termogravimétrica.* Trabalho de Conclusão de Curso (Engenharia de Materiais), Universidade Federal do Rio de Janeiro, Rio de Janeiro, 2017.

DE OLIVEIRA NETO, G. C.; SHIBAO, F. Y.; GODINHO FILHO, M.; CHAVES, L. E. C. Produção mais limpa: estudo da vantagem ambiental e econômica na reciclagem de polímeros. *Interciência*, v. 40, n. 6, p. 364-373, 2015.

DE SOUZA, P. H. C. *Solar pyrolysis and electrical furnace pyrolysis of Luffa cylindrica fibers to obtain adsorbent biochar.* Dissertação (Mestrado) – Programa de Pós-graduação em Engenharia Química, Universidade Federal de Minas Gerais, Belo Horizonte, 2022.

DROBNY, J. G. *Technology of fluoropolymers.* 2 ed., CRC Press, Boca Raton, 2009.

EL-QELISH, M.; MAGED, A.; ELWAKEEL, K. Z.; BHATNAGAR, A.; ELGARAHY, A. M. Dual valorization of coastal biowastes for tetracycline remediation and biomethane production: A composite assisted anaerobic digestion. *Journal of Hazardous Materials*, v. 465, p. 133143, 2024.

ESTERLY, D. M. *Manufacturing of Poly (vinylidene fluoride) and evaluation of its mechanical properties.* Dissertação (Mestrado) - Ciência e Engenharia de Materiais, Virginia Polytechnic Institute and State University, Blacksburg, 2002.

FERNANDES, R. G. *Estudo de técnicas de recuperação de metais de resíduos de equipamentos eletroeletrônicos.* Trabalho de Conclusão de Curso (Engenharia Ambiental), Universidade de São Paulo, São Carlos, 2014.

GARCIA-NUNEZ, J. A.; PELAEZ-SAMANIEGO, M. R.; GARCIA-PEREZ, M. E.; FONTS, I.; ABREGO, J.; WESTERHOF, R. J. M.; GARCIA-PEREZ, M. Historical developments of pyrolysis reactors: a review. *Energy & Fuels*, v. 31, n. 6, p. 5751-5775, 2017.

GÜMÜŞ, H. Catalytic performance of polyvinylidene fluoride (PVDF) supported TiO2 additive at microwave conditions. *Journal of the Turkish Chemical Society Section A: Chemistry*, v. 7, n. 2, p. 361-374, 2020.

HAMAGUCHI, M.; CARDOSO, M.; VAKKILAINEN, E. Alternative technologies for biofuels production in kraft pulp mills - Potential and prospects. *Energies*, v. 5, n. 7, p. 2288-2309, 2012.

HEO, Y. J.; ZHANG, Y.; RHEE, K. Y.; PARK, S. J. Synthesis of PAN/PVDF nanofiber composites-based carbon adsorbents for CO_2 capture. *Composites Part B: Engineering*, v. 156, p. 95-99, 2019.

HONG, S. M.; LIM, G.; KIM, S. H.; KIM, J. H.; LEE, K. B.; HAM, H. C. Preparation of porous carbons based on polyvinylidene fluoride for CO2 adsorption: A combined experimental and computational study. *Microporous and Mesoporous Materials*, v. 219, p. 59-65, 2016.

IPPOLITO, J. A.; CUI, L.; KAMMANN, C.; WRAGE-MÖNNIG, N.; ESTAVILLO, J. M.; FUERTES-MENDIZABAL, T.; CAYUELA, M. L.; SIGUA, G.; NOVAK, J.; SPOKAS, K.; BORCHARD, N. Feedstock choice, pyrolysis temperature and type influence biochar characteristics: a comprehensive meta-data analysis review. *Biochar*, v. 2, n. 4, p. 421-438, 2020.

KASPAR, P.; SOBOLA, D.; ČÁSTKOVÁ, K.; KNÁPEK, A.; BURDA, D.; ORUDZHEV, F.; DALLAEV, R.; TOFEL, P.; TRČKA, T.; GRMELA, L.; HADAŠ, Z. Characterization of polyvinylidene fluoride (PVDF) electrospun fibers doped by carbon flakes. *Polymers*, v. 12, n. 12, p. 2766, 2020.

LAWLER, W.; BRADFORD-HARTKE, Z.; CRAN, M. J.; DUKE, M.; LESLIE, G.; LADEWIG, B. P.; LE-CLECH, P. Towards new opportunities for reuse, recycling and disposal of used reverse osmosis membranes. *Desalination*, v. 299, p. 103-112, 2012.

LEE, D. G.; LEE, B. C.; JUNG, K. H. Preparation of porous carbon nanofiber electrodes derived from 6FDA-Durene/PVDF blends and their electrochemical properties. *Polymers*, v. 13, n. 5, p. 720, 2021.

LEE, S. Y.; PARK, S. J. Carbon dioxide adsorption performance of ultramicroporous carbon derived from poly (vinylidene fluoride). *Journal of Analytical and Applied Pyrolysis*, v. 106, p. 147-151, 2014.

LENG, L.; HUANG, H. An overview of the effect of pyrolysis process parameters on biochar stability. *Bioresource Technology*, v. 270, p. 627-642, 2018.

LU, Q.; YANG, X. C.; DONG, C. Q.; ZHANG, Z. F.; ZHANG, X. M.; ZHU, X. F. Influence of pyrolysis temperature and time on the cellulose fast pyrolysis products: Analytical Py-GC/MS study. *Journal of Analytical and Applied Pyrolysis*, v. 92, n. 2, p. 430-438, 2011.

MAGED, A.; DISSANAYAKE, P. D.; YANG, X.; PATHIRANNAHALAGE, C.; BHATNAGAR, A.; OK, Y. S. New mechanistic insight into rapid adsorption of pharmaceuticals from water utilizing activated biochar. *Environmental Research*, v. 202, p. 111693, 2021.

MAGED, A.; ELGARAHY, A. M.; HANEKLAUS, N. H.; GUPTA, A. K.; SHOW, P. L.; BHATNAGAR, A. Sustainable functionalized smectitic clay-based nano hydrated zirconium oxides for enhanced levofloxacin sorption from aqueous medium. *Journal of Hazardous Materials*, v. 452, p. 131325, 2023b.

MAGED, A.; ELGARAHY, A. M.; HLAWITSCHKA, M. W.; HANEKLAUS, N. H.; GUPTA, A. K.; BHATNAGAR, A. Synergistic mechanisms for the superior sorptive removal of aquatic pollutants via functionalized biochar-clay composite. *Bioresource Technology*, v. 387, p. 129593, 2023a.

MANO, J. F.; LOPES, J. L.; SILVA, R. A.; BROSTOW, W. Creep of PVDF monofilament sutures: service performance prediction from short-term tests. *Polymer*, v. 44, n. 15, p. 4293-4300, 2003.

MOHAN, D.; PITTMAN JR, C. U.; STEELE, P. H. Pyrolysis of wood/biomass for bio-oil: a critical review. *Energy & Fuels*, v. 20, n. 3, p. 848-889, 2006.

OLIVEIRA JR, D. L. D. *Pirólise de resíduos plásticos visando à obtenção de produtos de alto valor agregado.* Dissertação (Mestrado) - Engenharia Química, Universidade Federal de Santa Maria, Santa Maria, 2016.

PAPUGA, S. V.; GVERO, P. M.; VUKIĆ, L. M. Temperature and time influence on the waste plastics pyrolysis in the fixed bed reactor. *Thermal Science*, v. 20, n. 2, p. 731-741, 2016.

PIVA, A. M.; BAHIENSE NETO, M.; WIEBECK, H. A reciclagem de PVC no Brasil. *Polímeros*, v. 9, p. 195-200, 1999.

PRABAKARAN, P.; MANIMUTHU, R. P.; GURUSAMY, S.; SEBASTHIYAN, E. Plasticized polymer electrolyte membranes based on PEO/PVdF-HFP for use as an effective electrolyte in lithium-ion batteries. *Chinese Journal of Polymer Science*, v. 35, p. 407-421, 2017.

RIBEIRO, M. J. P. M.; ABRANTES, J. C. C. Moagem em moinho de bolas: Estudo de algumas variáveis e otimização energética do processo. *Cerâmica Industrial*, v. 6, n. 2, p. 7-11, 2001.

SAWANT, S. R.; KALLA, S.; MURTHY, Z. V. P. Enhanced properties of the PVDF membrane with carboxylated MWCNT and sodium alginate for membrane distillation. *Journal of Environmental Chemical Engineering*, v. 11, n. 2, p. 109259, 2023.

SIGMA ALDRICH. *Charcoal activated*, 2024. Disponível em: < https://www.sigmaaldrich.com/FI/en/search/activated-charcoal?focus=products&page=1&perpage=30&sort=relevance&term=activated-charcoal&type=product>. Acesso em: 10 abril 2024.

SOBOLA, D.; KASPAR, P.; ČÁSTKOVÁ, K.; DALLAEV, R.; PAPEŽ, N.; SEDLÁK, P.; ...; HOLCMAN, V. PVDF fibers modification by nitrate salts doping. *Polymers*, v. 13, n. 15, p. 2439, 2021.

SON, I. S.; OH, Y.; YI, S. H.; IM, W. B.; CHUN, S. E. Facile fabrication of mesoporous carbon from mixed polymer precursor of PVDF and PTFE for high-power supercapacitors. *Carbon*, v. 159, p. 283-291, 2020.

SPINACÉ, M. A. D. S.; DE PAOLI, M. A. A tecnologia da reciclagem de polímeros. *Química Nova*, v. 28, p. 65-72, 2005.

SUEZ. *Membranas de fibra oca de ultrafiltração ZeeWeed*. SUEZ Water Technology & Solutions, 2021. Disponível em: <https://www.suezwatertechnologies.com.br/products/zeeweed-ultrafiltration>. Acesso em: 03 novembro 2021.

VAN DE VELDEN, M.; BAEYENS, J.; BREMS, A.; JANSSENS, B.; DEWIL, R. Fundamentals, kinetics and endothermicity of the biomass pyrolysis reaction. *Renewable Energy*, v. 35, n. 1, p. 232-242, 2010.

VIDAL, D. B. *Estudo da influência das condições de pirólise de compósito de PEBD/Al na produção de hidrocarbonetos.* Dissertação (Mestrado) – Programa de Pós-graduação em Energia, Universidade Federal do Espírito Santo, São Mateus, 2017.

XU, B.; HOU, S.; CHU, M.; CAO, G.; YANG, Y. An activation-free method for preparing microporous carbon by the pyrolysis of poly (vinylidene fluoride). *Carbon*, v. 48, n. 10, p. 2812-2814, 2010.

YAMASHITA, J.; SHIOYA, M.; KIKUTANI, T.; HASHIMOTO, T. Activated carbon fibers and films derived from poly (vinylidene fluoride). *Carbon*, v. 39, n. 2, p. 207-214, 2001.

ZANARDINI, M. H. *Cinética da conversão térmica na pirólise de compósitos de polietileno/alumínio.* Dissertação (Mestrado) - Engenharia Mecânica, Universidade Tecnológica Federal do Paraná, Ponta Grossa, 2019.

ZHANG, J.; LIU, J.; LIU, R. Effects of pyrolysis temperature and heating time on biochar obtained from the pyrolysis of straw and lignosulfonate. *Bioresource Technology*, v. 176, p. 288-291, 2015.

CHAPTER 4 - MEMBRANE CHAR-BENTONITE COMPOSITE PRODUCTION AND CHARACTERIZATION

4.1 LITERATURE REVIEW

Hagemann *et al.* (2018), in a review of the definitions, uses, and production of pyrogenic carbonaceous materials (PCMs), such as activated char, listed numerous possibilities for combining thermochemical processes between them and with non-thermal pre- and post-treatments in the production stage of these materials. Among the thermochemical treatments for converting the raw material are pyrolysis, discussed in Chapter 3 of this thesis, activation, and modification. Non-thermal pre- and post-treatments commonly used in the production of PCMs are washing, coating or impregnation, and mixing.

Activation aims to increase the concentration of pores in the char, its surface area, and adsorptive capacity, preserving the size and other characteristics of these pores inherent to the raw material used. Generally targeted according to the characteristics of the char, activation can be achieved either simultaneously with the pyrolysis process, in one-step activation, or after pyrolysis, in two-step activation (AMER & ELWARDANY, 2020; HAGEMANN *et al.*, 2018; LOZANO-CASTELLO *et al.*, 2001; SONG *et al.*, 2013).

The chemical modification of the char surface is the introduction of non-carbon portions on the surface of the char also to increase its adsorption capacity. The modification of an adsorbent can be carried out after or in place of the activation process, for specific adsorbate removal purposes (BHATNAGAR *et al.*, 2013; HAGEMANN *et al.*, 2018; RIVERA-UTRILLA *et al.*, 2011).

The mixture is a post-treatment that combines PCMs with other materials to produce the composites. This treatment aims to unite the different chemical characteristics of two or more materials to produce a composite with more interesting properties for application as an adsorbent (HSISSOU *et al.*, 2021; FARIKOV, 2013).

4.1.1 CHAR ACTIVATION

Physical and chemical methods are commonly used for char activation, giving different characteristics to the activated char produced (HAGEMANN *et al.*, 2018; LOZANO-CASTELLO *et al.*, 2001; SONG *et al.*, 2013).

Chemical activation is usually carried out before the pyrolysis step using dehydrating agents. Potassium hydroxide (KOH), zinc chloride ($ZnCl_2$), phosphoric (H_3PO_4) and sulfuric (H_2SO_4) acids are commonly used chemical dehydrating agents. These agents favor carbonization and the achievement of the desired porosity, being removed as residues at the end of the thermal treatment. Compared to physical activation, the chemical method is faster and occurs under lower temperatures, producing char with a higher surface area. In addition, dehydrating agents have dehydrogenation properties, being able to inhibit the formation of volatile by-products typical of pyrolysis, such as tar, and thus favor the yield of char (HAGEMANN *et al.*, 2018; LOPES *et al.*, 2013; LOZANO-CASTELLO *et al.*, 2001; SONG *et al.*, 2013).

On the other hand, the physical activation consists of the oxidation of the previously carbonized raw material through its contact with an activating agent at temperatures between 800 and 1000 °C. Oxidative gases such as carbon dioxide, water vapor, and air are applied as activating agents, among which water vapor is most commonly used and a combination of these agents is also possible. To develop the porous structure of the material, carbon atoms from inside the pores are selectively removed by the oxidative process (AHMADPOUR & DO, 1996; HAGEMANN *et al.*, 2018; LOZANO-CASTELLO *et al.*, 2001; SONG *et al.*, 2013). According to Amer & Elwardany (2020), the overheated activating agent performs two main functions during activation. The first is to isolate the char from the oxidative environment by ensuring that it does not burn. The second is to remove the tar residue that is blocking the finely structured pores within the char.

- *Activation of PVDF char*

Based on the relevant literature, the activation of PVDF char was investigated in only two works, whose objective was the production of adsorbents (TABLE 3.3). Using pure

PVDF or combined with other compounds as precursors, the studies have evaluated physical activation techniques.

Yamashita *et al.* (2001) aimed to evaluate the adsorption of methylene blue by comparing the use of PVDF fibers and films with and without dehydrofluorination. The authors used CO_2 at 500 cm^3/min and 850 °C to activate the pyrolyzed material. The activated char film produced reached an adsorption capacity of 538 mg/g for methylene blue.

Heo *et al.* (2018) also activated the porous char obtained from the hybrid composite of polyacrylonitrile (PAN) and PVDF for its application as a CO_2 adsorbent. The authors used steam at 900 °C and 5 mL/h for 60 min and a pressure of 1.2 bar. The pyrolyzed and activated material exhibited a reversible and satisfactory CO_2 adsorption performance of 2.21% by weight.

4.1.2 CHAR MODIFICATION

Char modification techniques can be grouped into oxidation, sulphuration, nitrogenization or ammonification, and coordinated ligand anchoring (BHATNAGAR *et al.*, 2013; HAGEMANN *et al.*, 2018; RIVERA-UTRILLA *et al.*, 2011).

Modification by oxidation is usually carried out using hydrogen peroxide (H_2O_2), nitric acid (HNO_3), or ozone (O_3) at low temperatures, between 25 and 100 °C. It is mainly aimed at creating oxidized functional groups on the char surface. This modification technique tends to impair the porous structure of char, decreasing its specific surface area and pore volume (HAGEMANN *et al.*, 2018; RIVERA-UTRILLA *et al.*, 2011).

Sulphuration and nitrogenization are modification techniques whose objective is to increase the basic character and, consequently, the polarity of the char surface, favoring the adsorption of polar pollutants. The use of sulfur dioxide (SO_2) or hydrogen sulfide (H_2S) in char modification also favors the adsorption capacity of mercury, while ammonia (NH_3) can be applied for copper removal. Like oxidative techniques, sulfur modification can reduce char porosity (HAGEMANN *et al.*, 2018; RIVERA-UTRILLA *et al.*, 2011).

Finally, coordinated binder anchoring, or simply impregnation, can be a chemical modification technique of the char surface or a non-thermal pre- or post-treatment step in char production, depending on the production step application and the applied temperature. It is based on the compound removal through the formation of complexes between the adsorbate and the binder impregnated in the char. Several compounds can be impregnated and used as extra specific sites for the adsorption of a given compound, modifying the textural and chemical properties of char (BHATNAGAR *et al.*, 2013; HAGEMANN *et al.*, 2018; RIVERA-UTRILLA *et al.*, 2011).

- *Char modification for pharmaceuticals removal*

Some studies about the modification of chars for the removal of pharmaceuticals, mainly by acid activating and magnetizing techniques associated or not with the thermal treatment of the material, have been published, as exemplified in Chart 4.1.

Chart 4.1 - Some studies on the modification of adsorbents for the removal of pharmaceuticals

Adsorbent	Modification	Pharmaceutical	Reference
Biochar from rice husk and biochar-clay mineral composite	Activating by carbon dioxide (CO_2)	Ciprofloxacin	Arif *et al.* (2022)
Biochar from shells of *Hairy Sterculia (Sterculia villosa)*	Acid activating by phosphoric acid (H_3PO_4) and magnetizing by co-precipitation with iron chloride ($FeCl_3$) and iron sulfate ($FeSO_4$)	Ciprofloxacin	Kumar *et al.* (2022)
Biochar from pinewood	Activating by potassium hydroxide (KOH) and impregnation with copper oxide (CuO)	Ciprofloxacin and Carbamazepine	Xue *et al.* (2022)
Biochar from coffee bean waste	Acid activating by phosphoric acid (H_3PO_4)	Diclofenac and Levofloxacin	Maged *et al.* (2021)
Biochar from *Sour Cherry (Prunus cerasus)* stalk waste	Acid activating by phosphoric acid (H_3PO_4)	Ciprofloxacin	Sayin, Akar & Akar (2021)
Biochar from sugarcane bagasse	Impregnation with gallium nitrate ($Ga(NO_3)_3$ and activating by hydrogen sulfide (H_2S)	Ciprofloxacin	Zheng *et al.* (2021)
Biochar from municipal sludge	Acid activating by phosphoric acid (H_3PO_4) and magnetizing by co-precipitation with zinc chloride ($ZnCl_2$) and iron chloride ($FeCl_3$)	Ciprofloxacin, Norfloxacin and Ofloxacin	Ma *et al.* (2020)

Source: The author herself

Kumar *et al.* (2022) chemically activated the shells of Hairy Sterculia (*Sterculia villosa).* using 88% phosphoric acid (H_3PO_4) solution and the biochar was prepared by carbonization at 400 °C in a muffle furnace. The biochar magnetizing was done using the technique of co-precipitation with iron chloride ($FeCl_3$), iron sulfate ($FeSO_4$), and a 5 M solution of sodium hydroxide (NaOH). The biochar modification effect was evaluated on the removal of ciprofloxacin and a maximum Langmuir model adsorption capacity of 81.97 mg/g was found. The authors highlighted the possibility of separating the adsorbent from a solution using an external magnetic field due to the impregnation of iron particles.

For the acid activating of biochar from coffee bean waste, Maged *et al.* (2021) also used phosphoric acid (H_3PO_4), but a 50% solution was used, it was applied after the raw material carbonization and it was followed by a thermally activating in a muffle furnace at 550°C for 90 min under N_2 atmosphere. The modified biochar potential as an adsorbent for diclofenac and levofloxacin removal was evaluated through experiments using batch and continuous operation modes. This modification methodology found Langmuir model adsorption capacities of 61.17 mg/g for DF and 110.70 mg/g for LVX.

The acid activating by phosphoric acid (H_3PO_4) was also used in the research of Sayin, Akar & Akar (2021) for the modification of biochar from Sour Cherry (*Prunus cerasus)* stalk waste and presented a high adsorption capacity of 410.06 mg/g for ciprofloxacin removal. The raw material was put in contact with the H_3PO_4 solution, in different mass ratios, before its pyrolysis on a tube furnace.

Ma *et al.* (2020) investigated the municipal sludge biochar modification by magnetizing with iron/zinc (Fe/Zn), activating with phosphoric acid (H_3PO_4), and by the combination of both (Fe/Zn + H_3PO_4). First, the authors made the pyrolysis of the raw material, and then, zinc chloride ($ZnCl_2$) and iron chloride ($FeCl_3$) were used in the magnetizing methodology with an 85% phosphoric acid (H_3PO_4) solution being the reagent applied to acid-activating. The modification methodologies were followed by another pyrolysis stage and by thermally activating processes in a muffle furnace at 450°C for 60 min, respectively. The combination of both was reached by applying the magnetizing methodology to the biochar pre-acid activated. The last modified biochar presented the

highest removal of ciprofloxacin, norfloxacin, and ofloxacin from the water with maximum adsorption capacities of 83.7, 39.3, and 25.4 mg/g, respectively.

Due to some technical similarities and despite the different objectives, activation and modification are often used synonymously.

4.1.3 COMPOSITES

The choice of raw materials used in synthesizing a composite depends mainly on the application to be given to it. In the case of adsorbent composites, materials capable of conferring characteristics such as porosity, surface area, and affinity for the adsorbate are prioritized. These compounds are usually classified according to their function in the composite formulation. The presence of substances capable of maintaining the composite structure, in addition to binding its components, is essential. The materials that give the composites the extra desired properties are called additives (HSISSOU *et al.*, 2021; FARIKOV, 2013).

- *Composites for pharmaceuticals removal*

Several studies have been documented regarding the composite production intended for use as adsorbents to remove pharmaceuticals. This is exemplified in Chart 4.2.

Chart 4.2 - Some studies on the production of composites for pharmaceutical removal by adsorption

Composite	Pharmaceutical	Reference
Corncob-based activated carbon (AC) + Titanium dioxide (TiO_2)	Ceftriaxone	Abdullah *et al.* (2023)
Bentonite + Chitosan	Doripenem, Ampicillin, and Amoxicillin	Bouaziz *et al.* (2023)
Silica (SI) + Poly(ethyleneimine) (PEI) + Poly(sodium methacrylate) (PMAA) or Polyacrylic acid (PAA)	Diclofenac	Fighir *et al.* (2023)
Calcium alginate + Activated carbon	Ibuprofen and Diclofenac	Wasilewska & Deryło-Marczewska (2022)
Sodium alginate (SA) + H_3PO_4 activated corncob-based biochar (PB)	Ciprofloxacin	Chen *et al.* (2021)
Generation-5 polyamidoamine (G-5 PAMAM) + Graphene oxide (GO) + Amine functionalized silica mesoporous (SBA-15-NH_2)	Ciprofloxacin, Ivermectin, and Tetracycline	Xikhongelo *et al.* (2021)
Iron oxide (Fe_3O_4) + Activated carbon (AC) + β-Cyclodextrin (CD) + Sodium alginate (SA)	Norfloxacin and Ciprofloxacin	Yadav *et al.* (2021)
Nanotitanium oxide-chitosan ($NTiO_2$-Chit) + Nanotitanium oxide-bentonite ($NTiO_2$-Bent)	Levofloxacin and Ceftriaxone	Mahmoud *et al.* (2020)
Calcium (Ca(II)) + Chitosan + β-Cyclodextrin	Paracetamol	Rahman & Nasir (2020)

Source: The author herself

Some materials, natural and synthetic, can be observed with a certain frequency in the composites produced in the studies presented in Chart 4.2.

Activated carbons are commonly used in the synthesis of adsorbent composites, as they alone can satisfactorily provide the final product with the desired porosity and surface area. Commercial activated carbons (Yadav *et al.* (2021) and Wasilewska & Deryło-Marczewska (2022)), and char produced from alternative raw materials such as corncob (Abdullah *et al.* (2023) and Chen *et al.* (2021)), can be used in composites production.

Chitosan (Bouaziz *et al.* (2023), Mahmoud *et al.* (2020), and Rahman & Nasir (2020)), Bentonite (Bouaziz *et al.* (2023) and Mahmoud *et al.* (2020)), and Silica (Fighir *et al.*, (2023) and Xikhongelo *et al.* (2021)) are natural materials also widely consumed in the manufacture of adsorbent composites.

Compounds such as β-cyclodextrin and sodium and calcium alginates are often used as complexing agents (Rahman & Nasir (2020) and Yadav *et al.* (2021)) and stabilizing, thickening, and/or gelling agents (Chen *et al.* (2021), Wasilewska & Deryło-Marczewska (2022) and Yadav *et al.* (2021)), respectively.

- *Bentonite*

Clay minerals, or simply clays, are inorganic materials, natural and abundant throughout the world. Some examples of clays include bentonite, kaolinite, illite, zeolite, and smectite. Alone, clays are widely applied as adsorbents for removing various contaminants due to properties such as substantial specific surface area, pore volume, negative surface charge, and hydrophilic surface (MAGED *et al.*, 2020a; MAGED *et al.*, 2020b).

Bentonite is an inorganic clay mineral, with a layered structure, of the 2:1 type and originating from the weathering of volcanic ash. It is mainly composed of montmorillonite and its quality is directly associated with the content of this other mineral component. Other clay materials, such as illite, kaolinite, and chlorite, and non-clay materials, such as silica, quartz, and feldspar, can also compose bentonite (ABDOU, AL-SABAGH & DARDIR, 2013; MAGED *et al.*, 2020b).

Individually, bentonite is already known as a great adsorbent, evaluated in several recent studies, and reaching until 99% adsorption efficiency for removing different pollutants (MAGED *et al.*, 2023b). Thus, bentonite is widely used as a raw material for composites due to its ability to enhance the performance of the new material by adding its adsorption capacity, and also because of its low cost and high availability worldwide (ABDOU, AL-SABAGH & DARDIR, 2013; MAGED *et al.*, 2020b).

4.2 MATERIAL AND METHODS

4.2.1 MEMBRANE CHAR PRODUCTION

The membrane char (MC) submitted to the preliminary modification tests and to the synthesis of the membrane char-bentonite composite (MCBT) was produced from

PVDF fibers previously cleaned and fragmented (CHAPTER 3, SECTION 3.2.1). These PVDF fibers were pyrolyzed in a stainless-steel tubular reactor of the fluidized bed type (SECTION 3.2.4) in batches of about 100 g under the optimal final temperature of 584°C for the optimal residence time of 111 min, as optimized and validated in Chapter 3 of this study.

The MC produced in all batches was mixed, comminuted to below 100#, and, to remove the fines adhered to the surface of the particles, was washed 4 times with distilled water in the proportion 250:1 (grams of char:liters of distilled water) and dried in a Biobase oven (BJPX - Spring) at 120 °C for 2 hours.

4.2.2 PRELIMINARY REMOVAL TESTS

Based on its simplicity and concern as a pollutant in several countries, including Brazil (VELÁSQUEZ *et al.*, 2007), fluoride (F^-) was chosen for the preliminary adsorption tests using MC. Naturally present in groundwater, fluoride ions have a two-sided relationship with human health, one beneficial and the other harmful. Fluorine (F), the element from which these ions originate, is a fundamental trace element for the human body, mainly in the formation of tooth enamel and the mineralization of bones. However, its indiscriminate use poses risks to human health, from dental and skeletal fluorosis to gastrointestinal symptoms and brain damage (ALI *et al.*, 2016; EDMUNDS & SMEDLEY, 2013; ZUO *et al.*, 2018).

A factorial design of experiments was used to evaluate the effects of the independent variables MC dosage (D), initial concentration of fluoride (C_0), and Falcon tube volume (V) on the final concentration of fluoride (dependent variable). The factorial design of experiments was performed in 2 levels and 3 factors (2^3), without central points, generating a total of 8 tests into cubic points. The levels evaluated for the independent variables were defined based on:

- In the MC dosages evaluated in possible subsequent tests: 1, 3, and 5 g/L or 5, 10, and 15 g/L.

- At the fluoride content of 10 mg/L found by Velásquez *et al.* (2007) in Verdelândia/MG, Brazil.
- In the possibility of fluoride release by MC due to the presence of this element in the PVDF structure.
- Due to possible effects of the Falcon tube volume under the agitation of the solution and, consequently, under the contact of the MC with the fluoride and the removal efficiency.

The conditions of the independent variables D, C_0, and V for the cubic (levels -1 and +1) points of the factorial design of experiments are shown in Table 4.1.

Table 4.1 - Experimental conditions of MC dosage (D), initial concentration of fluoride (C_0), and Falcon tube volume (V) for the cubic points

Independent variables	Levels	
	-1	$+1$
D (g/L)	3.0	10.0
C_0 (mg/L)	0.0	10.0
V (mL)	15	50

The adsorption tests were carried out in Falcon tubes of a certain volume (V), containing the MC dosage (D) and 10 mL of the fluoride solution with the initial concentration (C_0), as established by the experimental design. The 10 mg/L fluoride solution was prepared from the inorganic salt sodium fluoride (NaF). Distilled water was used as the 0 mg/L fluoride solution. The Falcon tubes were kept under agitation in a shaker at 200 rpm for 24 hours at 30 °C, then each sample was filtered through qualitative filter paper and the fluoride concentration was measured by a specific ion electrode using TISAB II solution. The same tests were carried out using CABOT's commercial activated char NORIT® GAC 1240W, for comparison purposes.

- *Membrane char washing tests*

Washing tests were performed using sodium hydroxide (NaOH) solutions at various concentrations, MC-to-solution ratios, and contact times to remove any remaining fluoride molecules from the MC structure. Single and multiple washes (up to 6 times)

were carried out using 0.25 and 0.5 M NaOH solutions with MC dosages of 100 and 200 g/L, for 1 and 2 hours. The preliminary fluoride removal tests were repeated. All experiments were performed in triplicate.

4.2.3 PRELIMINARY MODIFICATION/COMPOSITE SYNTHESIS TESTS

Some preliminary tests of MC modification and MC-based composite synthesis were carried out to understand its applicability as an adsorbent material. Different methodologies from the literature were adapted, combined, and are presented in Chart 4.3.

Chart 4.3 - Preliminary MC modification and MC-based composite synthesis tests

Modification	Methodology	Reference
MC acid activation (AMC)	• 75% phosphoric acid (H_3PO_4) and MC (1:4 w/v ratio) • Magnetic stirring for 5 h at 80 °C • Hot water bath for 2 h at 50 °C • Filtration and drying • Furnace for 111 min at 584ºC (heating 5º C/min and atmosphere 0.06 L/min of N_2) • Cooling to room temperature, washing, and drying at 105 °C.	Kumar *et al.* (2022), Ma *et al.* (2020) and Maged *et al.* (2021)
MC magnetization or co-precipitation (MMC)	• 3.33 g of iron chloride ($FeCl_3$), 1.83 g of iron sulfate ($FeSO_4$), 2.5 g of MC and 100 mL of distilled water • Magnetic stirring for 1 h at 80 °C • 30 mL (stepwise) of 3M sodium hydroxide (NaOH) • Magnetic stirring for 5 h at 80 °C • Decantation, supernatant discard, washing, and drying at 105 °C.	Kumar *et al.* (2022) and Ma *et al.* (2020)
MC alkali-acid activation (AAMC)	• 200 mL of 2M sodium hydroxide (NaOH) and 2 g of MC • Magnetic stirring for 1 h at 90 °C • Hot water bath + Sonication for 2 h at 50 °C • Filtration, washing, and drying • 200 mL of 65% nitric acid (HNO_3) and 2 g of MC • Magnetic stirring for 1 h at room temperature • Filtration, washing, and drying at 105 °C.	Tang *et al.* (2018)
MC-Fe-Chitosan composite	• 0.5 g of chitosan and 100 mL of distilled water • Magnetic stirring for 1 h at room temperature • 4 g of iron chloride ($FeCl_3$), 2 g of iron sulfate ($FeSO_4$) and 100 mL of distilled water • Magnetic stirring for 10 min at room temperature • 100 mL of chitosan suspension, 100 mL of iron solution and 1 g of MC • Sonication for 1 h at room temperature • 10 mL of 8M ammonium hydroxide (NH_4OH_4) • Magnetic stirring for 1 h at 50 °C temperature • Magnetic separation, washing, and drying at 60 °C.	Danalıoğlu *et al.* (2017)

Adsorption tests using the modified MC samples and MC-based composite were carried out in glass bottles containing 50 mg of adsorbent (AMC, MMC, AAMC, or MC-Fe-Chitosan) and 50 mL of 30 ppm solution of different adsorbates (dyes or pharmaceuticals). The bottles were kept under agitation in a shaker at 200 rpm for 24 hours at room temperature. Then, each sample was filtered through syringe filters, and

the absorbate final concentration was measured with a UV–vis spectrophotometer at the appropriate wavelength.

4.2.4 MEMBRANE CHAR-BENTONITE COMPOSITE PRODUCTION

The membrane char-bentonite composite (MCBT) was prepared in a mass ratio 3:1 (MC:BT) using mixture operations and thermal treatments. Thus, 5 g of bentonite (BT) was added to 400 mL of distilled water and kept under ultrasonication for 1 hour at room temperature to produce a homogenous suspension. Stepwise, 15 g of MC was added to the BT suspension and magnetic stirred for 4 hours. The composite was separated from the liquid fraction by centrifugation, dried at 80°C overnight, and ground to below 100#. A thermal heating treatment was applied to the composite in a muffle furnace for 30 min at 450 °C achieved with a heating rate of 10 °C/min. After naturally cooling to 120°C, the composite was removed from the muffle furnace and subjected to a thermal shock in 400 mL of water at 5°C for 15 min. Finally, the MCBT was separated by centrifugation, dried at 80 °C overnight, and ground to below 100#.

4.2.5 MCBT CHARACTERIZATION STUDIES

Thermogravimetric analysis (TGA) of MCBT was performed on a NETZSCH TG thermal analyzer at a heating rate of 5 °C/min. The functional groups of the MCBT sample were studied using Fourier transform infrared spectroscopy (FTIR) on a JASCO FTIR 4600 Japan. The crystalline structure of the MCBT was evaluated using X-ray powder diffraction (XRD) analysis on a diffractometer (Shimadzu, LabX XRD-6100) with Cu-Kα monochromatic radiation wavelength (λ) of 1.5405 Å, accelerating voltage of 40 kV, and 30 mA current, from 3 to 35° on the 2θ angle. The structural features of the MCBT sample were characterized by Raman spectroscopy (LabRam ARAMIS IR2). The surface area, pore size, and pore volume were obtained from the N_2 adsorption-desorption isotherm data obtained by Tristar® II Plus. The surface morphology and elemental distribution of the MCBT were studied by scanning electron microscope with integrated energy dispersive X-ray spectroscopy (SEM-EDS) on a Schottky FE-SEM/JEOL 7900 JSM-F.

4.2.6 MCBT COST EVALUATION

The cost estimation for MCBT production was determined by the sum of feedstock/reagents expenses and energy consumption costs (MAGED *et al.*, 2023a). The cost of MC was determined in Section 3.3.6 (CHAPTER 3), the price of bentonite is neglected (free) and no chemicals were used during the synthesis process. The energy consumption cost of the MCBT composite production was calculated for each electrical equipment utilized using the consumed power (kW), the device factor load (0.5 for half-operation mode and 1.0 for full-operation mode), the operated time (h), and the energy price (0.05 €/kWh) (MAGED *et al.*, 2023b).

4.3 RESULTS AND DISCUSSION

4.3.1 PRELIMINARY FLUORIDE REMOVAL TESTS

The results of the final concentration of fluoride and the amount of fluoride released per gram of MC in the factorial design experiments for preliminary evaluation of the effects of the factors MC dosage (D), initial fluoride concentration (C_0), and Falcon tube volume (V) are shown in Table 4.2.

Table 4.2 - Final fluoride concentration and amount of fluoride released in the preliminary tests using MC

Test	MC dosage (g/L)	Initial fluoride concentration (mg/L)	Falcon tube volume (mL)	Final fluoride concentration (mg/L)	Amount of fluoride released (mg/g)
1	3.0	0.0	15	6.55	2.17
2	3.0	0.0	50	6.58	2.18
3	10.0	0.0	15	16.16	1.61
4	10.0	0.0	50	20.01	2.00
5	3.0	10.0	15	16.78	1.76
6	3.0	10.0	50	17.71	2.07
7	10.0	10.0	15	25.57	1.41
8	10.0	10.0	50	29.30	1.78

Analyzing Table 4.2, it is possible to verify the release of fluoride by the MC in all tests, since the final concentration is higher than the initial one. Thus, it was possible to calculate the amount of fluoride released per mass unit of MC, in mg/g, also available in Table 4.2.

The release of fluoride by MC can be justified by the presence of fluorine in the structure of PVDF, the raw material used in the production of MC, as presented in the characterization studies in Section 3.3.5. During pyrolysis, fluorine molecules may not have been expelled from the carbon chain of the PVDF fibers and, when in contact with the aqueous solution, have become soluble in water.

The significance of the effects of the variables can be verified by comparing the t-value of each variable with the critical t-value calculated for a confidence level of 95% (α = 0.05). When the t-value is greater than the critical t-value, it is assumed that the effect of the independent variable on the dependent variable is significant.

In this sense, only the effects of the factors MC dosage and initial fluoride concentration are significant on the final fluoride concentration. This is an expected result since the more MC is added and the higher the initial fluoride concentration, the higher the final concentration should be, adding the initial and released amounts of fluoride. The effect of the Falcon tube volume was not significant for the rotation of 200 rpm applied in the tests. Finally, the interactions between the variables were also not significant.

Regarding the amount of fluoride released, none of the independent variables or interactions between them show significant effects. This analysis corroborates the expectation since when calculating the amount of fluoride released, the initial concentration is subtracted and divided by the MC dosage. Thus, assuming that the average amount of fluoride released by the MC was 1.87±0.28 mg/g, the MC washing tests with sodium hydroxide (NaOH) solution were performed.

The results of the final concentration of fluoride and the percentage removal of fluoride in the factorial design experiments using CABOT as the adsorbent are shown in Table 4.3.

Table 4.3 - Final fluoride concentration and fluoride removal in the preliminary tests using CABOT

Test	CABOT dosage (g/L)	Initial fluoride concentration (mg/L)	Falcon tube volume (mL)	Final fluoride concentration (mg/L)	Fluoride removal (%)
1	3.0	0.0	15	0.06	*
2	3.0	0.0	50	0.07	*
3	10.0	0.0	15	0.01	*
4	10.0	0.0	50	0.09	*
5	3.0	10.0	15	8.07	19.3
6	3.0	10.0	50	7.60	24.0
7	10.0	10.0	15	7.06	29.4
8	10.0	10.0	50	6.95	30.5

(*) Initial fluoride concentration equal to zero mg/L.

As expected, CABOT, in addition to not releasing fluoride, was capable of removing it (TABLE 4.3). The minimum final concentrations of fluoride observed in tests with an initial concentration equal to zero should not be considered as fluoride release since this was the concentration found in the distilled water used in the tests, in addition to being an error value associated with proximity to the lower limit of the quantification method. At the initial fluoride concentration of 10 mg/L, CABOT removed 25.8±0.1% of fluoride on average, with no significant effects of any of the independent variables or interactions between them. This average removal achieved by CABOT was not enough to adapt the fluoride concentration to the minimum of 1.5 mg/L required by legislation (WHO, 2008; BRASIL, 2021). Therefore, in possible subsequent tests, higher MC dosages, of 5, 10, and 15 g/L or more, should be evaluated.

The effect of the Falcon tube volume was not significant at 200 rpm for both the MC and CABOT. In this sense, possible future adsorption tests could be carried out in 15 mL Falcon tubes, optimizing the use of available space in the shaker without compromising removal efficiency.

Despite the efficiency of the NaOH application on the regeneration of adsorbents saturated with fluoride pointed out in the literature (NIGRI, 2016), its use as a washing agent significantly reduced the amount of fluorine released by the MC, but not completely. After conducting the various washing methodologies, varying NaOH concentration, MC-to-solution ratio, and contact time, the adsorption tests showed that the MC still released, on average, 0.23 mg/g of fluoride in the aqueous solution.

4.3.2 PRELIMINARY MODIFICATION/COMPOSITE SYNTHESIS TESTS

The results of adsorption capacity and efficiency removal of the adsorbents produced in the preliminary modification and composite synthesis tests are shown in Table 4.4.

Table 4.4 - Adsorption capacity and efficiency removal of the adsorbents produced in the preliminary MC modification and MC-based composite synthesis tests

Adsorbent	Adsorbate	Adsorption capacity (mg/g)	Efficiency removal (%)
MC acid activation (AMC)	Ciprofloxacin	9.1	32.3
	Methylene blue	3.3	0.9
	Acid orange	2.0	0.6
MC magnetization or co-precipitation (MMC)	Ciprofloxacin	9.4	32.1
	Methylene blue	1.0	10.7
	Acid orange	2.6	26.2
MC alkali-acid activation (AAMC)	Ciprofloxacin	0.3	1.6
	Tetracycline	1.1	4.4
MC-Fe-Chitosan composite	Ciprofloxacin	6.7	1.9
	Tetracycline	55.6	14.9
	Acid orange	94.2	26.5

The results of the adsorption tests in Table 4.4 did not show promising results. However, comparing the adsorbent materials produced via activation with the adsorbent composite, it was decided to continue the study with the synthesis of an MC-based composite.

4.3.3 MCBT CHARACTERIZATION STUDIES

- *Thermogravimetric (TG-DTG) analysis*

Figure 4.1 presents TG-DTG curves to examine the thermal characteristics, degradation kinetics, and decomposition patterns of MCBT. The TG-DTG curves illustrate the weight loss of MCBT as a function of temperature. The main result obtained from the TG-DTG analysis of the MCBT composite revealed a weight loss of 11.38% at 415 ºC, coupled with a small exothermic peak at the same temperature and

a subsequent substantial endothermic peak around 620 ºC in the DTA curve. The observed weight loss at 415 ºC indicates a significant thermal event, signifying the decomposition of the MCBT components (MC and bentonite). This loss is normally attributed to the removal of volatile components such as residual or adsorbed moisture commonly found in carbonaceous materials. The small exothermic peak at this temperature suggests that the decomposition process is accompanied by a release of energy, possibly indicative of the initial stages of combustion or oxidation of the organic components within the MC.

Figure 4.1 - TG/DTG curves of MCBT

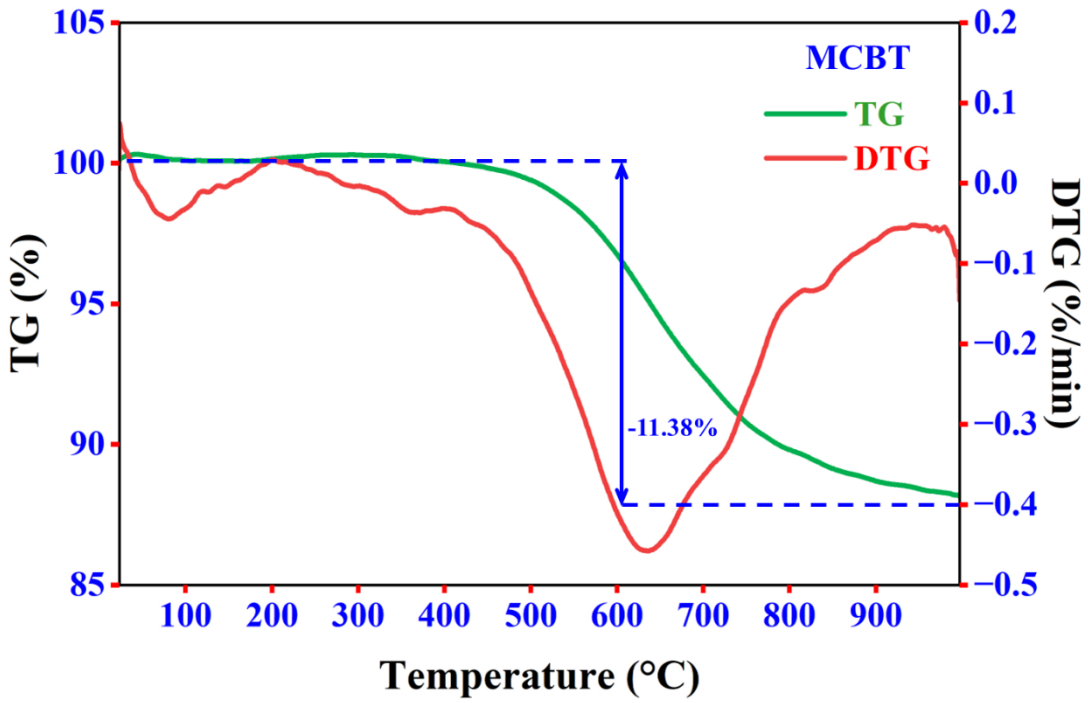

Furthermore, the subsequent large endothermic peak observed around 620 ºC implies a substantial absorption of heat during this temperature range. This phenomenon may be associated with the decomposition of more complex organic or inorganic constituents within the composite, such as the breakdown of certain minerals present in bentonite clay or further transformations of the carbonaceous residues. The combined exothermic and endothermic events in close succession suggest a multi-step decomposition process involving different phases of the composite. The char, being the primary carbonaceous component, likely undergoes initial combustion, leading to the exothermic peak, followed by subsequent reactions or transformations

contributing to the endothermic peak. Moreover, the temperature range of 415 ºC to 620 ºC aligns with typical decomposition temperatures of organic and inorganic materials, and the observed peaks underscore the complexity of the composite's thermal behavior. The presence of bentonite clay may influence the overall decomposition kinetics, either catalytically or by contributing to structural transformations.

- *Fourier-transform infrared (FT-IR) analysis*

The FTIR analysis of MCBT provides valuable information about the chemical composition and structural characteristics of this material (FIGURE 4.2). The presence of transmittance peaks in the FTIR spectrum of MCBT can be attributed to functional groups typically found in carbonaceous materials (MC) and bentonite (BT). The peak at 3600 cm^{-1} is attributed to the stretching vibrations of hydroxyl (OH) groups, indicating the presence of moisture or residual water in the composite. This peak is often associated with adsorbed or physically bound water within the material. This may also be associated with N-H stretching vibration, signifying the presence of a surface functional group of amino groups (MAGED *et al.*, 2021). The peak in the range of 1600-1700 cm^{-1} indicates the presence of C=C, which was also present in MC (CHAPTER 3, SECTION 3.3.5) probably as a result of PVDF structure thermal degradation, which contributes to the reactivity of the adsorbent surface and consequently its adsorption capacity. The band at 1100 cm^{-1} is typically associated with Si-O stretching vibrations, suggesting the contribution of bentonite clay to the MCBT composite. This peak signifies the presence of silicate structures in the clay, confirming the successful incorporation of the clay into the composite matrix. The peaks at 600 cm^{-1} and 500 cm^{-1} are characteristic of bending vibrations of the Si-O-Si bonds in the bentonite clay. These bands further support the presence of the clay component in the composite and indicate the preservation of the clay's mineralogical structure.

Figure 4.2 - FTIR spectra of MCBT

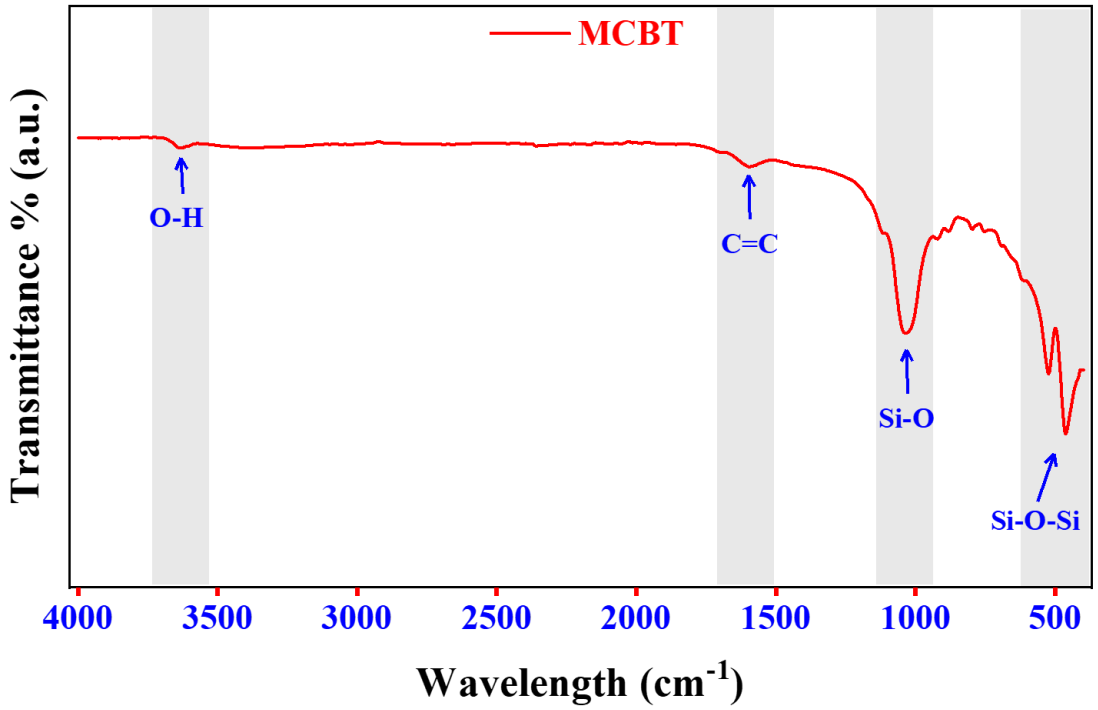

- *X-ray powder diffraction (XRD) analysis*

Figure 4.3 shows the XRD analysis of the MCBT, providing information about the structural properties of the composite. In the XRD pattern of MCBT, distinct peaks are observed around 6.5°, 20°, 25° and 44°. The intense peak observed at 6.5° in the XRD analysis is characteristic of smectite (within the bentonite clay). The smectite clay minerals exhibit a significant basal reflection (001) at low angles, and the peak at 6.5° (2θ) is associated with the spacing between the layers of the smectite crystal structure. The intensity of the peak indicates the abundance and well-defined crystalline nature of the smectite in the composite. Additionally, the peak at 20° is a characteristic reflection associated with the crystalline structure of bentonite clay. This confirms the successful incorporation of the clay into the composite, and the position of this peak may provide information about the clay's mineralogical composition. The presence of peaks at 36° and 44° suggests the existence of crystalline phases associated with the MC. These peaks may arise from the carbonaceous residues in the char or potentially from the interaction of the char with minerals in the bentonite. Overall, the obtained XRD results collectively indicate a composite material with a combination of amorphous and crystalline phases. The integration of bentonite clay introduces well-

defined crystalline structures, while the MC char contributes to both amorphous and crystalline features.

Figure 4.3 - XRD pattern of MCBT

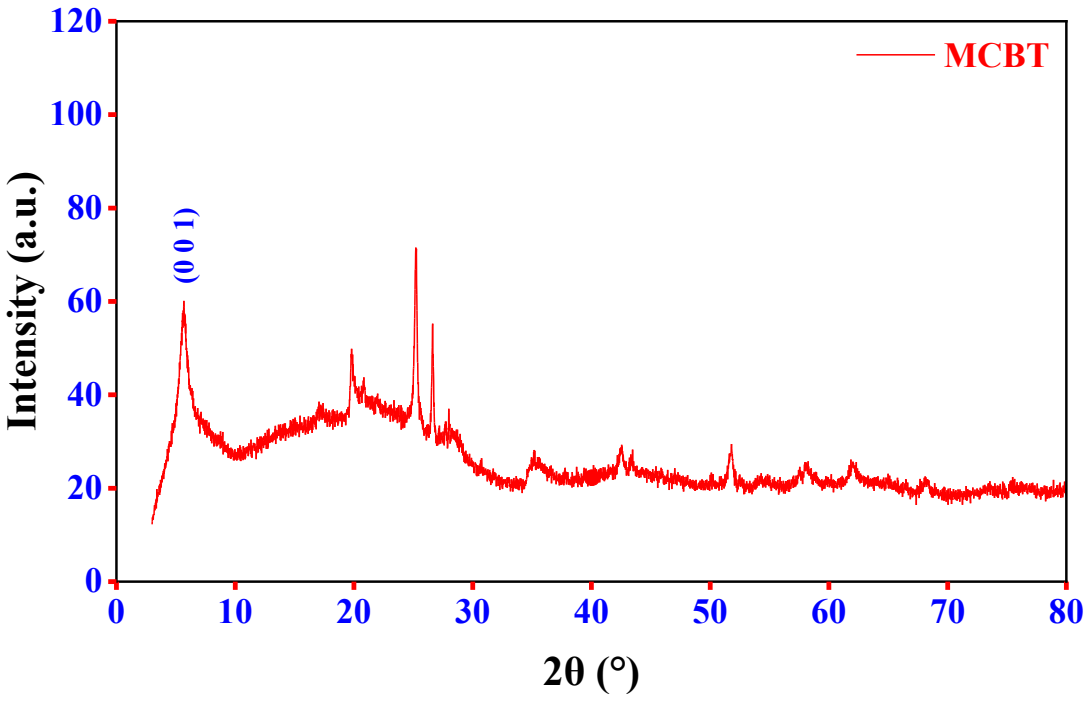

- *Raman analysis*

Raman spectroscopy was employed to validate the molecular composition and structural characteristics of the MCBT produced, as represented in Figure 4.4. The evaluation of the degree of graphitization (G band) and the presence of disordered carbon structures (D band) can be carried out using Raman analysis. The peak at 1348 cm^{-1} (D band) is associated with sp^3-hybridized carbon, while the G-band at 1582 cm^{-1} is related to the vibration of sp^2-hybridized carbon (Hong *et al.*, 2016). Compared to the MC Raman spectrum (CHAPTER 3, FIGURE 3.14), both D and G bands presented lower intensity, resulting in an I_D/I_G ratio also lower, equal to 0.66. The band at 507 cm^{-1} can be associated with bentonite (BT) added to MC to produce the composite. Raman analysis of MCBT is crucial to adapt its properties for application as an adsorbent. The combination of these Raman peaks reflects the hybrid nature of the composite, encompassing both inorganic (clay minerals) and organic (carbonaceous residues) components. The degree of disorder and crystallinity in the carbon structures, as

revealed by the D and G bands, provides insights into the carbonization process and the potential applications of the MCBT composite as a homogenized adsorbent.

Figure 4.4 - Raman spectra of MCBT

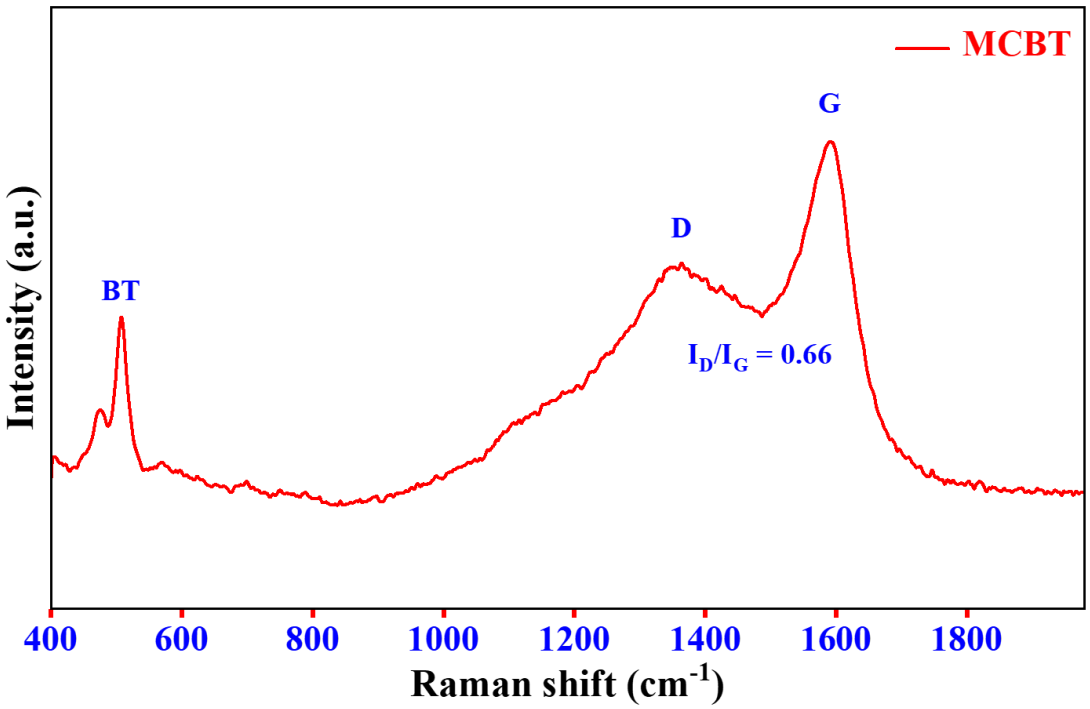

- *Surface and textural analysis*

The SEM analysis, which aims to investigate the surface morphology of the MCBT, is presented in FIGURE 4.5. As expected, MCBT presents a flake morphology with irregular shapes and a non-compact structure, characteristic of porous carbons. The presence of irregularly shaped particles and aggregates is indicative of the composite's complex composition, incorporating both organic and inorganic components. Additionally, the porous nature of the MCBT composite is crucial for adsorption applications. Furthermore, the distribution and dispersion of particles throughout the composite are evident from the SEM micrographs. The intimate intermingling of the clay and char components suggests a successful blending process, contributing to the overall homogeneity of the material. This homogeneous distribution is essential for ensuring consistent properties and performance in potential applications.

Figure 4.5 - SEM micrographs for MCBT

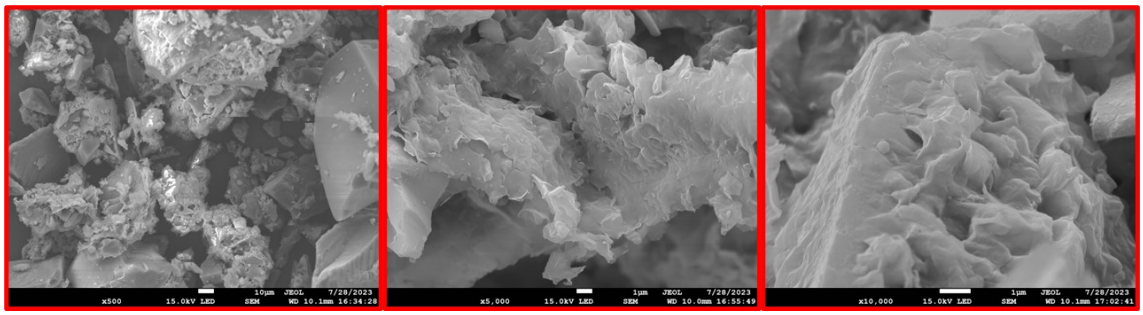

Figure 4.6 shows the EDS elemental analysis of the MCBT sample. The result indicates that carbon (C) is the most abundant element in the sample (56.2%), as expected due to its majority raw material, the carbonaceous material MC. Aluminum (Al, 7.7%) and silica (SiO_2, 8.7%) derived from bentonite were also identified in the MCBT, not previously detected in the MC (CHAPTER 3, SECTION 3.3.5). A surface area of 398 m^2/g for MCBT was determined through BET analysis. Total pore volume was measured at 0.18 cm^3/g. This high total pore volume is generally advantageous for application as an adsorbent. The average pore diameter was 1.8 nm, categorizing the material as microporous carbon.

Figure 4.6 - EDS elemental analysis for MCBT

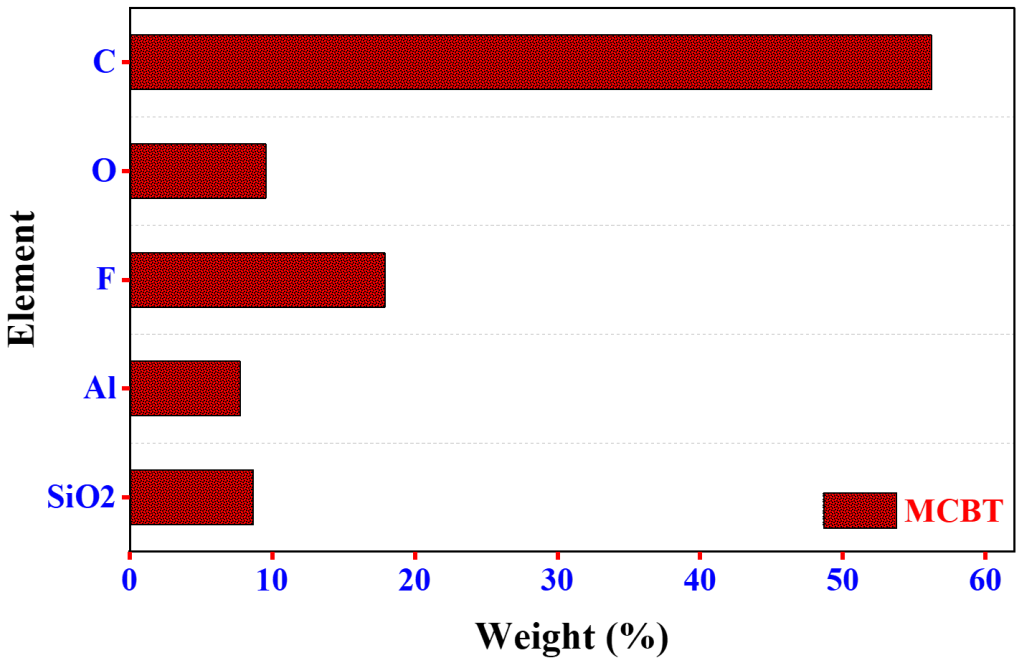

4.3.4 MCBT COST EVALUATION

From produced MC (CHAPTER 3) and bentonite, a simple procedure can be used to manufacture the MCBT composite without needing costly reagents or complex equipment. Based on the obtained results, MCBT is produced at a moderate temperature, and depending on the furnace's capacity, the synthesis process can be scaled up.

To assess the composite's economic feasibility and potential for large-scale adsorbent application, it is crucial to estimate the production costs. The price of raw materials, such as feedstock and reagents, as well as the energy consumed determine the cost of composites. Table 4.5 displays the specific production costs for MCBT. When compared to commercial adsorbents, the preparation cost of MCBT was found to be inexpensive, estimated at 0.85 €/kg. The low costs of MC and bentonite, being possible to collect it without cost or buy for 0.64 €/kg, and the decreased electricity use are responsible for the low synthesis cost of MCBT (TABLE 4.5). In general, when the process is used more widely to produce more composite, the costs decrease even more.

Table 4.5 - Cost analysis of producing 1 kg of MCBT

Items		Consumed amount	Price (€)	Total cost (€)
Materials				
	Membrane char	0.75 kg	0.12 €/kg*	0.09
	Bentonite	0.25 kg	Free[ϒ]	0.00
Energy				
	Ultrasonicator (400 W/h)	0.40 kWh	0.05 €/kWh	0.02
	Magnetic stirrer (650 W/h)	2.60 kWh	0.05 €/kWh	0.13
	Muffle furnace (4000 W/h)	2.00 kWh	0.05 €/kWh	0.10
	Drying oven (425 W/h)	10.20 kWh	0.05 €/kWh	0.51
Total				0.85

(*) Price estimated in Section 3.3.6.

(ϒ) Collected from Matrouh City, Egypt, without cost (MAGED *et al.*, 2020a).

4.4 CONCLUSIONS

During the preliminary tests for fluoride (F^-) removal using MC was observed an average of 1.87±0.28 mg/g of F^- released by the MC, and a residual release of 0.23 mg/g of F^- even after MC washing tests with sodium hydroxide (NaOH) solution.

MC modification by acid activation, magnetization/co-precipitation, and alkali-acid activation, furthermore membrane char-Fe-chitosan composite synthesis, were investigated in preliminary tests. However, the results of the adsorption tests using these MC modified and the composite produced for dyes and pharmaceuticals removal did not show promising results.

A synthesis methodology of a composite mixing MC and bentonite was presented and this produced membrane char-bentonite composite (MCBT) was characterized. MCBT characterization studies showed the obtaining of a homogeneous material, as supported by Raman and SEM analysis, with a surface area of 398 m^2/g, total pore volume of 0.18 cm^3/g, and microporous average pore diameter of 1.8 nm, as pointed by the N_2 adsorption-desorption isotherm data. Those proprieties are generally advantageous for the application of a material as an adsorbent. The cost evaluated of 0.85 €/kg also favors the interest of using MCBT as a low-cost alternative adsorbent.

REFERENCES

ABDOU, M. I.; AL-SABAGH, A. M.; DARDIR, M. M. Evaluation of Egyptian bentonite and nano-bentonite as drilling mud. *Egyptian Journal of Petroleum*, v. 22, n. 1, p. 53-59, 2013.

ABDULLAH, M.; IQBAL, J.; REHMAN, M. S. U.; KHALID, U.; MATEEN, F.; ARSHAD, S. N.; ...; FAZAL, T. Removal of ceftriaxone sodium antibiotic from pharmaceutical wastewater using an activated carbon based TiO2 composite: Adsorption and photocatalytic degradation evaluation. *Chemosphere*, v. 317, p. 137834, 2023.

AHMADPOUR, A.; DO, D. D. The preparation of active carbons from coal by chemical and physical activation. *Carbon*, v. 34, n. 4, p. 471-479, 1996.

ALI. S.; THAKUR, S. K.; SARKAR, A.; SHEKKAR, S. Worldwide contamination of water by fluoride. *Environmental Chemistry Letters*, v. 14, n. 3, p. 291-315, 2016.

AMER, M.; ELWARDANY, A. Biomass Carbonization. In: *Renewable Energy - Resources, Challenges and Applications.* IntechOpen, p. 211-232, 2020.

ARIF, M.; LIU, G.; UR REHMAN, M. Z.; YOUSAF, B.; AHMED, R.; MIAN, M. M.; ...; NAEEM, A. Carbon dioxide activated biochar-clay mineral composite efficiently removes ciprofloxacin from contaminated water-Reveals an incubation study. *Journal of Cleaner Production*, v. 332, p. 130079, 2022.

BHATNAGAR, A.; HOGLAND, W.; MARQUES, M.; SILLANPÄÄ, M. An overview of the modification methods of activated carbon for its water treatment applications. *Chemical Engineering Journal*, v. 219, p. 499-511, 2013.

BOUAZIZ, N.; KOUIRA, O.; AOUAINI, F.; BUKHARI, L.; KNANI, S.; ZNAIDIA, S.; LAMINE, A. B. Adsorption of antibiotics by bentonite-chitosan composite: Phenomenological modeling and physical investigation of the adsorption process. *International Journal of Biological Macromolecules*, p. 125156, 2023.

BRASIL. *Portaria nº 888 de 4 de maio de 2021.* Dispõe sobre os procedimentos de controle e de vigilância da qualidade da água para consumo humano e seu padrão de potabilidade. Ministério da Saúde, Brasília, 2021.

CHEN, J.; OUYANG, J.; CAI, X.; XING, X.; ZHOU, L.; LIU, Z.; CAI, D. Removal of ciprofloxacin from water by millimeter-sized sodium alginate/H3PO4 activated corncob-based biochar composite beads. *Separation and Purification Technology*, v. 276, p. 119371, 2021.

DANALIOĞLU, S. T.; BAYAZIT, Ş. S.; KUYUMCU, Ö. K.; SALAM, M. A. Efficient removal of antibiotics by a novel magnetic adsorbent: Magnetic activated carbon/chitosan (MACC) nanocomposite. *Journal of Molecular Liquids*, v. 240, p. 589-596, 2017.

EDMUNDS, W. M.; SMEDLEY, P. L. Fluoride in natural waters. In: *Essentials of Medical Geology*, Springer, p. 311-336, 2013.

FAKIROV, S. Nano-/microfibrillar polymer–polymer and single polymer composites: The converting instead of adding concept. *Composites Science and Technology*, v. 89, p. 211-225, 2013.

FIGHIR, D.; PADURARU, C.; CIOBANU, R.; BUCATARIU, F.; PLAVAN, O.; GHERGHEL, A.; ...; TEODOSIU, C. Removal of Diclofenac and Heavy Metal Ions from

Aqueous Media Using Composite Sorbents in Dynamic Conditions. *Nanomaterials*, v. 14, n. 1, p. 33, 2023.

HAGEMANN, N.; SPOKAS, K.; SCHMIDT, H. P.; KÄGI, R.; BÖHLER, M. A.; BUCHELI, T. D. Activated carbon, biochar and charcoal: linkages and synergies across pyrogenic carbon's ABCs. *Water*, v. 10, n. 2, p. 182, 2018.

HEO, Y. J.; ZHANG, Y.; RHEE, K. Y.; PARK, S. J. Synthesis of PAN/PVDF nanofiber composites-based carbon adsorbents for CO_2 capture. *Composites Part B: Engineering*, v. 156, p. 95-99, 2019.

HONG, S. M.; LIM, G.; KIM, S. H.; KIM, J. H.; LEE, K. B.; HAM, H. C. Preparation of porous carbons based on polyvinylidene fluoride for CO2 adsorption: A combined experimental and computational study. *Microporous and Mesoporous Materials*, v. 219, p. 59-65, 2016.

HSISSOU, R.; SEGHIRI, R.; BENZEKRI, Z.; HILALI, M.; RAFIK, M.; ELHARFI, A. Polymer composite materials: A comprehensive review. *Composite Structures*, v. 262, p. 113640, 2021.

KUMAR, A.; PATRA, C.; KUMAR, S.; NARAYANASAMY, S. Effect of magnetization on the adsorptive removal of an emerging contaminant ciprofloxacin by magnetic acid activated carbon. *Environmental Research*, v. 206, p. 112604, 2022.

LOPES, C. W.; BERTELLA, F.; PERGHER, S. B. C.; FINGER, P. H.; DALLAGO, R. M.; PENHA, F. G. Síntese e caracterização de carvões ativados derivados do sabugo de milho. *Perspectiva Erechim*, v. 37, p. 27-35, 2013.

LOZANO-CASTELLO, D.; LILLO-RÓDENAS, M. A.; CAZORLA-AMORÓS, D.; LINARES-SOLANO, A. Preparation of activated carbons from Spanish anthracite: I. Activation by KOH. *Carbon*, v. 39, n. 5, p. 741-749, 2001.

MA, Y.; LI, P.; YANG, L.; WU, L.; HE, L.; GAO, F.; ...; ZHANG, Z. Iron/zinc and phosphoric acid modified sludge biochar as an efficient adsorbent for fluoroquinolones antibiotics removal. *Ecotoxicology and Environmental Safety*, v. 196, p. 110550, 2020.

MAGED, A.; DISSANAYAKE, P. D.; YANG, X.; PATHIRANNAHALAGE, C.; BHATNAGAR, A.; OK, Y. S. New mechanistic insight into rapid adsorption of pharmaceuticals from water utilizing activated biochar. *Environmental Research*, v. 202, p. 111693, 2021.

MAGED, A.; IQBAL, J.; KHARBISH, S.; ISMAEL, I. S.; BHATNAGAR, A. Tuning tetracycline removal from aqueous solution onto activated 2: 1 layered clay mineral: Characterization, sorption and mechanistic studies. *Journal of Hazardous Materials*, v. 384, p. 121320, 2020b.

MAGED, A.; KHARBISH, S.; ISMAEL, I. S.; BHATNAGAR, A. Characterization of activated bentonite clay mineral and the mechanisms underlying its sorption for ciprofloxacin from aqueous solution. *Environmental Science and Pollution Research*, v. 27, p. 32980-32997, 2020a.

MAGED, A.; EL-FATTAH, H. A.; KAMEL, R. M.; KHARBISH, S.; ELGARAHY, A. M. A comprehensive review on sustainable clay-based geopolymers for wastewater treatment: circular economy and future outlook. *Environmental Monitoring and Assessment*, v. 195, n. 6, p. 693, 2023b.

MAHMOUD, M. E.; EL-GHANAM, A. M.; MOHAMED, R. H. A.; SAAD, S. R. Enhanced adsorption of Levofloxacin and Ceftriaxone antibiotics from water by assembled composite of nanotitanium oxide/chitosan/nano-bentonite. *Materials Science and Engineering: C*, v. 108, p. 110199, 2020.

NIGRI, E. M. *Caracterização e estudo dos mecanismos de sorção de fluoretos em carvão de osso.* Tese de Doutorado - Universidade Federal de Minas Gerais, Belo Horizonte, MG, 141 p., 2016.

RAHMAN, N.; NASIR, M. Effective removal of acetaminophen from aqueous solution using Ca (II)-doped chitosan/β-cyclodextrin composite. *Journal of Molecular Liquids*, v. 301, p. 112454, 2020.

RIVERA-UTRILLA, J.; SÁNCHEZ-POLO, M.; GÓMEZ-SERRANO, V.; ÁLVAREZ, P. M.; ALVIM-FERRAZ, M. C. M.; DIAS, J. M. Activated carbon modifications to enhance its water treatment applications: An overview. *Journal of Hazardous Materials*, v. 187, n. 1-3, p. 1-23, 2011.

SAYIN, F.; AKAR, S. T.; AKAR, T. From green biowaste to water treatment applications: Utilization of modified new biochar for the efficient removal of ciprofloxacin. *Sustainable Chemistry and Pharmacy*, v. 24, p. 100522, 2021.

SONG, M.; JIN, B.; XIAO, R.; YANG, L.; WU, Y.; ZHONG, Z.; HUANG, Y. The comparison of two activation techniques to prepare activated carbon from corn cob. *Biomass and Bioenergy*, v. 48, p. 250-256, 2013.

TANG, L.; YU, J.; PANG, Y.; ZENG, G.; DENG, Y.; WANG, J.; ...; FENG, H. Sustainable efficient adsorbent: alkali-acid modified magnetic biochar derived from sewage sludge for aqueous organic contaminant removal. *Chemical Engineering Journal*, v. 336, p. 160-169, 2018.

VELÁSQUEZ, L. N. M.; FANTINEL, L. M.; UHLEIN, A.; ARANHA, P. R. A.; VARGAS, A. M. D.; IGLESIAS, M. M.; JUNQUEIRA, A. E. *Investigação hidrogeológica do flúor em aqüíferos carbonáticos do médio São Francisco-MG e epidemiologia da fluorose dentária associada*. Relatório CNPq - Instituto de Geociências, Universidade Federal de Minas Gerais, Belo Horizonte, 2007.

WASILEWSKA, M.; DERYŁO-MARCZEWSKA, A. Adsorption of non-steroidal anti-inflammatory drugs on alginate-carbon composites - equilibrium and kinetics. *Materials*, v. 15, n. 17, p. 6049, 2022.

WHO. *Guidelines for Drinking-water*. v. 1 - Recommendations, 3 ed., World Health Organization, Geneva, 2008.

XIKHONGELO, R. V.; MTUNZI, F. M.; DIAGBOYA, P. N.; OLU-OWOLABI, B. I.; DÜRING, R. A. Polyamidoamine-functionalized graphene oxide–SBA-15 mesoporous composite: adsorbent for aqueous arsenite, cadmium, ciprofloxacin, ivermectin, and tetracycline. *Industrial & Engineering Chemistry Research*, v. 60, n. 10, p. 3957-3968, 2021.

XUE, Y.; GUO, Y.; ZHANG, X.; KAMALI, M.; AMINABHAVI, T. M.; APPELS, L.; DEWIL, R. Efficient adsorptive removal of ciprofloxacin and carbamazepine using modified pinewood biochar–A kinetic, mechanistic study. *Chemical Engineering Journal*, v. 450, p. 137896, 2022.

YADAV, S.; ASTHANA, A.; SINGH, A. K.; CHAKRABORTY, R.; VIDYA, S. S.; SUSAN, M. A. B. H.; CARABINEIRO, S. A. Adsorption of cationic dyes, drugs and metal from

aqueous solutions using a polymer composite of magnetic/β-cyclodextrin/activated charcoal/Na alginate: Isotherm, kinetics and regeneration studies. *Journal of Hazardous Materials*, v. 409, p. 124840, 2021.

YAMASHITA, J.; SHIOYA, M.; KIKUTANI, T.; HASHIMOTO, T. Activated carbon fibers and films derived from poly (vinylidene fluoride). *Carbon*, v. 39, n. 2, p. 207-214, 2001.

ZHENG, X.; HE, X.; PENG, H.; WEN, J.; LV, S. Efficient adsorption of ciprofloxacin using Ga2S3/S-modified biochar via the high-temperature sulfurization. *Bioresource Technology*, v. 334, p. 125238, 2021.

ZUO, H.; CHEN, L.; KONG, M.; QIU, L.; LÜ, P.; WU, P.; YANG, Y., CHEN, K. Toxic effects of fluoride on organisms. *Life Sciences*, v. 198, p. 18-24, 2018.

CHAPTER 5 - ADSORPTION TESTS: REMOVAL OF ANTIBIOTICS

5.1 LITERATURE REVIEW

Batch adsorption tests allow preliminary evaluation of the adsorption process under various parameters (pH, contact time, adsorbent dosage, and initial adsorbate concentration) in the fluid phase. Under constant temperature conditions, by constructing isotherms and adjusting experimental data to literature isotherm models, it is possible to determine the adsorption capacity and process efficiency in equilibrium studies. It is also possible to evaluate the contact time between adsorbate and adsorbent in kinetic studies (LARGITTE & PASQUIER, 2016; MESQUITA, 2016; MESQUITA *et al.*, 2017a; METCALF & EDDY, 2014; NASCIMENTO *et al.*, 2014; NIGRI *et al.*, 2017; QIU *et al.*, 2009; WORCH, 2012).

Operational and dynamic parameters, including adsorption capacity and removal efficiency, can be obtained from the breakthrough curve constructed in continuous adsorption tests (CAVALCANTI, 2009; MESQUITA *et al.*, 2017b; XAVIER *et al.*, 2018). The fluidized and fixed bed operating modes are defined by how the adsorbent is made available in the continuous operation system. In the fluidized bed, the fluid phase is typically fed at the bottom of the column at a sufficient velocity to fluidize the adsorbent particles, forming the bed. In the fixed bed, the adsorbent is held in the column between two inert layers, and the adsorbate concentration along the bed varies with the flow of the fluid phase, whether upward or downward. Upward flow is preferred to minimize bed compaction effects and the formation of preferential pathways (CAVALCANTI, 2009; MESQUITA *et al.*, 2017b; NIGRI *et al.*, 2017).

5.1.1 EQUILIBRIUM: ADSORPTION ISOTHERMS

The equilibrium point of an adsorption system depends directly on the interaction between adsorbate and adsorbent, which in turn is influenced by the characteristics of each one of them and by the system conditions, such as temperature, pH, and the presence of other substances in the fluid phase. Assuming the adsorption of a single adsorbate at a constant temperature, an adsorption isotherm can be constructed to study the equilibrium of the system, according to Equation 5.1 and Figure 5.1 (METCALF & EDDY, 2014; WORCH, 2012).

$$q_0 = f(C_e) \tag{5.1}$$

where q_0 is the amount of adsorbate adsorbed per unit mass of adsorbent (mg/g) and C_e is the adsorbate concentration at equilibrium (mg/L) under constant temperature.

Figure 5.1 - Adsorption isotherm for single adsorbate under constant temperature

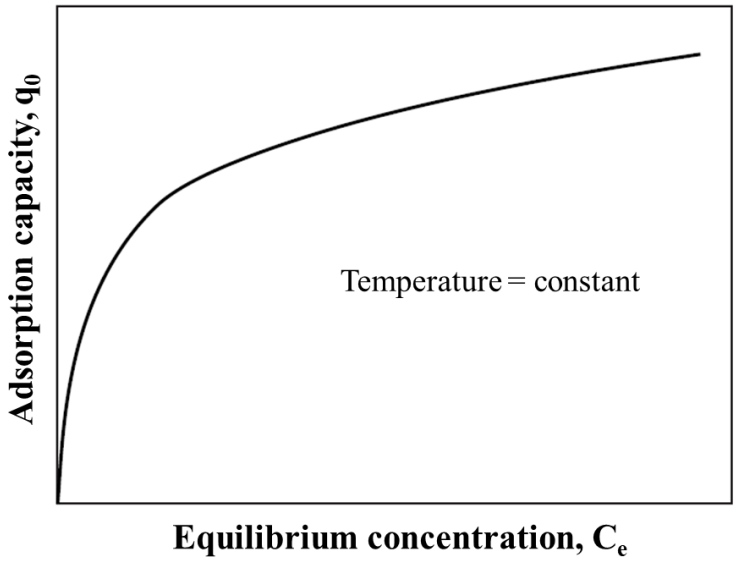

Source: Adapted from Worch (2012)

The determination of the adsorption capacity at equilibrium (q_0) or the amount of adsorbate adsorbed per unit mass of adsorbent at equilibrium (mg/g), is done experimentally under constant temperature considering the initial (C_0) and equilibrium (C_e) concentrations of the adsorbate in the fluid phase in mg/L, the volume of the fluid phase (V) in L and the mass of adsorbent (m) in g in the batch system (EQUATION 5.2) (METCALF & EDDY, 2014).

$$q_0 = \frac{(C_0 - C_e)\,.\,V}{m} \tag{5.2}$$

The isotherms can have different formats (FIGURE 5.2) that reveal the adsorption system and whether the adsorption capacity is proportional (linear) or independent (irreversible) to the adsorbate concentration in the fluid phase at equilibrium or, even, whether the adsorption capacity is high for low equilibrium concentrations (favorable or extremely favorable) or the opposite (not favorable) (MCCABE, SMITH & HARRIOTT, 2004).

Figure 5.2 - Adsorption isotherms formats

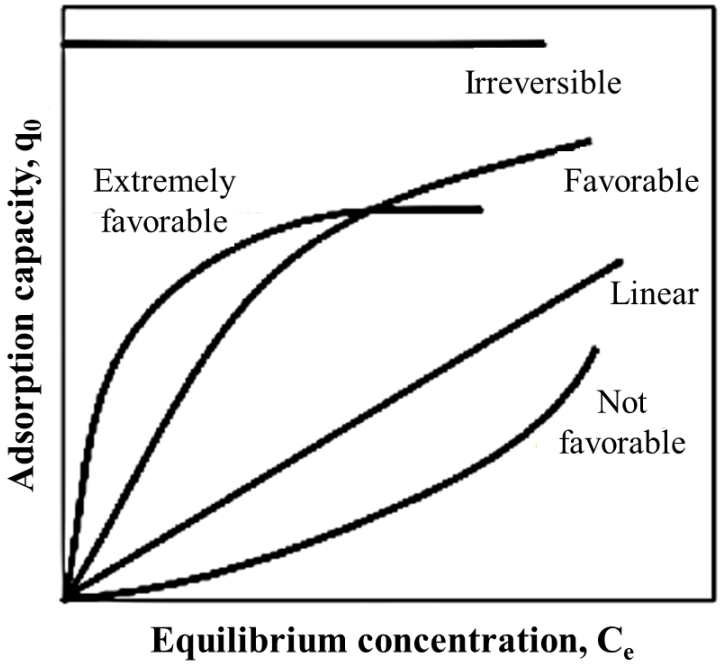

Source: Adapted from Mccabe, Smith & Harriott (2004)

According to the recommendations of the International Union of Pure and Applied Chemistry technical report (IUPAC, 2015), physisorption isotherms can be classified into eight types (FIGURE 5.3) (THOMMES *et al.*, 2015).

Figure 5.3 - IUPAC classification of adsorption isotherms

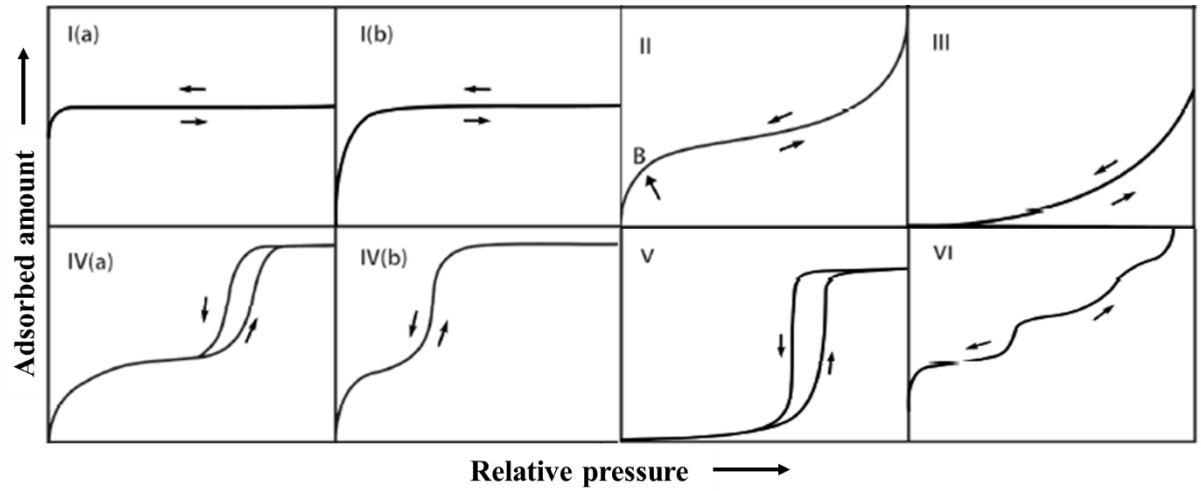

Source: Adapted from Thommes *et al.* (2015)

Type I isotherms correspond to monolayer adsorption of microporous materials with pore diameters smaller than 1 nm in I(a) and smaller than 2.5 nm in I(b). Type II isotherms characterize the adsorption onto non-porous materials by forming multilayers. In type III isotherms, the interactions between adsorbent and adsorbate

are relatively weak and an identifiable monolayer is not formed. Type IV isotherms show the adsorption on mesoporous adsorbents with a final saturation plateau of varying lengths. In isotherms of type IV(a) a hysteresis is observed, in which the adsorption and desorption isotherms do not coincide due to differences between the saturation pressures for condensation and evaporation inside the pores. Type IV(b) isotherms represent adsorbents with smaller mesopores, which are completely reversible. In type V isotherms, considered uncommon, the interactions between adsorbent and adsorbate are relatively weak as in type III isotherms, and hysteresis is observed as in type IV(a) isotherms. Finally, type VI isotherms describe multilayer adsorption onto highly uniform surfaces, in which layers form over varying relative pressure (THOMMES *et al.*, 2015).

The best-known mathematical models used to describe adsorption equilibrium under constant temperature were proposed by Freundlich and Langmuir in 1906 and 1918, respectively. These classical isotherm models require the determination of two parameters from experimental data for their application and each one has its simplifying assumptions and limitations. As there is no universal isotherm model to describe the adsorption equilibrium, the applicability of a given model to the experimental system needs to be tested (METCALF & EDDY, 2014; WORCH, 2012).

- *Freundlich isotherm*

The Freundlich isotherm was obtained empirically and is currently widely used to describe adsorption systems on activated carbon and zeolites in water and wastewater treatment. This model considers the energetic heterogeneity of the adsorbent surface. As it assumes multilayer adsorption and does not predict saturation of the adsorbent, the Freundlich isotherm describes adsorption only in the concentration range in which it was obtained and cannot be extrapolated. The Freundlich isotherm model is given by Equation 5.3 (FREUNDLICH, 1906; MESQUITA, 2016; METCALF & EDDY, 2014; WORCH, 2012)

$$q_0 = K_F . C_e^{\frac{1}{n}} \tag{5.3}$$

where q_0 is the adsorption capacity at equilibrium (mg/g), K_F is the Freundlich constant related to the adsorption capacity and determining the curvature of the isotherm (mg/g), C_e is the adsorbate concentration in the fluid phase at equilibrium (mg/L) and n is the heterogeneity factor of the adsorbent. Values of n greater than 1 (one) refer to high adsorption capacities for low equilibrium concentrations, in favorable isotherms, while values lower than 1 (one) show unfavorable isotherms.

- *Langmuir isotherm*

The Langmuir isotherm model, developed from theoretical considerations, assumes the existence of energetically homogeneous pores on the surface of the adsorbent and considers the reversibility of adsorption that occurs in a single layer. Equation 5.4 describes the Langmuir isotherm (LANGMUIR, 1916; MESQUITA, 2016; METCALF & EDDY, 2014; WORCH, 2012).

$$q_0 = \frac{q_{max} \,.\, K_L \,.\, C_e}{1 + K_L \,.\, C_e} \tag{5.4}$$

where q_0 is the adsorption capacity at equilibrium (mg/g), q_{max} is the maximum adsorption capacity for the monolayer coverage (mg/g), K_L is the Langmuir constant related to the free energy of adsorption and corresponding to the affinity between adsorbent and adsorbate (L/mg) and C_e the concentration of adsorbate in the fluid phase at equilibrium (mg/L).

5.1.2 ADSORPTION KINETICS

The kinetics study lets us understand the adsorption progress until equilibrium. Equilibrium is not reached instantly, especially in porous materials, due to the adsorbate transfer resistance from the fluid phase to the interior of the adsorbent pores. These mass transfer resistances directly influence the speed of each step of the adsorption process (LARGITTE & PASQUIER, 2016; MESQUITA, 2016; NASCIMENTO *et al.*, 2014; QIU *et al.*, 2009; WORCH, 2012).

The equilibrium time and limiting step in the adsorption process can be estimated through kinetic modeling. Generally assuming constant temperature, spherical isotropic adsorbent particles, and adsorption rates much higher than diffusion rates,

the kinetic models usually involve the mass balance, the isothermal parameters, and the mass transfer equations of the adsorption system. The main kinetic models for determining the adsorption rate of batch systems, that is, the variation in adsorption capacity over time, are the pseudo-first-order and pseudo-second-order models, based on the kinetics of chemical reactions (LARGITTE & PASQUIER, 2016; MESQUITA, 2016; QIU *et al.*, 2009; WORCH, 2012).

- *Pseudo-first-order model*

The pseudo-first-order kinetic model, proposed by Lagergren in 1898 for solid/liquid adsorption systems, assumes that physisorption is the rate-limiting step of adsorption and is given by Equation 5.5 (LAGERGREN, 1898; MESQUITA, 2016; NASCIMENTO *et al.*, 2014; WORCH, 2012).

$$q_t = q_0 \left(1 - e^{-k_1 . t}\right) \tag{5.5}$$

where q_t is the adsorption capacity at time t (mg/g), q_0 is the adsorption capacity at equilibrium (mg/g) and k_1 is the pseudo-first-order adsorption rate constant (1/min).

The determination of the pseudo-first-order adsorption rate constant (k_1) can be done by plotting a graph of $\ln(q_0 - q_t)$ versus t, according to Equation 5.6 obtained from the integration of linearized Equation 5.5 for the boundary conditions ($q_t = 0$, $t = 0$) and ($q_t = q_t$, $t = t$) (NASCIMENTO *et al.*, 2014; WORCH, 2012).

$$\ln(q_0 - q_t) = \ln(q_0) - k_1 . t \tag{5.6}$$

- *Pseudo-second-order model*

The pseudo-second-order kinetic model is also applied to solid/liquid adsorption systems, considers chemisorption as the adsorption rate-limiting mechanism, and is described by Equation 5.7 (MESQUITA, 2016; NASCIMENTO *et al.*, 2014; WORCH, 2012).

$$q_t = \frac{k_2 . {q_0}^2 . t}{1 + k_2 . q_0 . t} \tag{5.7}$$

where q_t is the adsorption capacity at time t (mg/g), k_2 is the pseudo-second-order adsorption rate constant (g/mg.min) and q_0 is the adsorption capacity at equilibrium (mg/g).

Integrating linearized Equation 5.7 for the boundary conditions (q_t = 0, t = 0) and (q_t = q_t, t = t) Equation 5.8 is obtained, which is presented in linearized form in Equation 5.9. The values of the equilibrium adsorption capacity (q_0) and the pseudo-second-order adsorption rate constant (k_2) are, respectively, the intercept and the slope of the curve obtained by plotting a graph of $\frac{t}{q_t}$ versus t (NASCIMENTO *et al.*, 2014; WORCH, 2012).

$$\frac{t}{(q_0 - q_t)} = \frac{1}{{q_0}^2} + k_2.t \tag{5.8}$$

$$\frac{t}{q_t} = \frac{1}{k_2.{q_0}^2} + \frac{t}{q_0} \tag{5.9}$$

5.1.3 DYNAMIC: CONTINUOUS ADSORPTION

To understand how distance acts on the continuous adsorption process, it is necessary to understand the bed as layers of adsorbent that reach equilibrium one by one, from the beginning to the end of the column, in the direction of fluid phase flow containing the adsorbate with an initial concentration (C_0). Therefore, the amount of material adsorbed in the column, in addition to time, also varies throughout the layers. However, the boundary between a saturated layer and an empty layer is not explicit, due to the different adsorption rates. This unmarked boundary between two layers of the column is called the mass transfer zone (MTZ). This is a bed region that is not empty but is not yet saturated, that is, it is the active region of the bed, in which the mass transfer is taking place. Thus, it is said that the shape of the MTZ reflects the mass transfer resistance, and the greater the resistance, the lower the degree of inclination of the MTZ. As shown in Figure 5.4, the MTZ moves along the entire bed until it is completely saturated (MESQUITA, 2016; WORCH, 2012).

Figure 5.4 - Displacement of the mass transfer zone by a fixed bed (MTZ: mass transfer zone; C_0: initial adsorbate concentration; t: time)

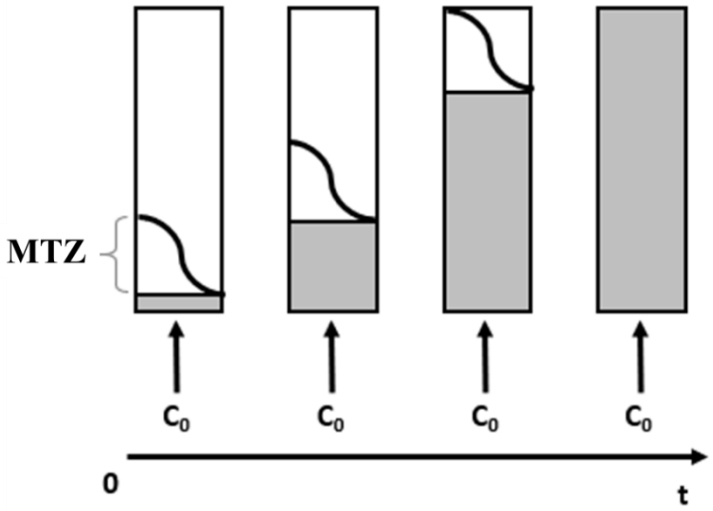

Source: Adapted from Xavier (2018)

Aiming to study the adsorption dynamics, are constructed breakthrough curves that describe the adsorbate concentration profile in the fluid phase as a function of time in the graphical form of C/C_0 versus t, where C is the adsorbate concentration in the fluid phase at the time t and C_0 is the initial adsorbate concentration in the fluid phase (FIGURE 5.5). The determination of C takes place at the column outlet. Thus, as at time zero, all the adsorbent is empty, adsorption takes place fully and the value of C at the column outlet is zero, with a consequent relative concentration (C/C_0) equal to zero. With the formation of the MTZ and the complete saturation of the bed, C equals C_0 and the breakthrough curve reaches 1 on the relative concentration axis (MESQUITA, 2016; XAVIER, 2018).

Figure 5.5 - Real and ideal breakthrough curves in a fixed bed adsorption column (BC: breakthrough curve; C/C_0: relative concentration; C_b/C_0: relative breakthrough concentration; C_e/C_0: relative exhaustion concentration; t: time; t_b: breakthrough time; t_e: exhaustion time)

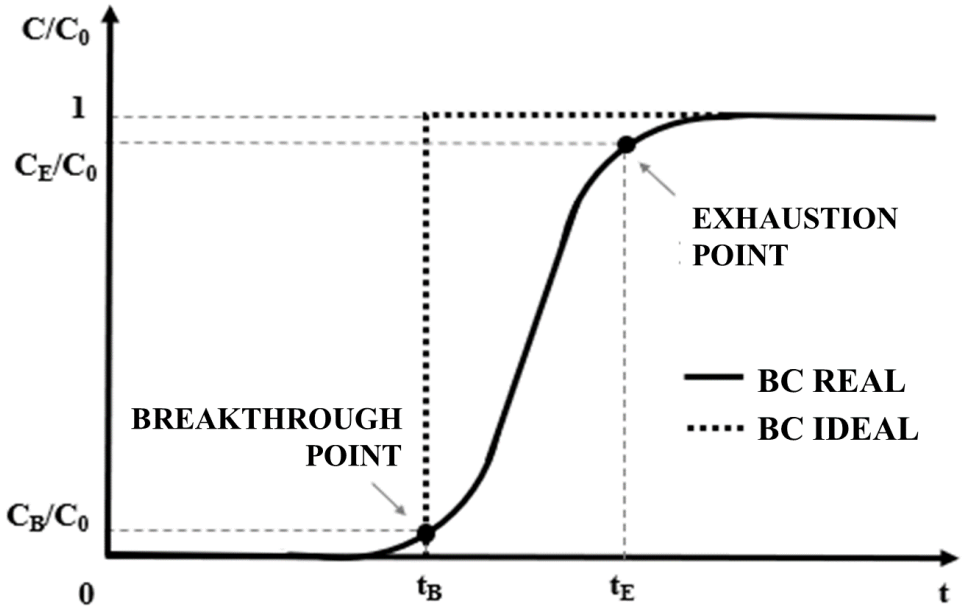

Source: Adapted from XAVIER (2018)

The breakthrough point and the exhaustion point delimit the region of the breakthrough curve in which the MTZ shifts, that is, the interval in which the bed is no longer empty, but has not yet been completely saturated. It is usual to define the breakthrough concentration (C_b) as the adsorbate concentration in the fluid phase 5% above the adsorbate initial concentration and the exhaust concentration (C_e) as the concentration equal to 95% of the initial adsorbate concentration. However, the choice of this breakthrough concentration (C_b) varies according to the desired removal efficiency in the process, generally defined to meet legal requirements. The breakthrough curve is a mirror image of MTZ, also presenting a sigmoidal shape and being related to the mass transfer resistance in the same way (MESQUITA, 2016; WORCH, 2012; XAVIER, 2018).

The time until the bed is empty and the outlet adsorbate concentration (C) has not yet exceeded the breakthrough concentration (C_b), called breakthrough time (t_b), is the parameter that determines the column's service time. It is desired that a column operates for as long as possible in this condition, maximizing its service time. After the breakthrough time, the column no longer meets the need for removing adsorbate from the fluid phase. In ideal cases, in which the adsorption rate is speedy, the bed is saturated after the breakthrough, soon reaching the exhaustion time (t_e), reducing the

time for the relative concentration (C/C_0) to go from 0 to 1 on the curve breakthrough, a time in which column efficiency is no longer sufficient. Thus, an ideal breakthrough curve differs from a real breakthrough curve, whose adsorption kinetic is slow due to the degree of inclination of its curves, as shown in Figure 5.5 (METCALF; EDDY, 2014; WORCH, 2012; XAVIER *et al.*, 2018).

The determination of the adsorption capacity (q_0) of a real continuous system can be done by applying integral mass balance equations to the respective breakthrough curves. These equations apply to all types of adsorbents, but they neglect the adsorption kinetics (METCALF & EDDY, 2014; WORCH, 2012). The adsorption capacity (q_0) is determined by applying a generic mass balance (EQUATION 5.13), to the breakthrough curve. Assuming the breakthrough time of the ideal curve corresponding to no adsorbate leaving the column, that there are no adsorbate formation or consumption reactions, and that the accumulated adsorbate is divided into the adsorbent and the fluid phase contained in the empty volume of the bed, the Equation 5.14 is presented (METCALF & EDDY, 2014; WORCH, 2012).

$$[Accumulation] = [Input] - [Output] + [Generation] - [Consumption] \quad (5.13)$$

$$q_0 \,.\, m \; + \; C_0 \,.\, V_L = \; C_0 \,.\, Q \,.\, \int_{t=0}^{t=\infty} \left(1 - \frac{C}{C_0}\right) dt \quad (5.14)$$

where q_0 is the adsorption capacity of the column (mg/g), m is the mass of adsorbent in the bed (g), C_0 is the initial concentration of adsorbate (mg/L), V_L is the volume of the bed filled by the fluid phase (L), Q is the volumetric flow rate of the fluid phase (L/min) and C is the adsorbate concentration in the fluid phase at the time t (mg/L).

5.2 MATERIAL AND METHODS

5.2.1 MEMBRANE CHAR-BENTONITE COMPOSITE PRODUCTION

The membrane char-bentonite composite (MCBT) submitted to the adsorption tests was synthesized as described in Section 4.2.4, using the membrane char (MC) produced under the optimized pyrolysis conditions (CHAPTER 3) and the bentonite (BT).

5.2.2 BATCH ADSORPTION TESTS

Adsorption tests in batch mode were carried out utilizing MCBT adsorbent to assess its effectiveness in removing Tetracycline (TC) and Enrofloxacin (ENR) from aqueous solutions. In the equilibrium batch experiments, capped 100 mL glass bottles were utilized. Each bottle contained an MCBT dosage, a measured volume of TC or ENR solution, and a known TC or ENR concentration for each experiment specifically. The prepared bottles, comprising TC or ENR and the MCBT, underwent agitation (200 rpm) on an orbital shaker for a predetermined duration of up to 300 minutes at an average room temperature. To adjust the pH of the solutions, freshly prepared solutions of 0.1 M NaOH/HCl were used. Additionally, various experimental conditions were examined to improve the batch adsorption process for TC and ENR onto MCBT. These conditions included solution pH (from 2.0 to 9.0), adsorbent dosage (from 0.1 to 1.5 g/L), interaction time between TC or ENR and MCBT (from 0 to 300 min), initial TC or ENR concentration (from 10 to 200 mg/L), and ionic strength (NaCl, from 0 to 0.1 M). Duplicate experiments were conducted for each set of conditions. Following equilibrium, the suspension was filtered using a syringe filter, and the residual TC or ENR concentration was determined using a UV–vis spectrophotometer at a wavelength of 357 nm or 277 nm, respectively. Finally, the adsorption capacity (q_0) and the removal efficiency (R%) for TC and ENR by MCBT were calculated using Equations 5.2 and 5.15, respectively.

$$R\% = \frac{C_0 - C_e}{C_0} * 100 \tag{5.15}$$

where R% is the adsorbate removal efficiency (%) and C_0 and C_e are the adsorbate's initial and equilibrium concentrations in the fluid phase (mg/L), respectively.

The Freundlich (EQUATION 5.3) and the Langmuir (EQUATION 5.4) isotherm models were employed in the non-linear form to predict the maximum adsorption capacity and gain insights into the specific relationship between the adsorbate (TC or ENR) and the MCBT. For the kinetic studies, the experimental data were fitted to the non-linear forms of the pseudo-first-order (EQUATION 5.6) and pseudo-second-order (EQUATION 5.7) models to assess TC and ENR adsorption rate and mechanism onto MCBT. Isotherm

and kinetics mathematical modeling were done using MATLAB R2020a software and the adjustment of the experimental data to respective models was assessed through the coefficient of determination (R^2) (EQUATION 5.16).

$$R^2 = 1 - \frac{\sum_{i=1}^{n}\left(Y_i - \hat{Y}_i\right)^2}{\sum_{i=1}^{n}(Y_i - \bar{Y})^2} \quad (5.16)$$

where Y_i is the experimental value, $\hat{Y}_i$ is the value predicted by the model, and $\bar{Y}$ is the mean of the experimental values.

5.2.3 FIXED-BED COLUMN ADSORPTION TESTS

The MCBT was evaluated in continuous mode to assess the practical application of the produced adsorbent. A fixed-bed column study was conducted using a glass column (130.0 x 5.0 mm, Omnifit™) and a peristaltic pump to maintain effluent flow through the fixed bed. Two layers of glass wool and glass sphere were appropriately positioned to sandwich the MCBT during the experiment, preventing any loss of adsorbent. Different flow rates (2.0 and 5.0 mL/min), TC and ENR concentrations (5.0 and 10.0 mg/L) at pH 5.0, and MCBT mass (50.0 and 100.0 mg) were investigated in the fixed-bed column studies. Effluent samples were collected at different time intervals and analyzed using a UV–vis spectrophotometer at a wavelength of 357 nm or 277 nm for TC and ENR, respectively. All column experimental runs were performed in duplicate under identical conditions. Moreover, breakthrough curves were plotted to evaluate the fixed-bed column's adsorption capacity, and the fixed-bed parameters were estimated.

5.3 RESULTS AND DISCUSSION

5.3.1 BATCH ADSORPTION TESTS

- *Influence of pH*

Essentially, the key to maximizing the removal of any given pollutant is understanding how the pH of the solution affects the adsorption. Furthermore, the pH of the solution can affect the solubility of the pollutant and the surface charge of the adsorbent, both of which are essential elements in the adsorption process. Thus, by conducting experimental sets at different pH values ranging from 2 to 9, the impact of initial pH for the adsorption of TC and ENR employing MCBT was investigated (FIGURE 5.6).

Figure 5.6 - Effect of pH (2.0 – 9.0) on TC and ENR adsorption using MCBT

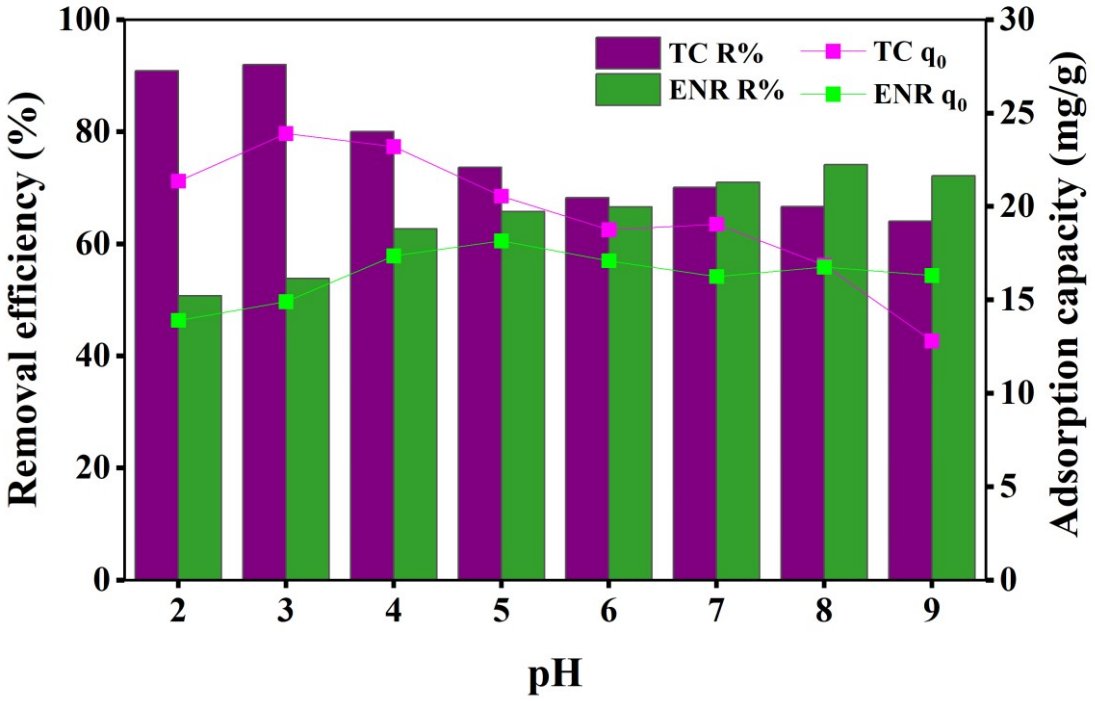

The adsorption is largely controlled by the pH of the solution. The surface charge of the adsorbent and the molecular form of the adsorbate are also impacted by the pH of the solution, and these factors rely on the pH_{ZPC} of the solid phase. Figure 5.7 shows that the pH_{ZPC} measured value of MCBT was 4.36 revealing that the MCBT surface carries a positive charge at pH values below the pH_{ZPC} and, conversely, a negative charge at pH values above the pH_{ZPC} value.

Figure 5.7 - pH_{ZPC} measurements of MCBT

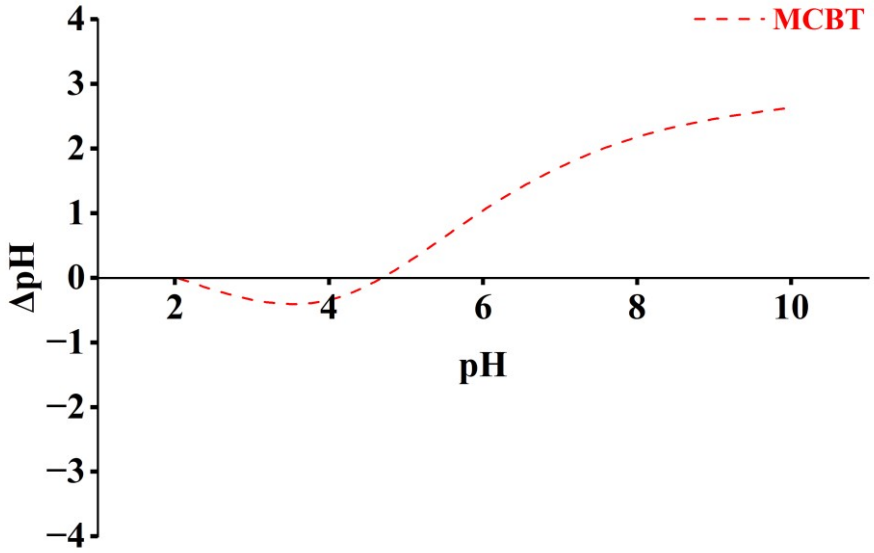

To evaluate a possible release of fluoride by MCBT in water, as occurred with MC (SECTION 4.3.1), an investigation of the stability of the composite was carried out. Figure 5.8 demonstrates the impact of solution pH (ranging from 2 to 9) on MCBT stability. The results showed that acidic and basic media slightly impacted MCBT with a small increase in fluoride leaching compared to neutral pH conditions. Overall, the results obtained proved that the synthesized MCBT is more stable than pure MC regarding the fluoride leaching.

Figure 5.8 – Release of fluoride in the solution from MCBT at pH (2.0 – 9.0) with 1.0 g/L MCBT at 25 °C and 200 rpm for 24 h shaking using ICP-OES

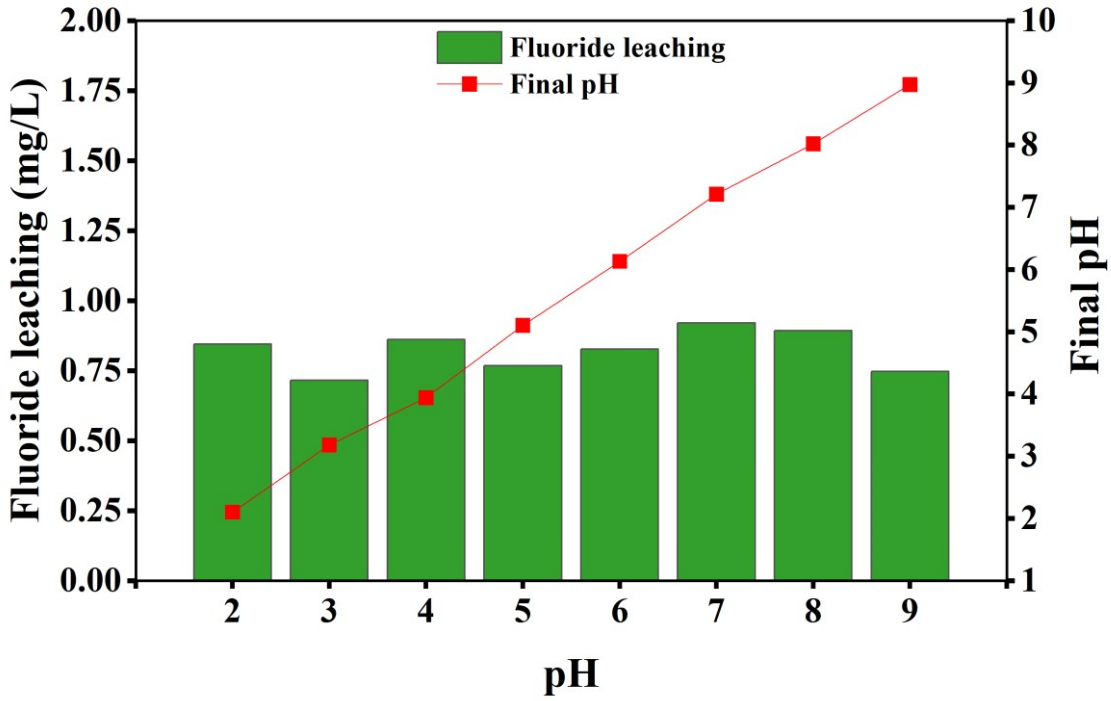

The amount of TC that was adsorbed decreased gradually as the pH of the solution increased (FIGURE 5.6). At pH 3, MCBT showed the maximum TC adsorption (92%), which then gradually decreased to pH 9 (64%). On the other hand, the removal efficiency of ENR enhanced, rising from 51% (pH 2) to 74% (pH 8). Therefore, pH 5 was established to be the ideal pH for TC and ENR removal by MCBT.

- *Influence of adsorbent dosage*

The amount of adsorbent employed can strongly impact the pollutant removal efficiency and the total cost of the adsorption process. Figure 5.9(a-b) illustrates the impact of varying adsorbate dosage (from 0.1 to 1.5 g/L) on the adsorption capacities and removal efficiency of TC and ENR by MCBT. It can be shown that the R% of TC and ENR increased from 10.1% to 91.0% and from 22.0% to 94.8%, respectively, but did not reach a plateau or saturation point Figure 5.9(a-b). These results validate the adsorption ability of TC and ENR by MCBT. The initial attainability of various adsorption sites for the adsorption can be associated with the significant improvement in the R%

of MCBT in response to changes in their amount. On the other hand, as shown in Figure 5.9(a-b), the adsorption capacity is indirectly proportional to the R%, in a negative correlation. The insufficient interaction between TC and ENR molecules with per unit weight of the adsorbent can account for the observed decrease in the MCBT adsorption capacities with increasing adsorbent concentrations, from 28.0 to 16.8 mg/g and from 59.5 to 17.1 mg/g, respectively. The ideal dosage for TC and ENR removal by MCBT was therefore determined to be 1.0 g/L.

Figure 5.9 - Effect of adsorbent dosage (0.1 – 1.5 g/L) on (a) TC and (b) ENR adsorption onto MCBT

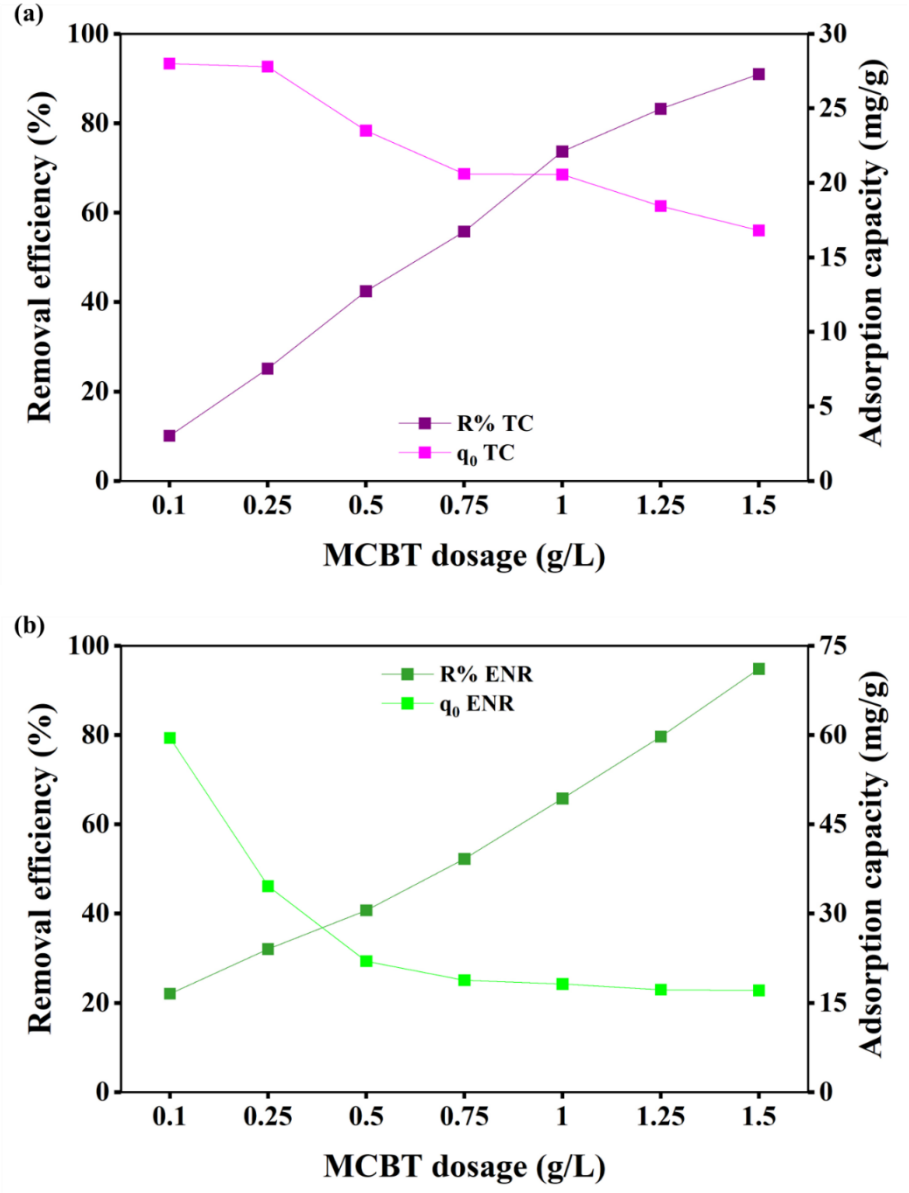

- *Influence of contact time*

For 300 minutes the adsorption capacities of MCBT for TC and ENR (FIGURE 5.10) were evaluated. According to the experimental findings, MCBT's adsorption capacity for both TC and ENR increased expressively in the first 20 minutes (rapid initial adsorption). Moreover, the adsorption rate gradually decreased as the contact period increased until it achieved equilibrium, or a static state, signifying that no more adsorption took place, reaching a plateau at near 20.0 mg/g.

Figure 5.10 - Non-linear adsorption kinetic modeling (0 – 300 min) of TC and ENR using MCBT

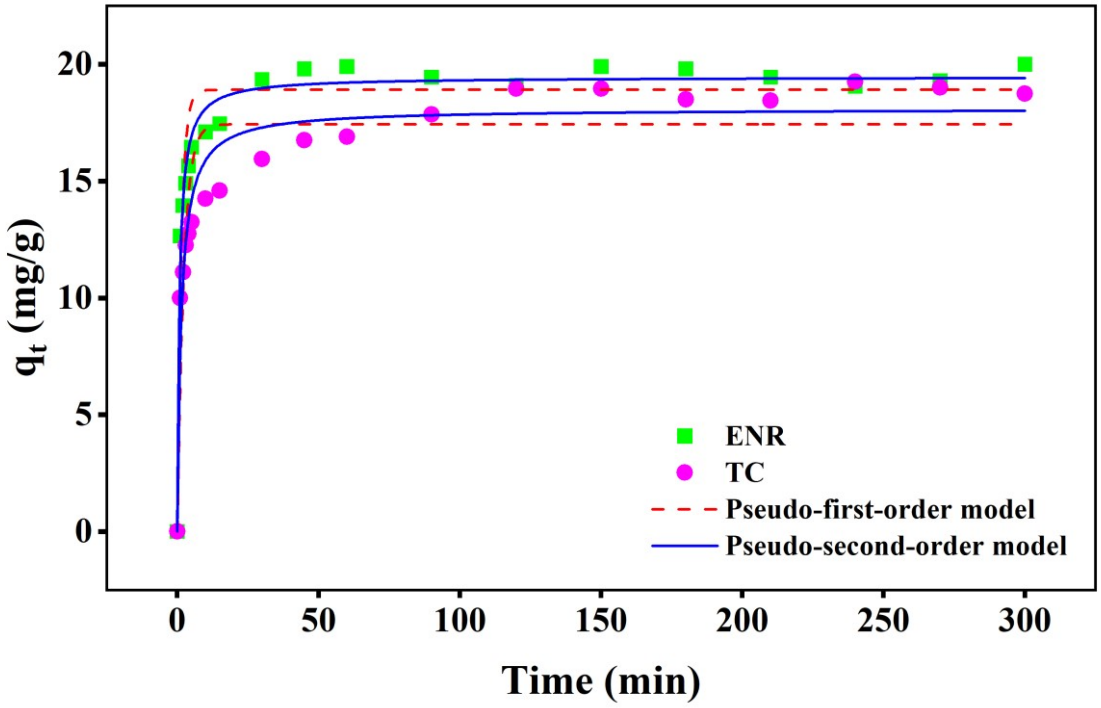

The fitting curves for the two kinetic models (pseudo-first-order and pseudo-second-order) are shown in Figure 5.10, together with the associated computed parameter values (TABLE 5.1). In comparison to the other model used, the kinetic data of MCBT showed a strong fit with the pseudo-second-order model for both TC (R^2 = 0.94) and ENR (R^2 = 0.98). Strong chemisorption interactions, such as ion exchange chemical reactions, complexation, pore filling, and H-bonding reactions, are implied to exist between MCBT and TC or ENR molecules by this model, which is based on experimental results (Liao *et al.*, 2023). The best-fitted model was shown to be valid when the theoretical adsorption capacities ($q_{e,cal}$), as determined by the pseudo-

second-order model, were found to coincide with the experimental value ($q_{e,exp}$). Additionally, it was observed that the adsorption capacity of ENR (20.0 mg/g) was only slightly greater than that of TC (18.8 mg/g).

Table 5.1 - Kinetic model parameters of TC and ENR adsorption onto MCBT

Antibiotic	Pseudo-first-order model			
	k_1 (1/min)	$q_{e,cal}$ (mg/g)	$q_{e,exp}$ (mg/g)	R^2
TC	0.44 ± 0.07	17.43 ± 0.51	18.80	0.85
ENR	0.69 ± 0.09	18.91 ± 0.37	20.00	0.92
	Pseudo-second-order model			
	k_1 (1/min)	$q_{e,cal}$ (mg/g)	$q_{e,exp}$ (mg/g)	R^2
TC	0.04 ± 0.01	18.09 ± 0.36	18.80	0.94
ENR	0.07 ± 0.01	19.46 ± 0.20	20.00	0.98

- *Influence of initial concentration*

As the main concentration was raised to 200 mg/L, the adsorption capacity of MCBT for TC and ENR showed a plateau behavior (FIGURE 5.11). This is explained by the fact that the porous structure of MCBT has no sufficient number of accessible and unoccupied adsorptive sites. The diminished steric repulsive forces between the adsorbed and diffused antibiotic molecules may also be responsible for this.

Figure 5.11 - Non-linear adsorption isotherm modeling (10 – 200 mg/L) of TC and ENR using MCBT

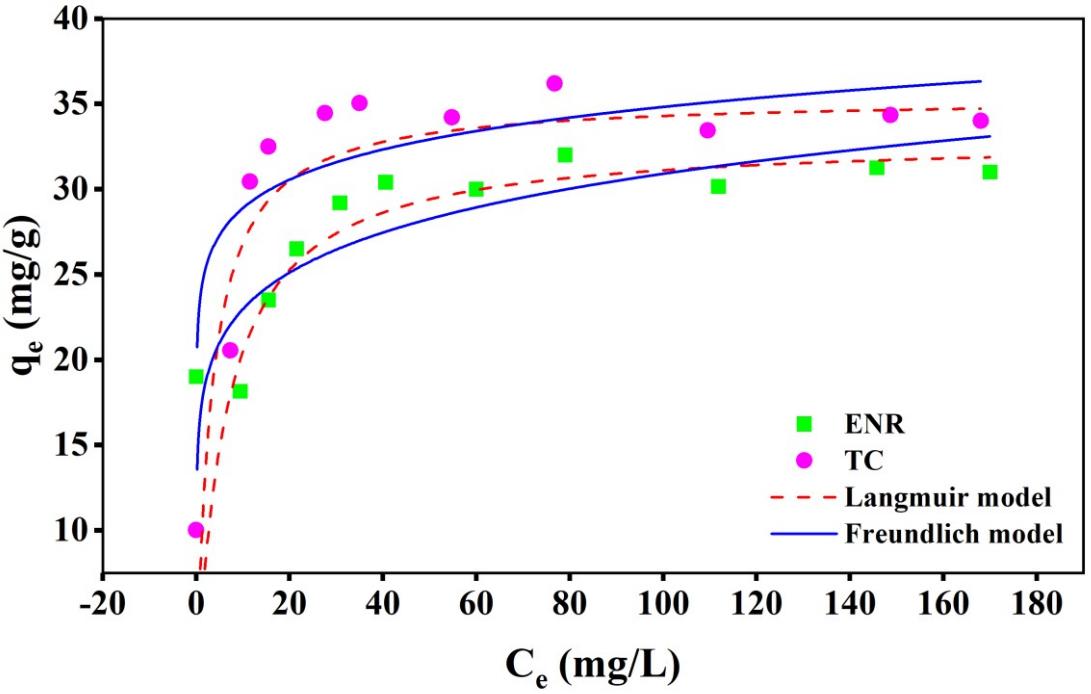

Using two non-linearized isotherms (Freundlich and Langmuir) models (FIGURE 5.11), the experimental data was also used to evaluate the TC and ENR adsorption onto MCBT. The parameters of these models were computed (TABLE 5.2). The isotherm data of MCBT towards TC and ENR molecules was best fitted by the Langmuir isotherm model, based on R^2 of 0.73 and 0.82, respectively. Due to a strong interaction between adsorbent and adsorbate, the Langmuir isotherm revealed that adsorption occurs at certain homogeneous sites within the MCBT surface, which is limited to the creation of monolayer adsorption (MAGED *et al.*, 2020). Furthermore, it was also found that TC's monolayer adsorption capacity (34.00 mg/g) was only slightly higher than ENR's (31.30 mg/g). Additionally, the Langmuir model was used to determine the maximum monolayer adsorption capacity of TC and ENR on the MCBT composite, which were determined to be 35.39 and 33.02 mg/g, respectively.

Table 5.2 - Isotherm model parameters of TC and ENR adsorption onto MCBT

Antibiotic	Langmuir model			
	$q_{max,cal}$ (mg/g)	k_L (dm^3/mg)	$q_{e,exp}$ (mg/g)	R^2
TC	35.39 ± 24.92	0.31 ± 0.20	34.00	0.73
ENR	33.02 ± 2.06	0.16 ± 0.06	31.30	0.82
	Freundlich model			
	K_F (mg/g)(L/mg)$^{1/n}$	n	R^2	
TC	23.99 ± 3.45	0.08 ± 0.04	0.34	
ENR	17.13 ± 2.31	0.13 ± 0.06	0.65	

- *Influence of ionic strength*

Improving pollutant adsorption requires an understanding of ionic strength because it provides insight into electrostatic interactions, solution chemistry, and treatment effectiveness in intricate environmental matrices. Determining the adsorption capacity and the removal efficiency of MCBT adsorbent towards TC and ENR in the presence of dissolved ions (NaCl), replicating the elements present in wastewater, is sufficient to evaluate the ionic strength (FIGURE 5.12). In this multi-component system, there was a decrease in the MCBT adsorbent's ability to remove TC (from 68.3 to 42.5%). A distinct adsorption trend was seen in the case of ENR with a small variation in the removal efficiency (from 74.6 to 75.1%) when in a multi-component system.

Figure 5.12 - Effect of ionic strength (NaCl: 0 – 0.1 M) on TC and ENR adsorption onto MCBT

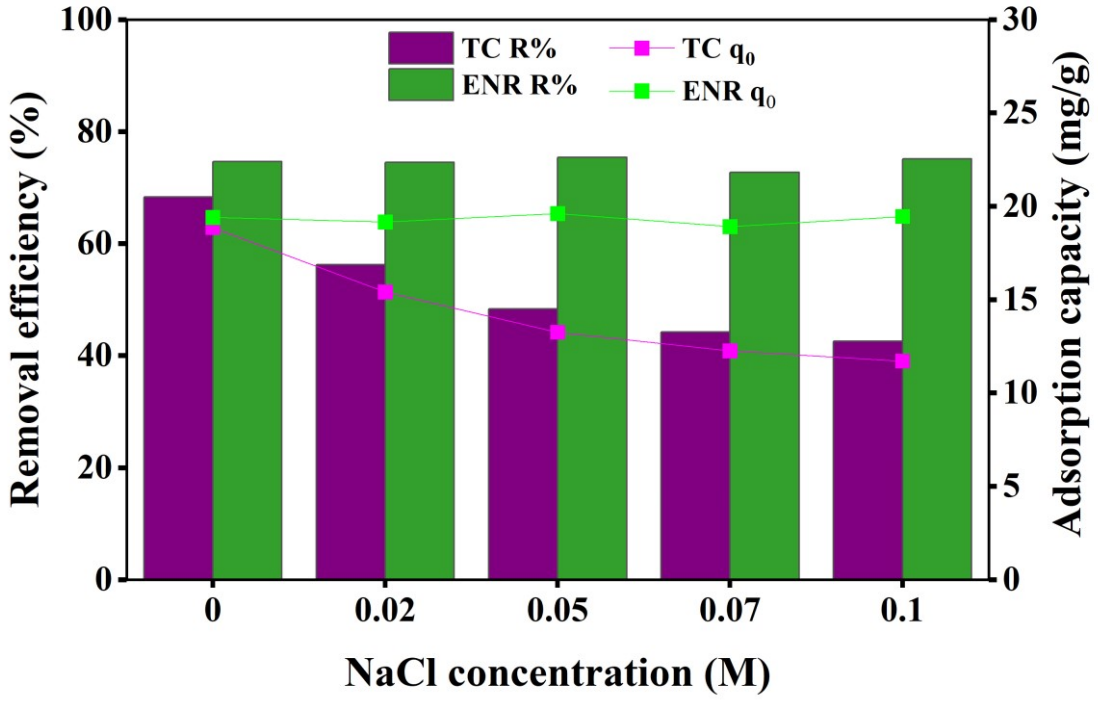

5.3.2 FIXED-BED COLUMN ADSORPTION TESTS

- *Influence of operating parameters*

The dynamic adsorption (fixed-bed column) investigations were carried out based on the ideal batch system settings to evaluate the applicability (scale-up procedure) of MCBT for TC and ENR removal. For each antibiotic, four experimental runs were carried out. These runs included the following parameters: MCBT amount packed in the column (mass of 50.0 and 100.0 mg), adsorbate flow rate (2.0 and 5.0 mL/min), and TC or ENR inlet concentration (initial concentration of 5.0 and 10.0 mg/L) (FIGURE 5.13).

Figure 5.13 - Breakthrough curves of TC and ENR adsorption onto MCBT at (a) Run 1, (b) Run 2, (c) Run 3, and (d) Run 4

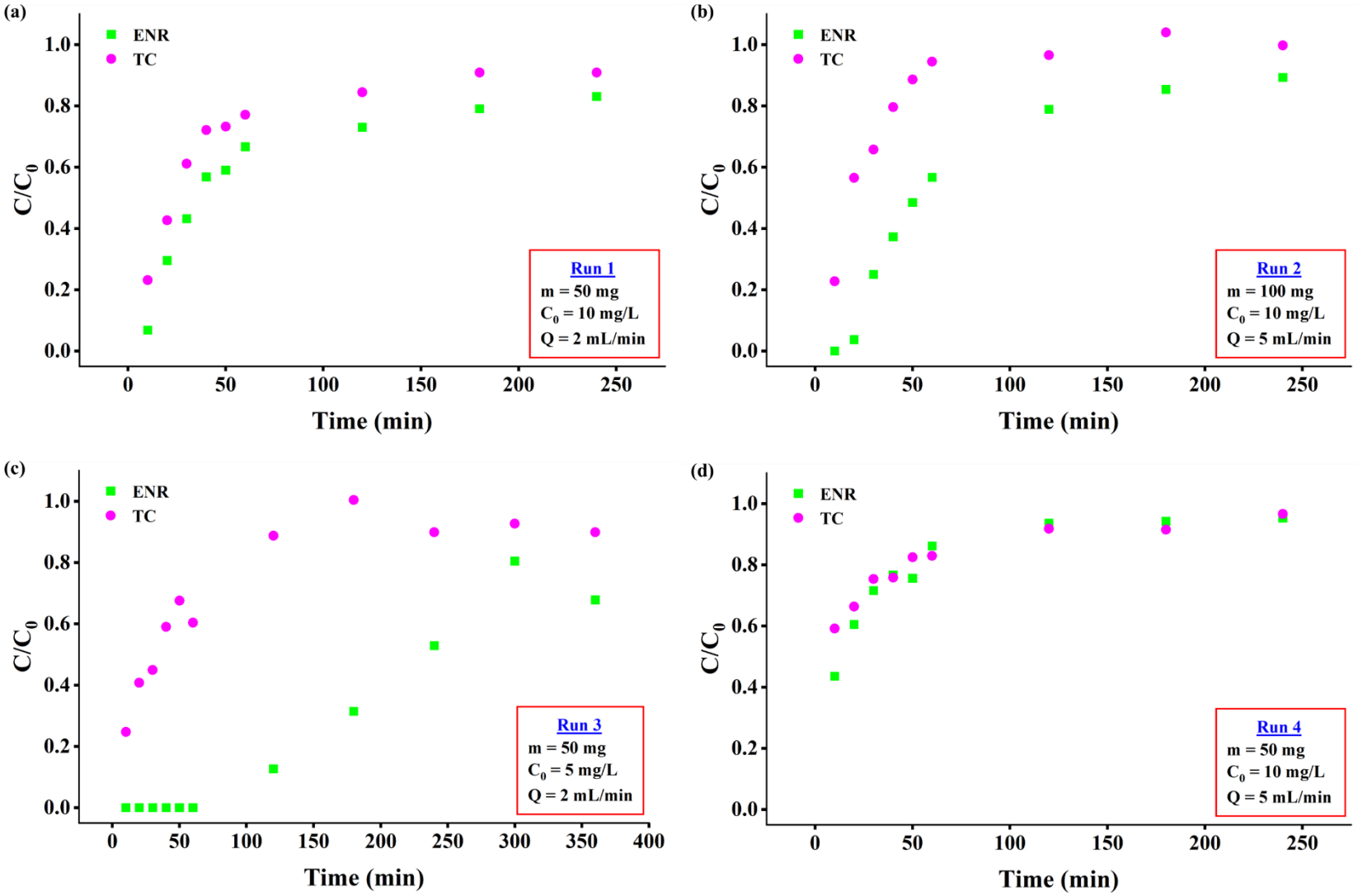

Variations in bed height (MCBT amounts packed) have a major impact on mass transfer processes, fluid dynamics, and the overall performance of continuous flow systems in column experiments. In Figure 5.13(b-d), the impact of MCBT amounts packed (Runs 2 and 4) was plotted. The breakthrough curves that were produced demonstrated that there was a significant improvement in column performance when the packed bed mass was increased from 50 to 100 mg. Under the conditions used for comparison purposes (FIGURE 5.13(b-d)), when a smaller amount of packaged MCBT (50.0 mg) is used (Run 4), the removal of antibiotics does not occur completely from the beginning of column operation and it is not possible to observe the breakthrough point of the column for both antibiotics. For TC a maximum removal of 40% is noted while for ENR this value reaches 60%. When the amount of packaged MCBT is doubled (100.0 mg) in Run 2, removals of 80% and 100% are achieved for TC and ENR, respectively, and the breakthrough can be visualized in the ENR curve. This result can be explained by increasing the intraparticle diffusion rate, the amount of accessible active sites, and the physical contact between TC and ENR molecules and MCBT (OMITOLA *et al.*, 2022).

Additionally, by adjusting the intake flow rate at 2 and 5 mL/min (Runs 1 and 4, respectively) while keeping the other parameters constant (50 mg of adsorbent amount and 10 mg/L of initial concentration), the effect of flow rate on TC and ENR adsorption onto MCBT was evaluated (FIGURE 5.13(a-d)). Even in a decrease in flow rate, Figure 5.13(a) showed that the removal of antibiotics does not occur completely from the beginning of column operation for both antibiotics. These results can be explained by a lack of residence time, which prevents MCBT and TC or ENR molecules from interacting and, as a result, lowers the adsorption potential. That situation points to probably slow adsorption, needing more contact time between adsorbent and adsorbate (AHMED & HAMEED, 2018).

Using two different antibiotic concentrations (5.0 and 10.0 mg/L), the effect of the initial concentration on breakthrough curves for MCBT was evaluated in Runs 1 and 3 while keeping other parameters constant (FIGURE 5.13(a-c)). The main discovery for these two runs was that the breakthrough time for MCBT was higher with decreasing the initial concentration of ENR, in contrast to the concentration of 10.0 mg/L. On the other hand, for TC removal, reducing the antibiotic's initial concentration did not affect

significantly the breakthrough curve. The observed increase in the breakthrough time of ENR could be explained by the slow rate of MCBT adsorption site occupancy, reinforcing the analysis of the flow rate effects above (DOVI *et al.*, 2022).

5.4 CONCLUSIONS

The adsorption capacity of the membrane char-bentonite composite (MCBT) produced in this study to remove antibiotics like Tetracycline (TC) and Enrofloxacin (ENR) from the water was investigated. Under best conditions, the maximal adsorption capacities of 34.0 mg/g for TC and 31.3 mg/g for ENR were achieved. The Langmuir best fitting in the isotherm studies revealed that adsorption only occurs in monolayer at specific homogenous spots on the MCBT surface. By this model, maximal adsorption capacities of 35.39 and 33.02 mg/g for TC and ENR onto MCBT composite were calculated. In TC and ENR adsorption onto MCBT in continuous mode were investigated the effects of MCBT amount packed in the column, adsorbate flow rate, and TC or ENR initial concentration. These studies suggest that the adsorption would likely be slow, probably due to a slow rate of MCBT adsorption site occupancy, and requiring longer contact times between the adsorbent and the adsorbate.

REFERENCES

AHMED, M. J.; HAMEED, B. H. Removal of emerging pharmaceutical contaminants by adsorption in a fixed-bed column: a review. *Ecotoxicology and Environmental Safety*, v. 149, p. 257-266, 2018.

CAVALCANTI J. E. W. A. *Manual de Tratamento de Efluentes Industriais*. 3 ed., [s.l.], Engenho Editora Técnica Ltda, São Paulo, 2009.

DAI, Y. D.; SHAH, K. J.; HUANG, C. P.; KIM, H.; CHIANG, P. C. Adsorption of nonylphenol to multi-walled carbon nanotubes: Kinetics and isotherm study. *Applied Sciences*, v. 8, n. 11, p. 2295, 2018.

DOVI, E.; ARYEE, A. A.; KANI, A. N.; MPATANI, F. M.; LI, J.; QU, L.; HAN, R. High-capacity amino-functionalized walnut shell for efficient removal of toxic hexavalent chromium ions in batch and column mode. *Journal of Environmental Chemical Engineering*, v. 10, n. 2, p. 107292, 2022.

FREUNDLICH, H. M. F. Over the adsorption in solution. *Journal of Physical Chemistry*, v. 57, n. 385471, p. 1100-1107, 1906.

LAGERGREN, S. K. About the theory of so-called adsorption of soluble substances. *Sven. Vetenskapsakad. Handingarl*, v. 24, p. 1-39, 1898.

LANGMUIR, I. The constitution and fundamental properties of solids and liquids. Part I. Solids. *Journal of the American Chemical Society*, v. 38, n. 11, p. 2221-2295, 1916.

LARGITTE, L.; PASQUIER, R. A review of the kinetics adsorption models and their application to the adsorption of lead by an activated carbon. *Chemical Engineering Research and Design*, v. 109, p. 495-504, 2016.

LIAO, X.; CHEN, C.; LIANG, Z.; ZHAO, Z.; CUI, F. Selective adsorption of antibiotics on manganese oxide-loaded biochar and mechanism based on quantitative structure–property relationship model. *Bioresource Technology*, v. 367, p. 128262, 2023.

MAGED, A.; DISSANAYAKE, P. D.; YANG, X.; PATHIRANNAHALAGE, C.; BHATNAGAR, A.; OK, Y. S. New mechanistic insight into rapid adsorption of pharmaceuticals from water utilizing activated biochar. *Environmental Research*, v. 202, p. 111693, 2021.

MAGED, A.; KHARBISH, S.; ISMAEL, I. S.; BHATNAGAR, A. Characterization of activated bentonite clay mineral and the mechanisms underlying its sorption for ciprofloxacin from aqueous solution. *Environmental Science and Pollution Research*, v. 27, p. 32980-32997, 2020.

MCCABE, W. L.; SMITH, J. C.; HARRIOTT, P. *Unit operations of chemical engineering*. 5 ed., McGraw-Hill Education, Nova Iorque, 2004.

MESQUITA, P. L. *Uso de carvão de ossos bovinos na remoção de contaminantes orgânicos de concentrados de eletrodiálise e sua contribuição ao reuso de água na indústria de petróleo*. Tese (Doutorado) - Engenharia Metalúrgica, Materiais e de Minas, Universidade Federal de Minas Gerais, Belo Horizonte, 2016.

MESQUITA, P. L.; PIRES, M. A.; SOUZA, C. R.; SANTOS, N. T. G.; NUCCI, E. R.; ROCHA, S. D. F. Removal of refractory organics from saline concentrate produced by electrodialysis in petroleum industry using bone char. *Adsorption*, v. 23, n. 7, p. 983-997, 2017a.

MESQUITA, P. L.; SOUZA, C. R.; SANTOS, N. T. G.; ROCHA, S. D. F. Fixed-bed study for bone char adsorptive removal of refractory organics from electrodialysis concentrate produced by petroleum refinery. *Environmental technology*, v. 39, n. 12, p. 1544-1556, 2017b.

METCALF, L.; EDDY, H. P. *Wastewater engineering: treatment and reuse.* 5 ed., McGraw-Hill Education, Nova Iorque, 2014.

NASCIMENTO, R. F.; LIMA, A. C. A.; VIDAL, C. B.; MELO, D. Q.; CABRAL RAULINO, G. S. *Adsorção: Aspectos teóricos e aplicações ambientais.* Imprensa Universitária, Fortaleza, 2014.

NIGRI, E. M.; CECHINEL, M. A. P.; MAYER, D. A.; MAZUR, L. P.; LOUREIRO, J. M.; ROCHA, S. D. F.; VILAR, V. J. P. Cow bones char as a green sorbent for fluorides removal from aqueous solutions: batch and fixed-bed studies. *Environmental Science and Pollution Research*, v. 24, n. 3, p. 2364-2380, 2017.

OMITOLA, O. B.; ABONYI, M. N.; AKPOMIE, K. G.; DAWODU, F. A. Adams-Bohart, Yoon-Nelson, and Thomas modeling of the fix-bed continuous column adsorption of amoxicillin onto silver nanoparticle-maize leaf composite. *Applied Water Science*, v. 12, n. 5, p. 94, 2022.

QIU, H.; LV, L.; PAN, B. C.; ZHANG, Q. J.; ZHANG, W. M.; ZHANG, Q. X. Critical review in adsorption kinetic models. *Journal of Zhejiang University-Science A*, v. 10, n. 5, p. 716-724, 2009.

SUMALINOG, D. A. G.; CAPAREDA, S. C.; LUNA, M. D. G. Evaluation of the effectiveness and mechanisms of acetaminophen and methylene blue dye adsorption on activated biochar derived from municipal solid wastes. *Journal of Environmental Management*, v. 210, p. 255-262, 2018.

THOMMES, M.; KANEKO, K.; NEIMARK, A. V.; OLIVIER, J. P.; RODRIGUEZ-REINOSO, F.; ROUQUEROL, J.; SING, K. S. Physisorption of gases, with special reference to the evaluation of surface area and pore size distribution (IUPAC Technical Report). *Pure and Applied Chemistry*, v. 87, n. 9-10, p. 1051-1069, 2015.

WORCH, E. *Adsorption technology in water treatment - fundamentals, process, and modelling.* Walter de Gruyter GmbH & Co, Dresden, 2012.

XAVIER, A. L. P. *Modelagem e otimização da adsorção de metais tóxicos em coluna de leitofixo utilizando bagaço de cana-de-açúcar modificado quimicamente como adsorvente.* Tese de Doutorado - Universidade Federal de Ouro Preto, Ouro Preto, MG, 139 p., 2018.

XAVIER, A. L. P.; ADARME, O. F. H.; FURTADO, L. M.; FERREIRA, G. M. D.; DA SILVA, L. H. M.; GIL, L. F.; GURGEL, L. V. A.. Modeling adsorption of copper (II), cobalt (II) and nickel (II) metal ions from aqueous solution onto a new carboxylated sugarcane bagasse. Part II: Optimization of monocomponent fixed-bed column adsorption. *Journal of Colloid and Interface Science*, v. 516, p. 431-445, 2018.

CHAPTER 6 - REGENERATION TESTS

6.1 LITERATURE REVIEW

6.1.1 ACTIVATED CARBON REGENERATION

During the adsorption mechanism, the pores of the activated carbon become occupied by the adsorbate and saturated. After the exhaustion of these pores, activated carbon loses its applicability as an adsorbent and the cost of replacing the material presents itself as an unfavorable point for the adsorption process use on a large scale. As an ecologically and economically viable alternative, regeneration techniques can be applied to reuse activated carbon after its exhaustion (CAZETTA *et al.*, 2013; COSTA *et al.*, 2020; ZANELLA, TESSARO & FÉRIS, 2014).

The regeneration technique applied depends on the characteristics of the pollutant, the type of adsorption, the process costs, and even the form of the activated carbon, with the regeneration methodologies of granular carbons being more consolidated, compared to pulverized material (CAVALCANTI, 2009; CAZETTA *et al.*, 2013; COSTA *et al.*, 2020; EL GAMAL *et al.*, 2018; MESQUITA, 2016). Regeneration can be classified based on its release method from the pores, either by removal or decomposition of the adsorbate.

In regeneration techniques via pollutant desorption, mass transfer occurs from the surface of the activated carbon to another phase (ZANELLA, TESSARO & FÉRIS, 2014). Thermal regeneration, using inert gases, steam, or microwaves, is widely used in industry for the desorption of adsorbates. Despite the high energy consumption and possible losses of carbonaceous mass, this technique can remove different adsorbates simultaneously (CAZETTA *et al.*, 2013; COSTA *et al.*, 2020).

In regeneration by decomposition, complete mineralization of the adsorbate can occur, with chemical regeneration being the most common of these (ZANELLA, TESSARO & FÉRIS, 2014). Compared to thermal regeneration, chemical regeneration has lower costs and offers less risk of wear to the carbonaceous material (COSTA *et al.*, 2020). Basically, it is a solid-liquid extraction, by immersing activated carbon in a solution of sulfuric acid, nitric acid, or hydrochloric acid, or even in an alkaline solution, of sodium hydroxide or ammonia, for example (DUAN *et al.*, 2020). To select the solvent, it is

important to get information on its affinity with the adsorbate as well as to know how the adsorbate is joined to the adsorbent surface.

6.2 MATERIAL AND METHODS

6.2.1 MEMBRANE CHAR-BENTONITE COMPOSITE SATURATION

The membrane char-bentonite composite (MCBT) submitted to the regeneration tests was synthesized as described in Section 4.2.4, using the membrane char (MC) produced under the optimized pyrolysis conditions (CHAPTER 3) and the bentonite (BT).

The saturation of the MCBT with a solution of Tetracycline (TC) or Enrofloxacin (ENR) was carried out by keeping the adsorbent in contact with the antibiotic solution (30 mg/L of each solute) in an orbital shaker at 200 rpm, respecting the adsorbent dosage of 1 g/L and the equilibrium time of 2 hours, as defined in the studies described in Chapter 5.

6.2.2 REGENERATION TESTS

Regeneration tests in batch mode were carried out utilizing the saturated MCBT adsorbent to assess the nitric acid (HNO_3) and potassium hydroxide (KOH) (0.1 and 0.5 M) effectiveness in removing the Tetracycline (TC) and Enrofloxacin (ENR) adsorbed. Each regeneration cycle comprehends a desorption and an adsorption step. Capped 50 mL Falcon tubes containing 50 mg of MCBT and 50 mL of TC or ENR solution (30 mg/L) or eluent solution were utilized. The prepared tubes underwent agitation (200 rpm) on an orbital shaker for 2 hours at an average room temperature for each desorption and adsorption step. Duplicate experiments were conducted for each set of conditions. Following the agitation process, the suspension was centrifuged, and for the adsorption step the residual TC or ENR concentration was determined using a UV–vis spectrophotometer at a wavelength of 357 nm or 277 nm, respectively. Finally, the removal efficiency (R%) for TC and ENR by MCBT was calculated using Equation 5.15 (CHAPTER 5).

6.3 RESULTS AND DISCUSSION

Due to waste reduction, sustainability, and economic feasibility, adsorbent reusability is essential to adsorption operations. The active adsorption sites of the saturated MCBT composite were regenerated using two different regeneration agents (HNO_3 and KOH) with two different concentrations (0.1 and 0.5 M) (FIGURE 6.1(a-b)).

Figure 6.1 - Regeneration cycles of MCBT saturated with (a) Tetracycline and (b) Enrofloxacin

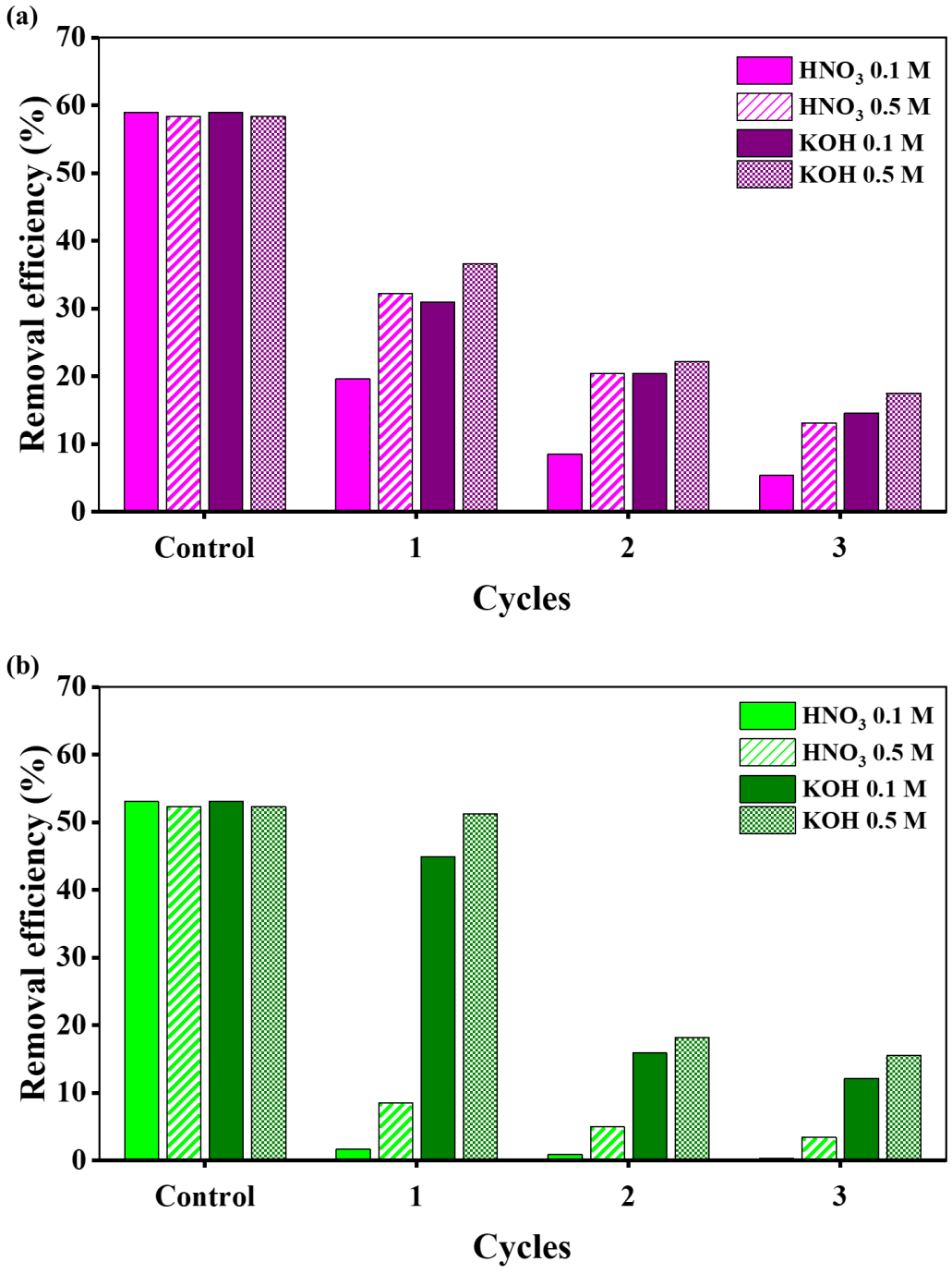

Following the third cycle of adsorption-desorption, the removal efficiency of MCBT in all eluent cases significantly decreased in the removal of TC (on average from 58.7 to 12.7%) and ENR (on average from 52.7 to 7.9%). On the other hand, it was possible to observe that utilizing KOH as the eluent for only one regeneration cycle of MCBT saturated with ENR can be effective in 0.5 M (from 52.3 to 51.2%, respectively) (FIGURE 6.1(b)). The obtained results of the regeneration tests were not satisfactory, indicating that only KOH was a favored eluent only for the desorption of ENR in one single desorption-adsorption cycle. These results can be explained by the strong chemisorption interactions implied to exist between MCBT composite and TC or ENR molecules by the pseudo-second-order model fitted in the kinetics studies (CHAPTER 5, SECTION 5.3.1).

6.4 CONCLUSIONS

The results of the regeneration tests were not satisfactory. Only KOH was able to desorb the ENR from MCBT in one single desorption-adsorption cycle. It might be explained by the strong chemisorption interactions between TC or ENR molecules and MCBT composite.

REFERENCES

CAVALCANTI J. E. W. A. *Manual de Tratamento de Efluentes Industriais*. 3 ed., [s.l.], Engenho Editora Técnica Ltda, São Paulo, 2009.

CAZETTA, A. L.; JUNIOR, O. P.; VARGAS, A. M.; DA SILVA, A. P.; ZOU, X.; ASEFA, T.; ALMEIDA, V. C. Thermal regeneration study of high surface area activated carbon obtained from coconut shell: Characterization and application of response surface methodology. *Journal of Analytical and Applied Pyrolysis*, v. 101, p. 53-60, 2013.

COSTA, L. R. C.; RIBEIRO, L. M.; HIDALGO, G. E. N.; FÉRIS, L. A. Evaluation of efficiency and capacity of thermal, chemical and ultrasonic regeneration of tetracycline exhausted activated carbon. *Environmental Technology*, v. 43, n. 6, p. 907-917, 2020.

DUAN, C.; MA, T.; WANG, J.; ZHOU, Y. Removal of heavy metals from aqueous solution using carbon-based adsorbents: A review. *Journal of Water Process Engineering*, v. 37, p. 101339, 2020.

EL GAMAL, M.; MOUSA, H. A.; EL-NAAS, M. H.; ZACHARIA, R.; JUDD, S. Bio-regeneration of activated carbon: A comprehensive review. *Separation and Purification Technology*, v. 197, p. 345-359, 2018.

MESQUITA, P. L. *Uso de carvão de ossos bovinos na remoção de contaminantes orgânicos de concentrados de eletrodiálise e sua contribuição ao reuso de água na indústria de petróleo*. Tese (Doutorado) - Engenharia Metalúrgica, Materiais e de Minas, Universidade Federal de Minas Gerais, Belo Horizonte, 2016.

ZANELLA, O.; TESSARO, I. C.; FÉRIS, L. A. Desorption-and decomposition-based techniques for the regeneration of activated carbon. *Chemical Engineering & Technology*, v. 37, n. 9, p. 1447-1459, 2014.

CHAPTER 7 - FINAL CONSIDERATIONS

7.1 CONCLUSIONS

The utilization of discarded PVDF ultrafiltration membranes for producing char/composite carries significant environmental implications. One of the most notable benefits is the diversion of these membranes from traditional disposal methods, such as landfilling or incineration. Landfilling can result in long-term environmental pollution, as PVDF membranes may take considerable time to degrade, and their incineration can release potentially harmful by-products into the atmosphere. Moreover, the environmentally conscious utilization of discarded PVDF ultrafiltration membranes is intricately linked with Sustainable Development Goals (SDGs), specifically SDG 12 - Responsible Consumption and Production. Therefore, diverting these membranes from traditional waste disposal routes and applying circular economy principles actively contribute to SDG 12's objective of achieving more sustainable and responsible consumption and production patterns. This entails reducing waste generation, conserving resources, and promoting the efficient use of materials as critical steps toward a more circular and less wasteful society. Also, the production of char/composite from discarded PVDF membranes can contribute to climate change mitigation by repurposing discarded materials and reducing the demand for virgin carbon sources aligned with SDG 13 - Climate Action. This circular economy approach minimizes greenhouse gas emissions associated with traditional waste disposal methods and promotes resource efficiency.

From the circular economy point of view, the conversion of discarded PVDF ultrafiltration membranes into char/composite exemplifies a circular economy approach centered on reducing waste, conserving resources, and promoting sustainable practices. This circularity is achieved by reintegrating materials into the production cycle, thereby extending their life cycle and creating value from waste. Embracing a circular economy paradigm entails a shift away from perceiving these ultrafiltration membranes as disposable, single-use items. Instead, these membranes are recognized as a resource that can be transformed into a valuable product, which is important in various applications and industries (i.e., water treatment, energy storage, and catalysis). This shift from a linear, "take-make-dispose" model to a circular one minimizes waste and reduces the need for virgin resources and the associated

environmental impacts of their extraction and production. Therefore, this approach is a promising strategy for managing discarded materials in an environmentally responsible and economically viable manner.

Polyvinylidene fluoride (PVDF) fibers obtained from discarded ultrafiltration (UF) membrane modules were pyrolyzed under optimized conditions of temperature (584 °C) and residence time (111 min), producing a membrane carbon (MC) with an iodine index of 242.35 mg/g. Carbonaceous material with thermal stability and graphitic domains, the MC produced by the removal of fluoride or hydrogen fluoride molecules from the PVDF, presented a surface area of 345 m^2/g, total pore volume of 0.16 cm^3/g, and microporous character. Adding these characteristics to its estimated low cost of production of 0.14 €/kg, its use in a variety of industrial, environmental, and research applications proved to be pertinent.

A methodology to synthesize the membrane char-bentonite composite (MCBT) by combining MC and bentonite clay was proposed and described. The characterization studies of MCBT indicated the production of a homogenous material with a surface area of 398 m^2/g, total pore volume of 0.18 cm^3/g, and microporous average pore diameter of 1.8 nm. MCBT production cost of 0.85 €/kg with its physical-chemical characteristics observed are beneficial for its use as a low-cost adsorbent.

The performance of MCBT as an adsorbent for antibiotics Tetracycline (TC) and Enrofloxacin (ENR) removal in batch and continuous was investigated. Maximum adsorption capacities of 34.0 mg/g for TC and 31.3 mg/g for ENR onto MCBT were achieved in batch. The kinetic studies showed that the pseudo-second-order model best describes this process, and that chemisorption was the adsorption mechanism of removal. In isotherm studies, Langmuir's best fitting showed that adsorption only takes place in monolayers at particular homogeneous regions on the MCBT surface. Maximum adsorption capacities of TC and ENR onto MCBT composite were determined to be 35.39 and 33.02 mg/g, respectively, using this isotherm model. The effects of flow rate, TC or ENR initial concentration, and the amount of MCBT packed in the column were evaluated in continuous mode adsorption. The adsorption probably is slow and needs prolonged contact time between the adsorbent and the adsorbate to occur.

Finally, four different methodologies for the regeneration of MCBT saturated with TC and ENR were evaluated, combining two regeneration agents (HNO3 and KOH) with two different concentrations (0.1 and 0.5 M) in three cycles of adsorption-desorption. After the third cycle, in every scenario, the removal efficiency of MCBT dramatically decreased in the removal of both TC (from 58.7 to 12.7%) and ENR (from 52.7 to 7.9%). These results were unsatisfactory and the strong chemisorption interactions between TC or ENR molecules and the MCBT composite could account for it.

In summary, a char (MC) was produced from discarded polymeric ultrafiltration membranes and characterized. Furthermore, a membrane char-bentonite composite (MCBT) was synthesized, characterized, and evaluated as an adsorbent to remove antibiotics TC and ENR from water in both technical and economic aspects. In this way, the contributions from this study underscore the applicability of the produced MCBT in addressing challenges across environmental domains, contributing to sustainable solutions and resource-efficient practices.

7.2 ORIGINAL SCIENTIFIC CONTRIBUTIONS TO KNOWLEDGE

- *Presented at conferences*

CANDIDO, A. L. Q.; SILVA, I. P.; ROCHA, S. D. F.; COUTINHO DE PAULA, E. *Avaliação da aplicação de um adsorvente alternativo de baixo custo, produzido a partir de membranas de ultrafiltração descartadas, para remoção de fluoreto.* In: Eu faço IC, e você?, Belo Horizonte - MG, Brazil, 11 - 12 April 2023.

SILVA, I. P.; CASELLA, G. S.; CANDIDO, A. L. Q.; ROCHA, S. D. F.; COUTINHO DE PAULA, E. *Avaliação preliminar da adsorção de fluoreto em carvão produzido a partir de membranas de ultrafiltração descartadas*. In: 32º Congresso Brasileiro de Engenharia Sanitária e Ambiental, Belo Horizonte - MG, Brazil, 21 - 24 May 2023.

CANDIDO, A. L. Q.; SILVA, I. P.; ROCHA, S. D. F.; COUTINHO DE PAULA, E. *Initial evaluation of the application of an alternative adsorbent produced from discarded ultrafiltration membranes for fluoride removal.* In: II International Congress on Science, Biodiversity and Sustainability, Belo Horizonte - MG, Brazil, 4 - 7 June 2023.

- *Submitted to journals*

SILVA, I. P.; ROCHA, S. D. F.; PAULA, E. C. Development and application of adsorbents from byproducts of wastewater treatment: a mini-review. *Water Science & Technology*.

SILVA, I. P.; MAGED, A.; ABREU, V. P. L.; CANDIDO, A. L. Q.; BHATNAGAR, A.; ROCHA, S. D. F.; PAULA, E. C. Transfiguration of discarded PVDF ultrafiltration membranes: Optimization of pyrolysis parameters for high-value char production. *Environmental Technology & Innovation.*

- *To be submitted to journals*

SILVA, I. P.; MAGED, A.; PAULA, E. C; ROCHA, S. D. F.; BHATNAGAR, A. Pharmaceuticals removal from aqueous solution via composite based on discarded fluoride polyvinylidene (PVDF) membranes and bentonite clay: synthesis, sorption, and mechanistic studies.

APPENDIX A – ADAPTED METHODOLOGY FOR IODINE NUMBER DETERMINATION

The NBR 12073/1991 and ASTM D4607/1994 methodologies provide for the determination of the iodine number of activated carbon. As the adsorbate concentration in the solution directly affects the adsorptive capacity of the char, it is important that the normality of the standard iodine solution used is maintained at 1.0 N, and therefore the residual iodine concentration is 0.02 N. The presence of volatile compounds, such as sulfur, also affects the accuracy of these methodologies. It is important to highlight that the accuracy of these methodologies is only attested for iodine numbers between 600 and 1450 mg/g (ABNT, 1991; ASTM, 1994).

▪ SAMPLE PREPARATION

1. Comminute the char to 100% smaller than 0.15 mm (100#) using a pestle grate.
2. Weigh 1 g of pulverized char with an accuracy of 0.0001g.

▪ REAGENTS PREPARATION

• SODIUM THIOSULFATE SOLUTION 0.1 N

1.Dissolve 24.82 g of sodium thiosulfate ($Na_2S_2O_3$) in distilled water.

2.Add 0.1 g of sodium carbonate (Na_2CO_3).

3.Volume up to 1000 mL with distilled water in a volumetric flask.

4.Store the solution in an amber bottle, keeping it closed.

5.Let the solution rest for 24 hours before standardizing it.

Note: If there are solids inside the flask after the rest period, the solution must be filtered on qualitative filter paper before standardizing it.

• IODINE SOLUTION 0.1 N

1. Dissolve 19.1 g of potassium iodide (KI) in 100 mL of distilled water.
2. Add 12.75 g of metallic iodine (I) and stir until complete dissolution.
3. Volume up to 1000 mL with distilled water in a volumetric flask.
4. Store the solution in an amber bottle, keeping it closed.
5. Let the solution rest for 3 hours before standardizing it.

Note: The 0.1 N iodine solution must have an iodide-to-iodine weight ratio of 1.5 to 1.

• HYDROCHLORIC ACID SOLUTION 1:5

1.Dilute 200 mL of concentrated hydrochloric acid (HCl) in 1000 mL of distilled water.

- **POTASSIUM DICHROMATE SOLUTION 0.1 N**
  1. Dry potassium dichromate ($K_2Cr_2O_7$) in an oven at 150 °C for 2 hours.
  2. Dissolve 4.9035 g of dried potassium dichromate in distilled water.
  3. Volume up to 1000 mL with distilled water in a volumetric flask.
- **STARCH INDICATOR SOLUTION 0.5%**
  1. Dissolve 0.5 g of soluble starch in 2 mL of cold distilled water.
  2. Add 100 mL of boiling distilled water.
  3. Heat the solution while stirring until it turns light in color.
  4. If the solution's turbidity persists after a few minutes of heating, the solution must be filtered through qualitative filter paper.
  5. Cool the solution to room temperature.
  6. Store the solution in an amber bottle, keeping it closed.

Note: The solution must be used on the same day of preparation.

- **SOLUTIONS STANDARDIZATION**
  - **SODIUM THIOSULFATE SOLUTION 0.1 N**
    1. Transfer 3 g of potassium iodide (KI) to a 500 mL Erlenmeyer flask.
    2. Add 100 mL of the 1:5 HCl solution and homogenize.
    3. Add 25 mL of 0.1 N potassium dichromate solution.
    4. Add 100 mL of distilled water.
    5. Immediately titrate the mixture with 0.1 N sodium thiosulfate solution until it turns yellowish.
    6. Add approximately 3 drops of 0.5% starch indicator solution.
    7. Continue titrating the sample until one drop produces a greenish mixture.
    8. Record the total volume of 0.1 N sodium thiosulfate solution used in the titration.
    9. Carry out all steps in triplicate.

Note: Standardization must be carried out immediately before using the solution.

- **IODINE SOLUTION 0.1 N**
  1. Add 25 mL of 0.1 N iodine solution to a 100 mL Erlenmeyer flask.

2. Immediately titrate the sample with 0.1 N sodium thiosulphate solution until it turns yellowish.
3. Add approximately 3 drops of 0.5% starch indicator solution.
4. Continue titrating the sample until one drop produces a colorless mixture.
5. Carry out all steps in triplicate.

Note: Standardization must be carried out immediately before using the solution.

- **TEST EXECUTION**

1.Transfer the 1 g sample of dry pulverized char to a 250 mL Erlenmeyer flask previously dried at 130 °C for 30 min and equipped with a glass stopper.

2.Add 10 mL of the 1:5 HCl solution, cover the Erlenmeyer flask, and shake the mixture gently until the char is completely wet.

3.Loosen the Erlenmeyer lid and bring the mixture to boil for 30 seconds while stirring.

4.Remove the Erlenmeyer flask from the heating plate and let the mixture cool naturally to room temperature.

5.Add 100 mL of 0.1 N iodine solution, close the Erlenmeyer flask immediately, and shake vigorously for 30 seconds.

6.Filter the mixture quickly through qualitative filter paper.

7.Collect the first 20 to 30 mL of filtrate in a beaker to create an environment in the pipette.

8.Collect the remaining filtrate in another beaker and homogenize it with a glass rod.

9.Transfer 20 mL of the filtrate to a 100 mL Erlenmeyer flask using the pipette previously set.

10. Immediately titrate the filtrate sample with the standardized 0.1 N sodium thiosulfate solution until it turns yellowish.

11. Add approximately 3 drops of 0.5% starch indicator solution.

12. Continue titrating the sample until one drop produces a colorless mixture.

13. Record the total volume of 0.1 N sodium thiosulfate solution used in the titration.

14. Carry out steps 9 to 13 in triplicate.

Note: The filtering apparatus must be prepared in advance to avoid delays in filtering the samples.

- **IODINE NUMBER CALCULATION**

1.Calculate the normality of the potassium dichromate solution (N_D):

$$N_D = \frac{\frac{m}{V}}{MM} \times k$$

Where:

–m is the mass of potassium dichromate (g);

–V is the solution volume (L);

–MM is the molar mass of potassium dichromate (g/mol);

–k is the number of gram equivalents of potassium dichromate (electron-gram).

Example:

$$N_D = \frac{\frac{m}{V}}{MM} \times k = \frac{\frac{4.9035\ g}{1\ L}}{294.185\ \frac{g}{mol}} \times 6 = 0.10001\ N$$

2.Calculate the normality of the sodium thiosulfate solution (N_T):

$$V_D \times N_D = V_T \times N_T \rightarrow N_T = \frac{V_D \times N_D}{V_T}$$

Where:

–V_D is the volume of potassium dichromate solution used in the standardization (mL);

–N_D is the calculated normality of the potassium dichromate solution (N);

–V_T is the average volume of sodium thiosulfate solution spent in titrating the standardization of sodium thiosulfate solution (mL).

Example:

$$N_T = \frac{V_D \times N_D}{V_T} = \frac{25\ mL \times 0.10001\ N}{23.8\ mL} = 0.1051\ N$$

3.Calculate the normality of the iodine solution (N_I):

$$V_I \times N_I = V_T \times N_T \rightarrow N_I = \frac{V_T \times N_T}{V_I}$$

Where:

–V_I is the volume of iodine solution used in the standardization (mL);

–V_T is the average volume of sodium thiosulfate solution used in the titration of standardization of the iodine solution (mL);

–N_T is the calculated normality of the sodium thiosulfate solution (N).

Example:

$$N_I = \frac{V_T \times N_T}{V_I} = \frac{24.6\ mL \times 0.1051\ N}{25\ mL} = 0.1032\ N$$

4. Calculate the correction factor for the sodium thiosulfate solution (FC_T):

$$FC_T = \frac{N_T}{0.1\ N}$$

Where:

–N_T is the calculated normality of the sodium thiosulfate solution (N);

–0.1 N is the theoretical normality of the sodium thiosulfate solution.

Example:

$$FC_T = \frac{N_T}{0.1\ N} = \frac{0.1051\ N}{0.1\ N} = 1.05$$

5. Calculate the iodine solution correction factor (FC_I):

$$FC_I = \frac{N_I}{0.1\ N}$$

Where:

–N_I is the calculated normality of the iodine solution (N);

–0.05 N is the theoretical normality of the iodine solution.

Example:

$$FC_I = \frac{N_T}{0.1\ N} = \frac{0.1032\ N}{0.1\ N} = 1.03$$

6.Calculate factor A (A):

$$A = N_I \times 12693$$

Where:

–N_I is the calculated normality of the iodine solution (N);

Example:

$$A = N_I \times 12693 = 0.1032\ N \times 12693 = 1310.30$$

7.Calculate factor B (B):

$$B = N_T \times 126.93$$

Where:

–N_T is the calculated normality of the sodium thiosulfate solution (N);

Example:

$$B = N_T \times 126.93 = 0.1051\ N \times 126.93 = 13.33$$

8.Calculate the dilution factor (FD):

$$FD = \frac{V_{HCl} + V_I}{V_F}$$

Where:

–V_{HCl} is the volume of 1:5 hydrochloric acid solution used in the test (mL);

–V_I is the volume of iodine solution used in the test (mL);

–V_F is the volume of filtrate used in the test (mL).

Example:

$$FD = \frac{10\ mL + 100\ mL}{20\ mL} = 5.5$$

9.Calculate the sample's iodine number (IN):

$$IN = \frac{A - (FD \times B \times V_T)}{m}$$

Where:

–A is factor A;

–FD is the dilution factor;

–B is factor B;

–V_T is the average volume of sodium thiosulfate solution used to titrate the filtrate sample (mL);

–m is the mass of dry pulverized char used in the test (g).

Example:

$$IN = \frac{A - (FD \times B \times V_T)}{m} = \frac{1310.30 - (5.5 \times 13.33 \times 5.2\ mL)}{1.0001\ g} = 928.85\ \frac{mg}{g}$$

Note: Steps 1 to 8 must be carried out whenever new solutions are prepared.

REFERENCES

ABNT. *NBR 12073/1991 – Carvão ativado pulverizado – Determinação do número de iodo.* Associação Brasileira de Normas Técnicas, Rio de Janeiro, 1991.

ASTM. *ASTM D4607-94 - Standard test method for determination of iodine number of activated carbon.* American Society for Testing and Materials, 1994.